Shape Coexistence at the sub-shell closure 40

Emmanuel Clément

UNIVERSITE CAEN NORMANDIE

Habilitation à diriger des recherches

Par

Emmanuel CLEMENT

Shape Coexistence at the sub-shell closure 40

Soutenue le 11 Décembre 2019 devant la commission d'examen :

Dr. D. Lacroix	Président et Rapporteur
Pr. O. Dorvaux	Rapporteur
Dr. J. Giovinazzo	Rapporteur
Pr. S. Lenzi	Examinateur
Pr. P. Van Duppen	Examinateur
Dr. W. Korten	Examinateur
Dr. G. de France	Garant

à Nassima, Zaccharie et Balthazar

γ-rays always tell the truth

Tables of contents

Introduction 1

I Avant-Propos 5

1 Avant-Propos 7

II Shape coexistence at A=100, Z=40 11

2 Shape coexistence at A = 100, Z=40 13
2.1 Introduction . . . 13
2.2 Coulomb excitation experiment results . . . 15
2.3 $\mathcal{Q}_s$ systematics . . . 19
2.4 Overview with other experimental data . . . 23
2.4.1 Bands head overview . . . 23
2.4.2 Transition probabilities overview . . . 26
2.4.3 Rotational band and configuration mixing . . . 27
2.4.4 Particle-Core coupling scheme . . . 28
2.4.5 Experimental multi-messenger approach: the ^{96}Sr case . . . 29
2.5 Theoretical calculations for ^{96,98}Sr . . . 30
2.5.1 Mean field approach . . . 30
2.5.2 Shell model approach . . . 33
2.6 Conclusions . . . 34

III Shape coexistence in the neutron rich Ni isotopes 35

3 Shape coexistence at N=40 and Z=28 37
3.1 Introduction . . . 37
3.2 Lifetime measurement and transition probabilities around N=40 . . . 38
3.2.1 The $3/2^-_1$ state . . . 40
3.2.2 The $9/2^-_1$ state . . . 40
3.2.3 The $11/2^-_1$ state . . . 40
3.2.4 The $1/2^-_1$ state . . . 40
3.2.5 Summary of the experimental results . . . 41

3.2.6 Theoretical calculations 42
3.3 Shape Isomers and deformed state in the vicinity of ^{68}Ni 45
3.4 $\mathcal{Q}_s$ systematics 56
3.5 Conclusions 56

IV Shape coexistence around N=Z=40 **57**

4 Shape coexistence around N=Z=40 **59**
4.1 Introduction 59
4.2 Coulomb excitation experiment results 61
4.3 $\mathcal{Q}_s$ systematics 62
4.4 Probing the deformation from the first excited states in even-even isotopes 63
4.5 Probing the role of the $g_{9/2}$ from laser spectroscopy 66
4.6 Short overview of the theoretical approaches 67
4.6.1 Mean Field calculations in Se, Kr, Sr and Zr isotopes 67
4.6.2 Shell Model calculations in Se, Kr, Sr and Zr isotopes 72
4.7 Conclusions 74

V Conclusion **75**

Conclusion **77**

Bibliography **81**

Introduction

The nuclear shape coexistence is a spectacular and universal phenomena reflecting the competition between different microscopical configurations at low excitation energy corresponding to different nuclear shapes in a single nucleus [1]. In the nuclear chart, in most of the case, the nuclear shape coexistence involves a spherical configuration that coexistences with a deformed configuration. The corresponding states reflect the competition between spherical gap from major or sub-shell closure and the residual energy of the nuclear interaction which minimize the energy of the deformed configuration. The ground state and the low lying excited states corresponding to different shapes coexist in the same nucleus with a difference in excitation energy typically lower than 2 MeV. It illustrates the subtile equilibrium of the nuclear interaction near the ground state. This phenomena is therefore a strong constraint for modern nuclear models and its experimental description remains a challenge involving advanced heavy-ions facilities and experimental setup. In a unified description of shape coexistence [1] for nuclei close to proton shell closures, e.g. Z=20 (Ca [2]), 28 (Ni [3]), and 82 (Pb-Hg [4]), spherical configurations corresponding to closed shells compete with deformed configurations resulting from multi-particle multi-hole excitations above the proton shell closures that interact with neutrons which fill high-j intruder orbits. The significant gain in binding energy for this configuration arising from the pairing and the proton-neutron correlations energy decreases the excitation energy of the corresponding 0_2^+ state in even-even nuclei so that it appears at low excitation energy or even becomes the ground state [1]. Shape coexistence has been the subject of numerous theoretical works and almost all theoretical approaches have been compared with available experimental data. Recently, a major achievement was reached by the use of Monte Carlo Shell Model calculations. These calculations provide for the first time a microscopic description in the neutron rich Ni and Zr isotopes and in neutron deficient Hg isotopes with an accurate reproduction of the experimental data [5, 6, 7, 8]. A second achievement is the first measurements of spectroscopic quadruopole moment of short lived excited states using post-accelerated radioactive beams at ISOL facilities and safe Coulomb excitation technique [9, 10, 11, 12]. Very recently, single nucleon transfer shed a new light on the field [13]. The last decade has also shown that this exotic phenomena is not rare. From isolated case, islands of occurrence appeared all along the nuclear chart, at proton shell closures closed by high j-orbits, involving therefore a possible strong proton-neutron interaction via the tensor force. Finally, some cases appeared in the recent years close to doubly magic nuclei (^{42}Ca [14], ^{80}Ge [15], ^{56}Ni [16], ^{78}Ni [17]).

The experimental study of shape coexistence is long standing effort. Many experimental probes can be used to discover or characterized shape coexistence in an isotopic chain or in a given nuclei. Shape changes such as the transition from spherical to deformed nuclei can be identified by the

measurement of the excitation energy of the first excited 2^+ state in even-even nuclei. In odd-mass nuclei, having a non zero spin in the ground state, the charge radii or the spectroscopic quadrupole moment extracted from laser spectroscopy, are a clear signature of a shape change. The most emblematic case is the discovery of the charge radii staggering in the Hg isotopes [18, 19, 7] between the ground state and the isomeric state, suggesting a shape coexistence between spherical and deformed configuration. In heavy elements, α-decay have been used to identify excited 0^+ shape isomer in the light Pb isotopes [20]. E0 $0^{+m} \rightarrow 0^+$ transition by e^- decay is a unique signature of shape coexistence [21, 22, 23, 24, 25]. A large value of the monopole transition strenght $\rho^2(E_0)$ reflects a large difference in deformation or/and a large mixing of the 0^+ states wave function [26]. This large mixing can lead to the repulsion of the 0^+ states and increase the excitation energy of the 0_2^+ state. If both the monopole and quadrupole strenghts are known [27], the mixing amplitude of the wave functions can be deduced. This strenght distribution related to a significant mixing perturbates the relative excitation of the first 2^+ to the ground state (that increases) and the reduced E2 transition probability (which is reduced) from an extrapolation of the collective band at higher angular momentum. This low spin perturbation was interpreted as a signature of mixing related to shape coexistence. A complete illustration is the case of the neutron deficient Kr isotopes [28, 29, 30, 31, 32]. Ideally, one would like to measure directly the shape of both configurations. The quantities directly related to the charge distribution are the charge radii and the electric spectroscopic quadrupole moment. In odd mass nuclei, with states that differ from zero spin, such measurement can be achieved by laser spectroscopy under the condition that both the ground state and the shape isomer live long enough for the measurement. Deformation parameter for a 0^+ state cannot be directly measured since the zero spin prevents to define an orientation needed to define a shape. First 2^+ excited states built on top of the corresponding 0^+ state live from few pico-second to few nano-second. Laser spectroscopy remains impossible. The last decade has revolutionized the study of shape coexistence with the possibility of having post-accelerated radioactive beam at the Coulomb barrier in so-called ISOL facilities like GANIL-SPIRAL1, REX-ISOLDE and ISAC-TRIUMF. With beams intensity $> 10^3$ pps and efficient γ arrays like EXOGAM [33], MINIBALL [34] and TIGRESS [35], multistep safe Coulomb excitation [36, 37, 38, 39, 40, 41] becomes feasable. From these measurements, using second order effects in the Coulomb excitation cross section, the diagonal E2 matrix element $\langle J^\pi | E2 | J^\pi \rangle$ can be measured in short lived excited states. This quantity is directly related to the spectroscopic quadrupole moment ($\mathcal{Q}_s$) and its sign. A geometrical conversion allows to determine an axial deformation parameter β_2. Thus such measurements allow to determine the corresponding shape of excited states and therefore the *unique* way to prove shape coexistence in exotic nuclei involving short lived non-zero spin states.

Shape coexistence with protons and neutrons far from shell closures have been reasonnably well describes within the mean-field approaches using interactions like the Gogny or Skryme functionnals. In these calculations, two clear minima appear in the potential energy surface calculated as a function of the deformed axial (β) and triaxial (γ) degree of freedom. Each minima corresponds to a $J^\pi = 0^+$ state in even-even nuclei, from which collective structures are built. In the vicinity of proton major or sub-shell closure, a more microspical description of the low lying 0^+ state was developped by K. Heyde and co-workers [42]. Starting from the nuclear shell structure in medium-heavy and heavy nuclei, the excitation energy for low-lying 0^+ intruder states was investigated. Taking a simplified model with two particle-two hole (2p-2h) excitations across closed shells, the effects of pairing and proton-neutron (monopole and quadrupole components) with high-j in-

truder orbits residual interaction was highlighted. The resulting contribution of the pairing and quadrupole proton-neutron interaction allow the deformed state to gain enough binding energy to become the ground state. The spherical configuration doesn't vanish but appears as an excited configuration. It is a caracteristic of the shape coexistence phenomenum that it is not only an onset of deformation (as for N=90) or the local appearence of a spherical shape (as magic nuclei). But both configurations, spherical and deformed, coexist at low excitation energy and are in competition for the ground state configuration. Only subtle effects in the nuclear interaction make one or the other configuration a candidate for the ground state as minimum of the potential energy of the system. The microscopical description calls for more elaborated calculations. This was recently achieved using Monte Carlo Shell Model calculation in several region benchmarking the phenomenom of shape coexistence [5, 6, 7, 8]. However, it is worth mentioning that, in spite of all these great progresses, the comparaisons with spectroscopic data are always partial. Indeed, most of the advanced theoretical models are compared with experimental data of a given publication. Often, partial level schemes are compared on few isotopes and time to time reduced transition probabilities. Rarely, spectroscopic quadrupole moment from both excited states and ground states are compared at the same level. Even more rarely, monopole transition strenght $\rho^2(E_0)$, often evidencing for the first time shape coexistence by the observation of a $0^+ \rightarrow 0^+$ transition, are systematically compared. It can also be underligned that so far, the so-called $ab-initio$ calculations did not yet investigated such shape competition. It will be interesting to evaluate if such spectacular phenomena emerge from $first-principle$ approaches giving more insight in the microscopical origin of the deformation in atomic nuclei and by extension to shape coexistence. Finally, symmetries can play a major role. The islands of inversion have also been described in the Quasi-SU(3) and Pseudo-SU(3) dynamical symmetries framework [43, 44] and can be applied to many area of shape coexistence.

The sub-shell closure at nucleons number 40 plays a major role in the framework of the study of the shape coexistence. This sub-shell closure is not a strong shell closure defining magic or semi-magic nuclei as can be clearly seen from the mass measurements. Its appears as the 4^{th} major shell gap in the oscillator potential plus angular momentum but without spin-orbit. It is closing the *spdf* sequence, last orbit beeing the l=2 $2p$, by the l=4 $1g$ orbit. This natural Δ=2 difference calls for large quadrupole collectivity effect when nucleons are excited from the *spdf* shells to the g orbit. Thanks to the spin-orbit term, the $1g$ orbit is further splitted between the $1g_{9/2}$ (down in energy) and the $1g_{7/2}$ (increased energy) which define finally the strong N, Z = 50 shell closure responsible for the doubly magicity character of ^{100,132}Sn and ^{78}Ni isotopes. This proximity in energy between the $1g_{9/2}$ orbit and the pf shells is the seed for the competition between spherical states with nucleons occupying the pf shells and deformed configurations involving nucleons excitation into the $1g_{9/2}$ orbit. The occupancy of the $g-$orbit only doesn't provide sufficient gain in binding energy to allow the deformed configuration to become the ground state. Similarly to the $N = 20$ and $N = 28$ island of inversions, thus shape coexistence, are triggered by a proton-neutron interaction reducing the spin-orbit splitting induced by the tensor term of the interaction in its Δl=0 or Δl=1 channels. Proton-neutron interactions are the final trigger of shape coexistence provinding enough correlation energy to reduce the excitation energy of the deformed configuration. At $N = 20$, the $p - n$ Δl=0 interactions are $\pi d_{5/2}$-$\nu d_{3/2}$ and $\pi d_{3/2}$-$\nu d_{3/2}$ as at $N = 28$, the Δ=1 interactions are $\pi d_{5/2}$-$\nu f_{7/2}$ and $\pi d_{3/2}$-$\nu f_{7/2}$. This scheme can also be applied to isotopes involving *either* a proton or a neutron number 40 or *both* a proton and a neutron number 40 making this nucleon number unique in the nuclear chart.

At Z$\sim$ **40** and N$\sim$60, the $\pi(g_{7/2} - g_{9/2})$ spin-orbit splitting is reduced when neutrons are promoted into the $\nu g_{7/2}$ and less significantly into the $\nu h_{11/2}$ orbits from the $\nu d_{5/2}$ orbit. Neutron holes interact strongly in the Δl=1 channel with proton holes in the $\pi f_{5/2}$ orbit created by pair excitation across the Z=40 gap into the $\pi g_{9/2}$ orbit. This proton pair further interacts with a pair of promoted neutron in the $\nu g_{7/2}$ orbit in the Δl=0 channel. Theses strong $p-n$ interactions induce the sudden and unique onset of deformation leading to shape coexistence at N=60 in neutron rich Sr/Zr elements which desappears for elements $Z > 40$ and $Z < 37$. My contribution in this mass region is described in chapter II.

At Z$\sim$28 and N$\sim$ **40**, the $\pi(f_{5/2} - f_{7/2})$ spin-orbit splitting is reduced when neutron are excited across the N=40 gap and populate the $\nu g_{9/2}$ orbit from the $\nu f_{5/2}$ orbit. Neutron holes interact strongly in the Δl=0 channel with proton holes in the $\pi f_{7/2}$ orbit created by the pair excitation across the Z=28 gap into the $\pi p_{3/2}$ orbit. The resulting deformed configuration competes at $\sim$ 2MeV excitation energy with the spherical ground state in the ^{68}Ni isotope, and is almost degenerated in the ^{67}Co isotopes (Z=27) to become the ground state in the Z=26 ^{66}Fe nuclei. My contribution in this shape coexistence scenario is described in chapter III.

At Z$\sim$N$\sim$**40**, the description in term of particle-hole excitation of proton interacting with neutron populating high-j intruder orbits is not directly applicable. Being at and near the N=Z line, neutron-deficient isotopes of Ge, Se, Kr, Sr and Zr do not follow the large isospin asymmetry leading to shape coexistence with respect to the two previous cases. Both proton and neutron occupy same orbits and have similar occupancy of the $g_{9/2}$ orbit. This isospin symmetry seems to inihibit the competition between spherical and deformed configuration. A shape coexistence scenario between spherical and deformed states was proposed in ^{70,72,74}Ge and will not be discussed here. In neutron deficient, Se, Kr, Sr and Zr, prolate and oblate configurations compete for the ground state giving rise to a unique prolate-oblate shape coexistence scenario with very large mixing of the wave functions by opposition to the previous cases. The nearly identical microscopic configuration of both proton and neutron arise from the fact that naturally proton and neutron occupy same orbits. By opposition to the A$\sim$100 and ^{68}Ni regions where a proton-neutron interaction drives the shape competition, the N$\sim$Z region could be explained by mean field effects. The weak occupancy of the $g_{9/2}$ orbit gradually increases along the N=Z line and can be correlated to the level of triaxility of the ground state. My contribution in this shape coexistence scenario is described in chapter IV.

Partie I

Avant-Propos

Chapter 1

Avant-Propos

One of the key parameter in the description of the nucleus is its mass distribution. Since the first observations of rotational bands similar to molecules in nuclei, it is well established that they are breaking the spherical symmetry and get deformed. Almost all nuclei are far from the spherical shape. This deviation is called nuclear deformation. The most simplest nucleus, ^{2}H, has a non-zero quadrupole moment which indicates that on average a preference for a non-spherical shape for the nuclear interaction. The question of the description of the nuclear deformation, both theoretically and experimentally, remains a challenge in nuclear physics. On the theoretical side, one could summarize the open question to which degrees of freedom are relevant for the description of the nuclear shape. This lead to the development of non-spherical mean-field model at different orders or group-symmetry based approaches. The dominant symmetry is the axial symmetry with the so-called prolate and oblate deformation. Smaller corrections on the potential energy can be obtained by including the triaxial or the octupole degree of freedom.

Proton and neutrons create electric and magnetic fields in their orbits inside the nucleus. The V potential created by the charge distribution can be written in multi-pole moments such as :

$$V(R) = \underbrace{\frac{1}{R}\int \rho(r)dr}_{Electric\ monopole} + \underbrace{\frac{1}{R^2}\int z\rho(r)dr}_{Dipolar\ term} + \underbrace{\frac{1}{R^3}\int (3z^2 - r^2)\rho(r)dr}_{Quadrupolar\ term} + ... \tag{1.1}$$

The nuclear surface R can be written using the spherical shape corrected by the normalized spherical harmonic such as :

$$R(\theta, \phi) = R_0(1 + \sum_{\lambda=0}\sum_{\mu=-\lambda}^{\lambda} \alpha_{\lambda\mu} Y_{\lambda\mu}(\theta, \phi)) \tag{1.2}$$

The λ, μ indexes defined the degree of symmetry of the nuclear surface. When limited to the triaxial degree of freedom, the three non null terms are $\alpha_{2,0}$, $\alpha_{2,2}$ and $\alpha_{2,-2}$. The later can be written as a function of two deformations parameters β and γ defined as :

$$\begin{aligned} \alpha_{20} &= \beta cos\gamma \\ \alpha_{22} = \alpha_{2-2} &= \tfrac{1}{\sqrt{2}}\beta sin\gamma \end{aligned} \tag{1.3}$$

β represents the axial elongation and γ is the asymmetry also called the triaxial degree of freedom. Using the ellipsoidal description of the nuclear volume, β is proportional to the difference between the long and short axis such as $\beta = \frac{4}{3}\sqrt{\frac{\pi}{5}}\left(\frac{c-a}{R}\right)$.

The comparison of measured and calculated nuclear deformation and its evolution with mass, charge and angular momentum is a cornerstone of the nuclear researches. On the experimental side, there are many methods to estimate the nuclear deformation. However measuring directly β or γ is not possible. From the observation of excited states, one can deduce from geometrical models an axial deformation parameter β using for instance the excitation energy of the first 2^+ state. In collective models, the reduced transition probabilities measures the wave functions overlap between different excited states under a given electromagnetic operator. For instance the B(E2, $2_1^+ \rightarrow 0_1^+$) gives the wave function overlap between the 2_1^+ and 0_1^+ states using the electric quadrupole operator. For all multi-polarities, the reduced transition probability is proportional to the matrix element between states and can be written such as :

$$B(E\lambda, I_i \rightarrow I_f) = \frac{|\ \langle I_f\ ||\ M(E\lambda)\ ||\ I_i\rangle\ |^2}{2I_i + 1} \tag{1.4}$$

In deformed nuclei, the B(E2)'s are large, underlining that excited states have the same structure but differ by their angular momentum. Similarly, under the assumption of geometrical models, a β parameter can be deduced from the B(E2, $2_1^+ \rightarrow 0_1^+$).

The most accurate quantity to determine the nuclear deformation is the electric spectroscopic quadrupole moment. Its amplitude determines the overall deformation and its sign the prolate or oblate character. Similarly to the reduced transition probability, the spectroscopic quadrupole moment is proportional to the mean value of the E2 operator for a given state such as, in the laboratory frame :

$$eQ_s = \sqrt{\frac{16\pi}{5}}(2I+1)^{-1/2}\langle II20\mid II\rangle\langle I\ ||\ M(E2)\ ||\ I\rangle \tag{1.5}$$

This quantity can be translated in the nucleus reference frame (intrinsic quadrupole moment) by :

$$eQ_0 = \sqrt{\frac{16\pi}{5}}\frac{1}{\sqrt{2I_i+1}}\frac{\langle I_f\|M(E2)\|I_i\rangle}{\langle I_iK20|I_f0\rangle} \tag{1.6}$$

With $I_f \neq I_i$, one deduces a transitional quadrupole moment which is related to the reduced transition probability by :

$$B(E2, I_i \rightarrow I_f) = \frac{5}{16\pi}(eQ_0)^2\langle I_iK20|I_f0\rangle^2 \tag{1.7}$$

With $I_f = I_i$, the static quadrupole moment (Q_0) can be deduced and can be translated in β such as :

$$Q_0 = \frac{3}{\sqrt{5\pi}}ZR^2\beta\left(1 + \frac{1}{8}\sqrt{\frac{5}{\pi}}\beta\right) \tag{1.8}$$

A direct translation from the intrinsic to the laboratory frame is given by :

$$Q_0 = \frac{3K^2 - I(I+1)}{(I+1)(2I+3)}Q_s$$

In excited states, the reduced transitional probability can be deduced from the measurement of their lifetime such as :

$$\frac{1}{\tau} = 12.26 B(E2,\downarrow) E_\gamma^5 (1+\alpha)$$

τ is in [ps], the B(E2) in $[e^2 fm^4]$ and E_γ in [MeV]. The α coefficient is the total conversion coefficient. In this work, lifetimes ranging from 1 to 100 ps are measured using the plunger technique [45].

Experimentally, the ground state spectroscopic quadrupole moment can be measured at zero angular momentum in odd-mass nuclei using laser spectroscopy techniques [46]. For excited states, the spectroscopic quadrupole moment can be measured using the Coulomb excitation technique below the Coulomb barrier. At first order, the cross section is proportional to the Rutherford scattering cross section and the probability to populate the final state from the ground state under the electromagnetic field of the nucleus. The cross section can be written such as :

$$\underbrace{\frac{d\sigma}{d\Omega_{i\to f}}}_{Coulomb\ cross\ section} = \underbrace{\frac{d\sigma}{d\Omega}^{Ruth}}_{Rutherford\ cross\ section} \underbrace{\frac{\sum_{M_i M_f} \mid b_{if}^{Tot} \mid^2}{2I_i+1}}_{P_{i\to f}\ probability} \tag{1.9}$$

The b_{if}^{Tot} amplitude has a first order (1) and a second order (2) terms :

$$b_{if}^{(1)} = \frac{4\pi Z_1 e}{i\hbar} \sum_{\lambda\mu} \frac{1}{2\lambda+1} \langle i \mid M(E\lambda,\mu) \mid f \rangle S_{E\lambda,\mu}$$

$$b_{I_f M_f I_i M_i}^{(2)} = \left(\frac{1}{i\hbar}\right)^2 \sum_n \int_{-\infty}^{+\infty} \langle I_f M_f \mid V(t) \mid I_n M_n \rangle e^{i\omega_{fn}t} dt \times \int_{-\infty}^{t} \langle I_n M_n \mid V(t') \mid I_i M_i \rangle e^{i\omega_{ni}t'} dt'$$

with $S_{E\lambda,\mu}$ the Coulomb integrals. The total probabilities is :

$$P_{i\to f} \propto \mid b_{if}^{Tot} \mid^2 \propto \mid b_{if}^{(2)} \mid^2 + \mid b_{if}^{(1)} \mid^2 + 2 \mid b_{if}^{(1)} b_{if}^{(2)} \mid$$

The first order, (1), is proportional to the transitional E2 matrix element only while the second order, (2), is proportional to the diagonal E2 matrix element, i.e. the spectroscopic quadrupole moment via the interference term $\mid b_{if}^{(1)} b_{if}^{(2)} \mid$ [38]. The measurement of the Coulomb excitation cross section allows therefore to deduce both reduced transition probabilities and spectroscopic quadrupole moment.

Shape coexistence is a particular phenomenon in the study of the nuclear deformation. In that case, a significantly different microscopical configuration than the ground state can give rise to a different shape, corresponding to a second minimum in the potential energy, possibly degenerated with the ground state. The study of this phenomenon remains a challenge for both experimental and theoretical works. The modern challenges are the determination of the shape parameters of the coexisting structures, the coupling between them and how well they can be described by the theories. In the calculations, the main motivation is to understand the origin of the shape coexistence. At the mean-field level, the question is to identify the relevant symmetries. In a more microscopical

approach, it is essential to identify the relevant nucleon excitations and coupling between them. Theoretical calculations reached in the last decade a very high level of description of the experimental quantities, in particular based on the Monte Carlo Shell Model approach. The counter part is that the description in proton pair excitation above major shell gap coupled to neutron occupying intruder orbits is not experimentally verified. A long term prospective is therefore the possible direct constrain on this description.

In this manuscript, I have focussed my studies on the shape coexistence phenomena involving the nucleon sub-shell closure 40. The experimental work uses the three experimental techniques described previously: high resolution prompt γ-ray spectroscopy of exotic nuclei to extract the low spin levels scheme, excited states lifetime measurements using the plunger technique and safe Coulomb excitation of radioactive beams. This manuscript is not an introduction to the field. Introductions to the subject, to the experimental techniques and their analysis are available in my PhD manuscript [47].

On the contrary, the aim of this work is to summarize very briefly my experimental achievements and put them in the perspectives of more recent experimental works and theoretical calculations. The goal is to identify if the collection of experimental data, on each mass region in which I produced a result, have consistencies and if not, trying to identify them. In chapter 3, controversial experimental results are discussed in great details in the light of the most recent experimental and theoretical works. In all chapters, my personal experimental work are compared and placed in larger systematics including in-beam, β-decay and ground state properties experimental results. The counter part of this choice is that general introductions on each mass region are very brief. Part of the work in chapter 3 are the results of the PhD thesis of A. Dijon [48] and I. Celikovic [49] at GANIL.

In spite my significant involvement in the experimental activities at GANIL through the EXOGAM and AGATA projects [50, 51], this manuscript will not discussed this aspect of my careerer.

Partie II

Shape coexistence at A=100, Z=40

Chapter 2

Shape coexistence at A = 100, Z=40

2.1 Introduction

Neutron-rich nuclei with A$\sim$ 100 are amongst the best examples of interplays between microscopic and macroscopic effects in the nuclear matter. A rapid onset of quadrupole deformation is known to occur at N=60 in the neutron-rich Zr and Sr isotopes, making this region an active area for both experimental and theoretical studies. Already in the 60's, S.A.E. Johansson investigated the properties of light fission fragments of ^{252}Cf and observed an island of large and constant deformation around A=110 [52]. Since , a large set of experimental data becomes available in this mass region from ground state to high spin excited states.

A compilation of the mass and the charge radii ($\delta\langle r^2\rangle$) measurements was recently published in [46]. In fission fragments with A$\sim$100, the two neutron separation energy shows that the binding energy of Rb, Sr, Y and Zr isotopes rapidly increases at N=60 [53]. At the same neutron number, the systematics of the $\delta\langle r^2\rangle$ shows an abrupt increase of the nucleus radii. Therefore, the onset of stability has been interpreted as a consequence of a dramatic increase of the ground-state deformation. This onset of deformation is unique in the nuclear chart. Indeed, it occurs at exactly N=60 for several elements (Rb, Sr, Y and Zr) ; it is sudden (from spherical N=58 isotones to highly deformed N=60 isotones) ; it is not observed for Mo and Kr isotopes. This low-Z border in the Kr isotopes of this phenomenon has been recently established by means of mass measurements, where no deviation from the standard trend toward the drip line was observed at N=60 [54]. This localized effect points to the interaction between specific proton and neutron orbitals.

The systematics of the excitation energy for the first 2^+ states in the Sr and Zr isotopic chains show a sudden drop at N=60 (Fig.2.1) and by applying a simple geometrical model, one can relate it to a change of deformation from $\beta_2 = 0.1$ to $\beta_2 = 0.4$. On the other hand, in Kr isotopes, the energy of the first 2^+ state decreases smoothly between $^{94}Kr_{58}$ and $^{100}Kr_{68}$ indicating instead a smooth increase of the deformation [55, 56]. At N=60, the evolution of the E(4^+)/E(2^+) ratio

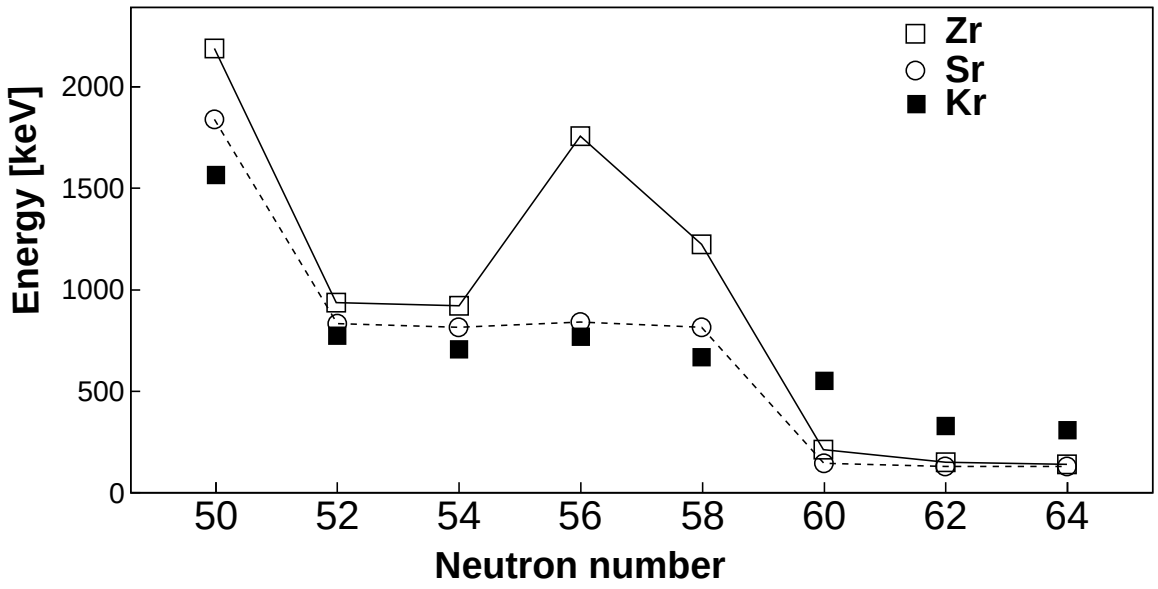

Figure 2.1: Systematics of experimental excitation energy of the 2_1^+ state as a function of the neutron number.

between Zr/Sr and Kr shows an abrupt change of trend consistent with a change in microscopical evolution [57].

The uniqueness of this shape change is illustrated in figure 2.2. The systematics of the excitation energy of the 2_1^+ states in neutron rich Sr and Sm isotopes is presented as a function of the neutron number added to the last neutron shell closure, N=50 and N=82 respectively. A maximum of excitation energy is observed at the shell closure and a minimum when 10 neutrons are added. In between, the transition from the spherical shape associated to the shell closure to the highly deformed 2_1^+ is gradual in Sm isotopes where it is sudden in Sr isotopes. Due to the sudden onset of deformation, this shape transition at N=60 and Z$\sim$40 has recently been identified as a *Quantum Phase Transition* with N as the order parameter [54, 58].

Finally, low-lying 0^+ states, indicating possible shape coexistence, have been identified in the Zr and Sr chains and, similar to the 2_1^+ state, a drop of the 0_2^+ energy is observed at N=60 (Fig.2.3). A shape coexistence scenario was therefore proposed where the 0_2^+ states for N<60 correspond to a deformed configuration, which then become the ground state at N=60, while the spherical configuration of the ground state for N<60 becomes non-yrast.

The structure of neutron-rich Sr isotopes beyond the first 2^+ state has been studied extensively in the past. In ^{96}Sr, the ground-state band was shown to have a vibrational-like character, and the small $B(E2; 2_1^+ \rightarrow 0_1^+)$ value extracted from the lifetime of 7(4) ps [59] is consistent with a nearly spherical ground state. Two low-lying 0^+ states at 1229 and 1465 keV were established by G. Jung *et al.* [60] and interpreted as candidates for a deformed band head, supporting the shape

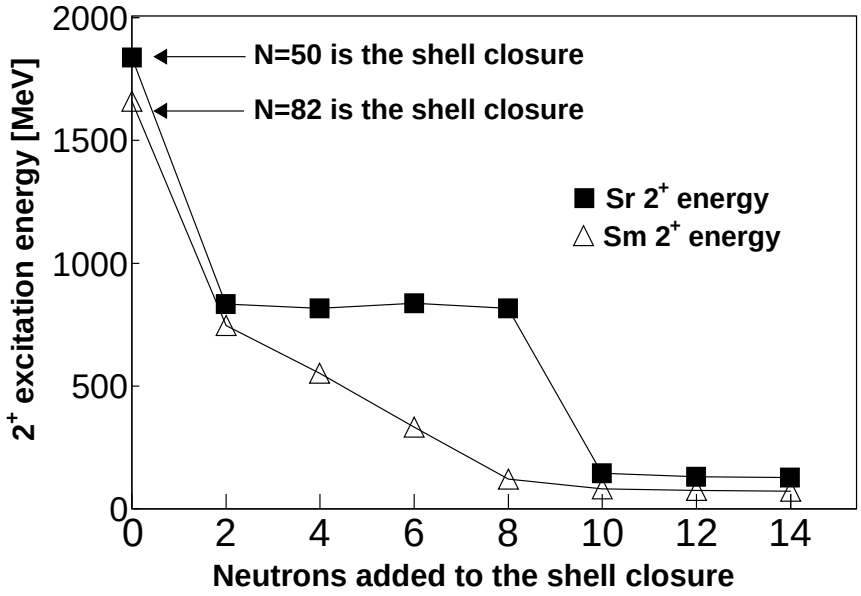

Figure 2.2: Systematics of experimental excitation energy of the 2_1^+ states in neutron rich Sr and Sm isotopes as a function of the neutrons added to the shell closure.

coexistence scenario. An extremely strong electric monopole transition of $\rho^2(E0) = 0.185(50)$ was observed between these two states [23, 24], indicating the presence of a sizeable deformation and strong mixing between the configurations. In ^{98}Sr, the ground-state band has a rotational character, and the large B($E2$) values between the excited states, deduced from lifetime measurements [61, 62, 63, 64, 59, 65, 66], are consistent with a deformed character of the ground state. A low-lying 0_2^+ state at 215.3 keV was established by F. Schussler *et al.* [25] and interpreted as the band head of a presumably spherical structure. A strong electric monopole transition of $\rho^2(E0) = 0.053(5)$ was measured between the 0_2^+ and the 0_1^+ states, again supporting the shape coexistence scenario [25, 67].

While these observables yield informations on the configuration of the ground state band and strongly support the shape coexistence scenario, the exact properties of co-existing non-yrast structures and the degree of their mixing with the ground-state configuration can only be inferred from both transition rates and spectroscopic quadrupole moments.

2.2 Coulomb excitation experiment results

The spectroscopic quadrupole moments and reduced transition probabilities in ^{96,98}Sr have been measured by low-energy Coulomb excitation of post-accelerated radioactive ion beams at REX-ISOLDE, which provided firm evidence for shape coexistence and configuration inversion in the

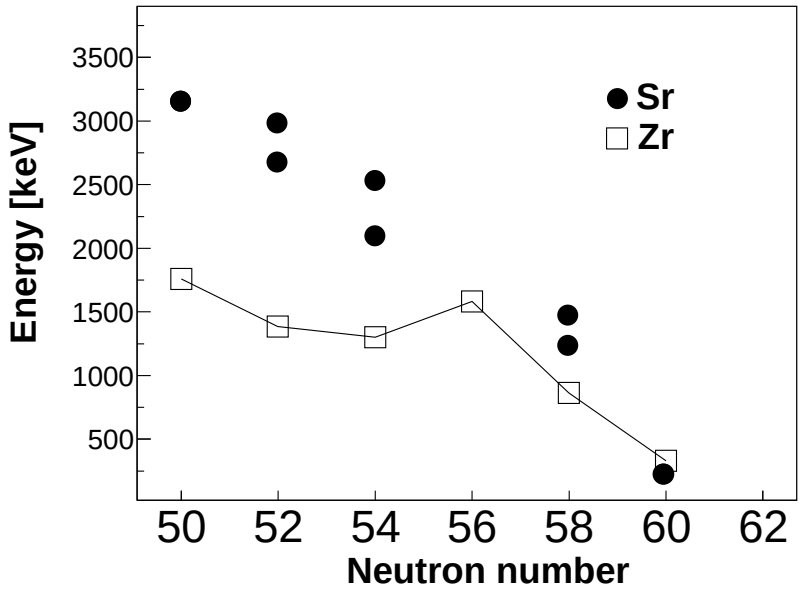

Figure 2.3: Systematics of experimental excitation energy of the $0^+_{2,3}$ states as a function of the neutron number.

neutron-rich Sr isotopes [10, 11, 68]. The corresponding level schemes are presented in figure 2.4.

To summarize the output of this rich set of experimental data :

- A Molecular extraction of a $^{96}Sr^{19}F^+$ beam was developed further broken in the REX-EBIS to deliver a pure secondary ^{96}Sr beam
- In REX-Trap/REX-EBIS β-decay of $^{98}Rb^+$ was developed to produce a secondary post-accelerated ^{98}Sr beam
- 2(9) E2 transitional matrix elements have been measured in ^{96}Sr (^{98}Sr), respectively.
- 1(5) E2 diagonal matrix elements have been measured in ^{96}Sr (^{98}Sr), respectively for the first time.
- The B(E2) transition strengths are in good agreement with the results from the most recent lifetime measurements.
- Using the precise lifetimes measurements as additional input in the analysis of the Coulomb excitation data enhanced the sensitivity to the reorientation effect and allowed extracting spectroscopic quadrupole moments for several excited states for the first time.
- In ^{96}Sr, the diagonal matrix element of the 2^+_1 state is found small and compatible with 0 in the error bars, and compatible with a nearly spherical state.

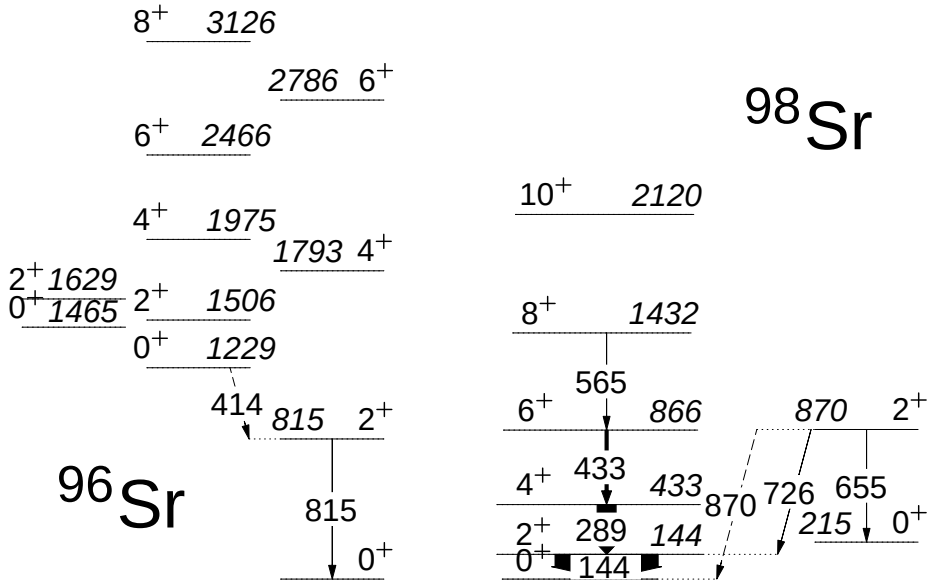

Figure 2.4: Experimental level schemes for ^{96}Sr and ^{98}Sr in [10, 11, 68].

- In ^{98}Sr, the diagonal matrix elements of the 2_1^+, 4_1^+, 6_1^+ and 8_1^+ states are large and negative underlying the large prolate deformation of the ground state band. On the contrary, the 2_2^+ diagonal matrix is found compatible with 0 indicating a spherical state similar to the 2_1^+ in ^{96}Sr. This is the first ever proof of shape coexistence in Sr isotopes and supports the shape inversion between ^{96}Sr and ^{98}Sr.

- The B(E2; $2_1^+ \rightarrow 0_1^+$) in ^{96}Sr is close to the B(E2; $2_2^+ \rightarrow 0_2^+$) in ^{98}Sr supporting their similar nature. In addition, the B(E2;$2_2^+ \rightarrow 0_1^+$) in ^{98}Sr are found an order of magnitude smaller than the B(E2; $2_2^+ \rightarrow 0_2^+$), suggesting a very weak mixing between the wave function of the coexisting states.

- The systematics of B(E2)'s along the ground state band is found similar in Sr and Zr as good rotational bands.

- They differ from the Mo isotopes which present a change from axial to triaxial rotational band.

- The transitional quadrupole moments calculated from the B(E2,$2_1^+ \rightarrow 0_1^+$) of ^{96,94}Kr, ^{96}Sr, ^{98}Zr and ^{100}Mo are found very similar supporting the fact that they lie out of the island of deformation.

- The spectroscopic quadrupole moments of the 2_1^+ state deduced from the diagonal E2 matrix elements in ^{96,94}Kr, ^{96,98}Sr and ^{100}Mo are found very similar and low, suggesting a certain level of triaxility in the deformed ^{98}Sr, similarly to the deformed ^{100}Mo.

- The matrix elements were interpreted in a phenomenological two-band mixing model for ^{98}Sr. The mixing angle for the 0^+ (2^+) states yield 0.87(1) (0.99(1)) respectively underlying the very weak mixing of the wave function in spite of their proximity in excitation energy.

- The purity of the wave functions increases rapidly with spin, explaining the increase in the spectroscopic quadrupole moments between the different 2^+ and 0^+ states.

- The quadrupole sum rule formalism was applied to derive shape parameters for the 0^+ states.

- The first rotational invariant, Q^2 (similar to $|\beta_2|$), is found small and very similar for the 0^+_1 (0^+_2) states in ^{96}Sr (^{98}Sr) respectively, confirming their weakly deformed character. On the contrary, the value is found large for the 0^+_1 in ^{98}Sr supporting the large deformation of the ground state band.

- The second rotational invariant, $cos3\delta$ (similar to γ) can only be calculated in ^{98}Sr with the available E2 matrix elements. It shows that both 0^+ states are triaxial with a value of $\gamma \sim 20°$. The similarity of the electromagnetic moments between the 0^+_1 in ^{96}Sr and 0^+_2 states in ^{98}Sr suggests that the 0^+_1 in ^{96}Sr should also present a certain level of triaxility.

- The sharp transition is associated to a very weak mixing between competing configuration, involving triaxility at very low spin, in contrast to the N∼Z cases in Kr and neutron deficient Hg for instance.

- The Davydov-Filippov model was applied on the $\langle 2^+_1|E2|2^+_1\rangle/\langle 2^+_1|E2|0^+_1\rangle$ matrix elements ratio as a function of the γ triaxial parameter. The experimental ratio is compatible with $\gamma \sim 27°$ close to the $20°$ extracted from the quadrupole sum rule formalism.

- The transition strengths and quadrupole moments were compared to theoretical calculations going beyond the static mean-field approach using the Gogny D1S interaction which well reproduce the shape coexistence in N=Z nuclei (see Chapter 4).

As mentioned, we applied a simple two-states mixing model to the measured reduced matrix elements in ^{98}Sr. In this model, the observed physical states $|I^+_1\rangle$ and $|I^+_2\rangle$ may be expressed as linear combinations of pure prolate and spherical configurations, $|I^+_p\rangle$ and $|I^+_s\rangle$, respectively:

$$|I^+_1\rangle = +\cos\theta_I \times |I^+_p\rangle + \sin\theta_I \times |I^+_s\rangle$$

$$|I^+_2\rangle = -\sin\theta_I \times |I^+_p\rangle + \cos\theta_I \times |I^+_s\rangle$$

Experimental data, in particular $E2$ matrix elements, can be used to calculate the mixing amplitudes, $\cos^2\theta_I$, between the two pure (unperturbed) configurations. Following the method described [9], and using the complete set of $E2$ matrix elements in ^{98}Sr we have extracted, small mixing angles for the 0^+ and 2^+ wave functions [10, 68, 11]. An evaluation of the mixing angles for the 0^+ and 2^+ states requires a large set of $E2$ matrix elements which are not available for many nuclei in this mass region. Assuming a negligible mixing between 2^+ states, one can extract an approximate mixing angle for the 0^+ states via

$$\tan\theta_0 = \frac{\langle 0^+_2|E2|2^+_1\rangle}{\langle 0^+_1|E2|2^+_1\rangle}.$$

Table 2.1: Values of $\cos^2\theta_0$ for the mixing angles between the 0^+ states in N=58,60 nuclei extracted using the approximation described in the text.

Elements	N=58	N=60
Pd	0.93	0.86
Ru	0.86	0.92
Mo	0.63	0.84
Zr	not measured	0.84
Sr	0.84	0.88

The $\cos^2\theta_0$ values obtained using the above expression for N=58,60 Sr, Zr, Mo, Ru and Pd nuclei are presented in Tab 2.1. For the $0_2^+ \rightarrow 2_1^+$ transition in ^{98}Zr, only an upper limit of the B(E2) is known. The result for ^{98}Sr is similar to the values determined for neighbouring nuclei. A rather weak mixing between coexisting structures is observed for nuclei in this mass region, both inside and outside the region of deformation. ^{100}Mo presents a certain level of mixing which could be related to a certain level of triaxiality as proposed from the systematics in B(E2) along the rotational band [69].

2.3 $\mathcal{Q}_s$ systematics

The diagonal $E2$ matrix elements extracted from the Coulomb excitation analysis can be translated into spectroscopic quadrupole moments, defined in the laboratory frame, using :

$$\mathcal{Q}_s = \sqrt{\frac{16\pi}{5}}\frac{1}{\sqrt{2I+1}}(I,I,2,0|I,I)\langle I\|E2\|I\rangle,$$

It can be compared to the spectroscopic quadrupole moments of the ground states obtained from laser spectroscopy for odd-mass neighbouring nuclei [70]. In order to eliminate spin, mass and charge dependences, we further convert the $\mathcal{Q}_s$ values to intrinsic quadrupole moment and to quadrupole deformation parameters β_2, assuming an axial symmetry:

$$\mathcal{Q}_s = \frac{3K^2 - I(I+1)}{(I+1)(2I+3)}\mathcal{Q}_0 = \frac{3K^2 - I(I+1)}{(I+1)(2I+3)}\frac{3}{\sqrt{5\pi}}ZeR^2\beta_2$$

where R is defined as R=$1.25\times A^{1/3}$ [fm].

The comparison for all known $\mathcal{Q}_s$ is shown in Fig.2.5 as a function of the neutron number for the odd-neutron Kr, Sr, Zr, Mo and Ru nuclei, and for the odd-proton Rb, Y, Nb and Tc isotopes [70]. The spherical neutron Nilsson orbitals are also indicated. The nuclei with N<60 have a low deformation with $\beta_2 \leq 0.2$. Our measurement of the spectroscopic quadrupole moment for the 2_1^+ state in ^{96}Sr fits well with the systematics. For N≥60, the deformations of the ground states of odd-mass isotopes, and in the ground state band of ^{98}Sr, are consistently large, whereas the β_2 value for the 2_2^+ state in ^{98}Sr is as low as those observed for N<60. Unfortunately, quadrupole moments for ^{90,92}Rb, $^{91-93,95-98}$Y, $^{94-98,100}$Nb and $^{99-101}$Mo have not been measured yet. The spectroscopic quadrupole moments in ^{88,90,92}Kr, ^{90,92,94}Sr and $^{92-94,96-100}$Zr are unknown. In the

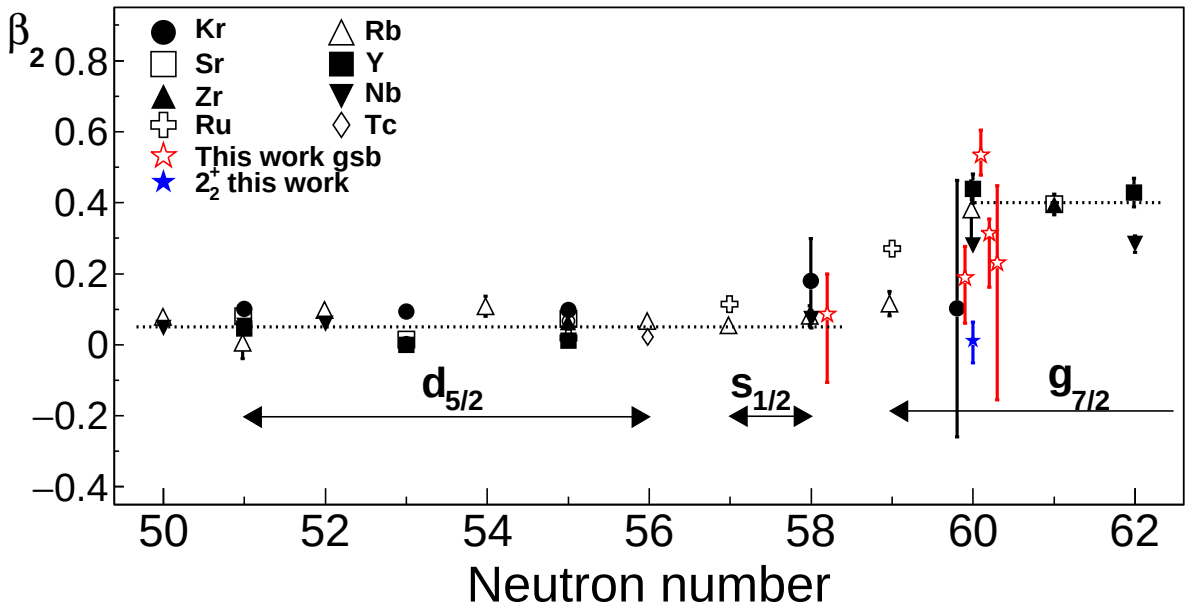

Figure 2.5: Quadrupole deformation parameter β_2 as a function of the neutron number in the Kr – Ru isotopic chains. The parameter is calculated assuming an axial symmetry. The values calculated from diagonal $E2$ matrix elements measured in the present experiment for J≠0 states in ^{96,98}Sr are compared to those obtained from laser spectroscopy for the ground states of odd-mass nuclei. States belonging to the ground state band (2_2^+) are labelled in red (blue), respectively. Spherical Nilsson orbits are mentioned for neutron.

stable ^{94,96}Mo and ^{98,100,102}Ru nuclei the quadrupole moments of the 2_1^+ states were measured using the reorientation effect with light-ion beams and yielded two alternative solutions in the Coulomb excitation analysis leading to different conclusions on the deformation. The data are therefore not displayed in the figures. This limitation could be overcome using multi-step Coulomb excitation with high-Z collision partners. The systematics shown in Fig. 2.5 is further extended by including the spectroscopic quadrupole moments of the 2_1^+ states in ^{94,96}Kr [55, 71], ^{98,100}Mo [72, 69] and ^{104}Ru [73], extracted from low-energy Coulomb excitation experiments. They follow consistently the trend observed in laser spectroscopy. Between N=50 and 58, when the $d_{5/2}$ and $s_{1/2}$ orbits are filled, the deformation is uniformly low ($\langle\beta_2\rangle \sim 0.1$) for all elements from Kr to Tc. From N=60, all deformation parameters are uniformly high ($\langle\beta_2\rangle \sim 0.5$) for all elements from Rb to Tc. Due to the large error bars, no conclusion can be drawn for ^{96}Kr. Unfortunately, ^{102}Mo is not yet measured as possible high even-Z border of the island of deformation. The onset of deformation when adding 2 neutrons to N=58 (ie. the $s_{1/2}$ orbit) to N=60 (ie filling the $g_{7/2}$) is consistently observed in both methods.

This systematics highlights a particular behaviour at N=59. As the onset of deformation is abrupt for all elements from Z=37 to 41 when adding a pair of neutrons, at N=59 a gradual effect

as function of the proton number emerges. The $^{96}_{37}Rb_{59}$ deformation is estimated at $\beta_2 \sim 0.17$, slightly higher than the N≤58 systematics and well below the N≥60 systematics. For $^{103}_{44}Ru_{59}$, the deformation is evaluated at $\beta_2 \sim 0.4$, slightly lower than the N≥60 systematics. Therefore, a more gradual shape change is suggested when only one neutron is added to the $g_{7/2}$ and when increasing the proton number in the pf shells. The shape change seems highly correlated to the occupancy of both proton and neutron in the mentioned orbits. Unfortunately, this gradual change between Sr and Tc cannot be quantified as no laser spectroscopy of this N=59 isotone (1/2 ground state spin) was performed so far.

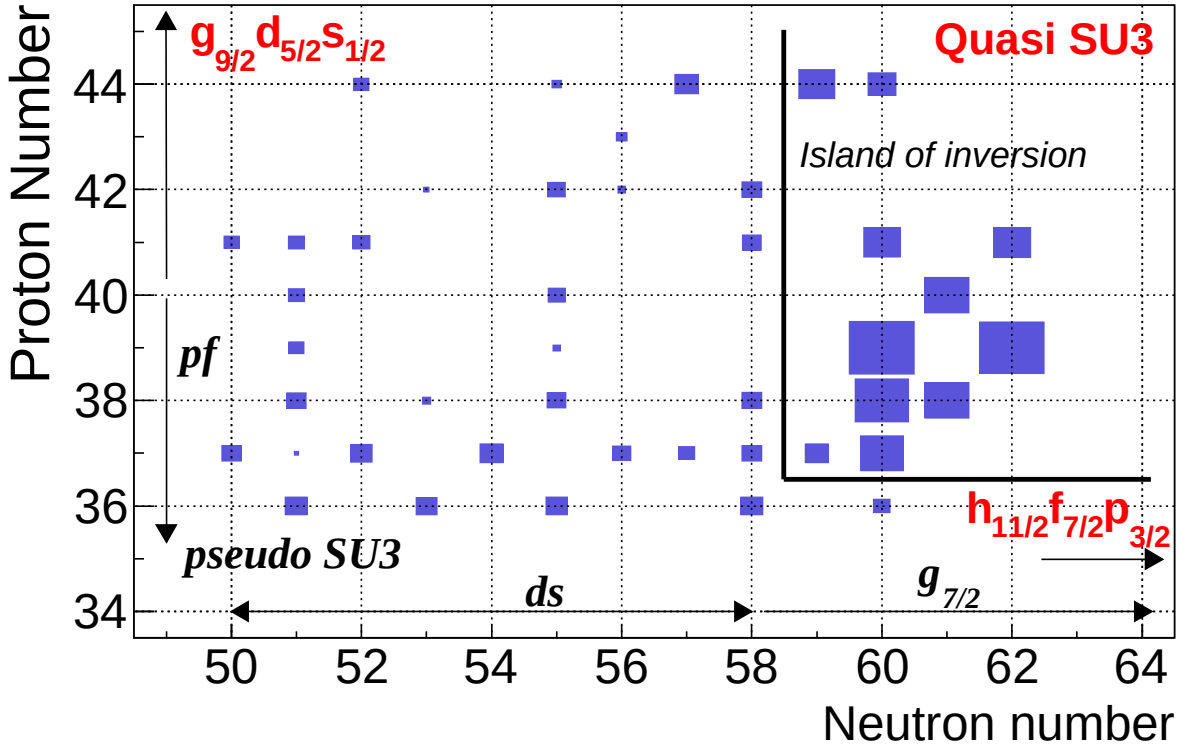

Figure 2.6: Experimental quadrupole deformation of the ground state for odd-neutron Kr, Sr, Zr, Mo and Ru nuclei, and for the odd-proton Rb, Y, Nb and Tc isotopes, and for the 2^+_1 state in even-even nuclei, as a function of the proton and neutron number. The sizes of the squares are proportional to β_2 under the assumption of axial symmetry. The Pseudo (*italic*) and Quasi (**red**) SU(3) orbitals are shown (see text).

In figure 2.6, the deformation is represented in the (N,Z) plan. The sizes of the squares in the plot are proportional to β_2. These systematics suffers from several missing experimental points. Large quadrupole deformations are observed for the ground states of odd-mass nuclei and for the first 2^+ states in even-even nuclei for elements between Z=37 and Z=44 at N=60 and beyond. With this two dimensional systematics, the island of deformation appears clearly and shows its boundaries. It appears that the Kr isotopes lie outside the island of deformation since the spec-

troscopic quadrupole moment in $^{96}Kr_{60}$ is low with respect to those in $^{97}Rb_{60}$ and $^{98}Sr_{60}$. This may indicate that for Z=36, the two neutrons beyond N=58 occupying the $g_{7/2}$ are insufficient to induce a large quadrupole deformation. The completion of the systematics, in particular for the Kr isotopic chain and N=59 isotones, are vital informations to further constrain the microscopic interpretation of the onset of deformation at N=60.

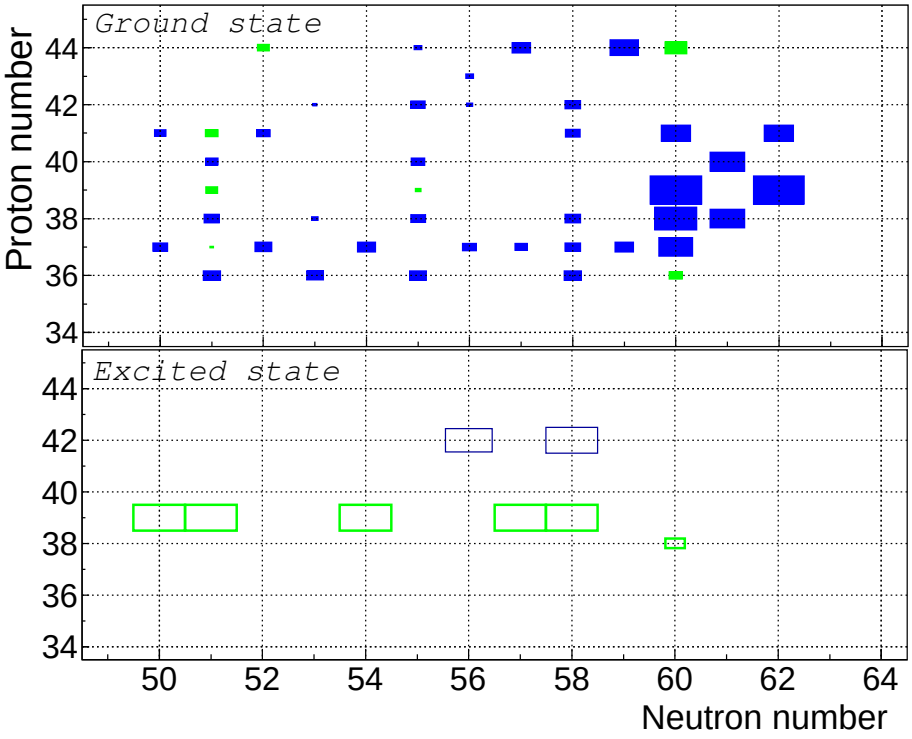

Figure 2.7: Algebraic deformation amplitude (β_2) in the (N,Z) plan from measured spectroscopic quadrupole moments. *Top*: for ground state or 2_1^+ states. *Bottom*: for isomers or $2_{2,3}^+$ states

In figure 2.7, the algebraic deformation is deduced (β_2). The blue (green) squares indicate prolate (oblate) deformations respectively. The first matrix shows the deformation for the ground states in odd-nucleon isotopes and the 2_1^+ state for even-even isotopes. The second matrix displays the long lived isomeric state deformation in odd-proton or odd-neutron isotopes extracted from the laser spectroscopy. In the case of the even-even nuclei, the 2_2^+ or 2_3^+ state built on top of the 0_2^+ state with the largest B(E2) is shown. The first systematics is similar to figure 2.6 and highlights the onset of deformation of prolate character. The second systematics reveals the lack of experimental data in spite of the large set of known long lived isomers. Unfortunately, only spectroscopic quadrupole moment in Y isotopes have been measured. In even-even nuclei, ^{98,100}Mo and ^{98}Sr have measured spectroscopic quadrupole moments. Consistently, for isotopes with N$\leq$58, non-yrast 2^+ states and isomers have very large deformation of prolate character in Mo and oblate character

in Y isotopes coexisting with weakly deformed ground state. Beyond N=58, only one deformation in excited configuration is measured in ^{98}Sr having a weak oblate deformation. This systematics shows again the consistency between the laser spectroscopy measurement and the Coulomb excitation data and the shape inversion at N=60. Below Z=40, the non-yrast configuration seems to be systematically of oblate character.

2.4 Overview with other experimental data

2.4.1 Bands head overview

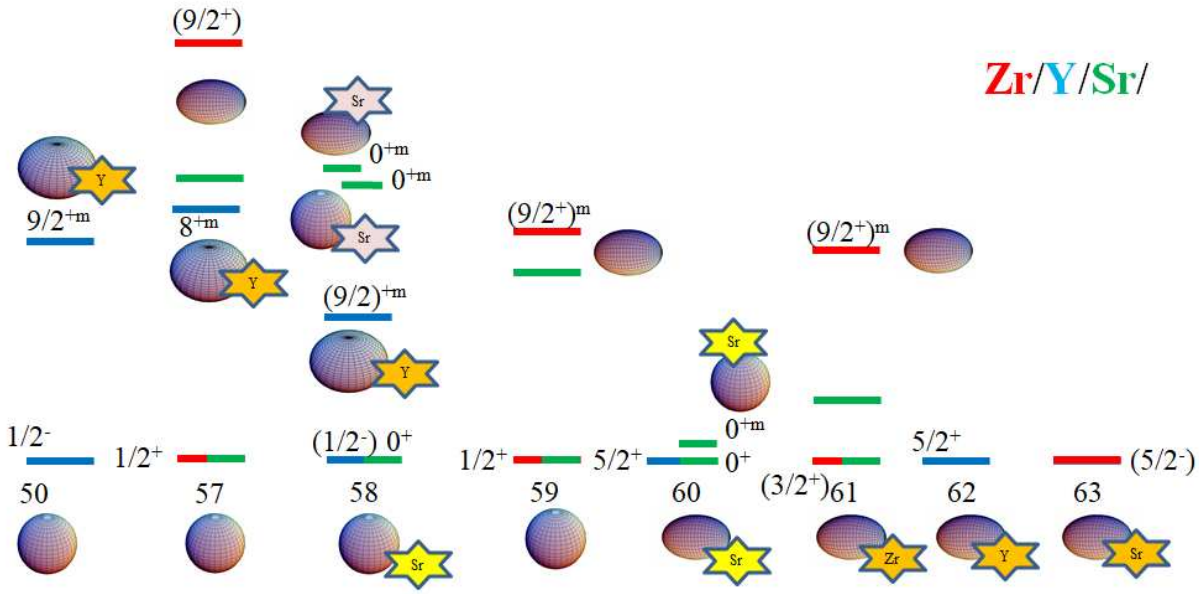

Figure 2.8: Systematics of ground and isomeric states spin/parity and confirmed deformation in Zr, Y and Sr isotopes. Orange stars indicate that the deformation parameter was extracted from laser spectroscopy. The yellow stars highlight the deformation measurement by safe Coulomb excitation. The pink stars underline the conclusion from the neutron transfer experiment in ^{96}Sr. Shapes without star are speculative deformation assignment.

Spectroscopy of fission fragments with mass A$\sim$ 100 produced in fission sources or induced fission of actinide has triggered a large experimental effort world-wide to probe the scenario of shape coexistence. Large set of γ-ray spectroscopy and electron spectroscopy at high spins are available in the literature. The onset of collectivity and deformation change in the ground state is now clearly established, even if not for all isotopic chains. On the contrary, the shape coexistence description is incomplete and systematics of excited and ground state deformation are very scarce. With the development of post-accelerated radioactive ion beams, experimental data with "direct" methods

are available and improve our description of shape coexistence in this mass region. The spin and parity of the ground state and long-lived isomers give strong indication on the involved Nilsson orbits. Figure 2.8 shows the systematics of measured ground states and isomeric states spin/parity and highlight confirmed deformation in Zr, Y and Sr isotopes as a function of the neutron number. Isotones are presented in the same column and a colour code indicates the element. For clarity, figure 2.9 shows the orbitals involved in the present discussion.

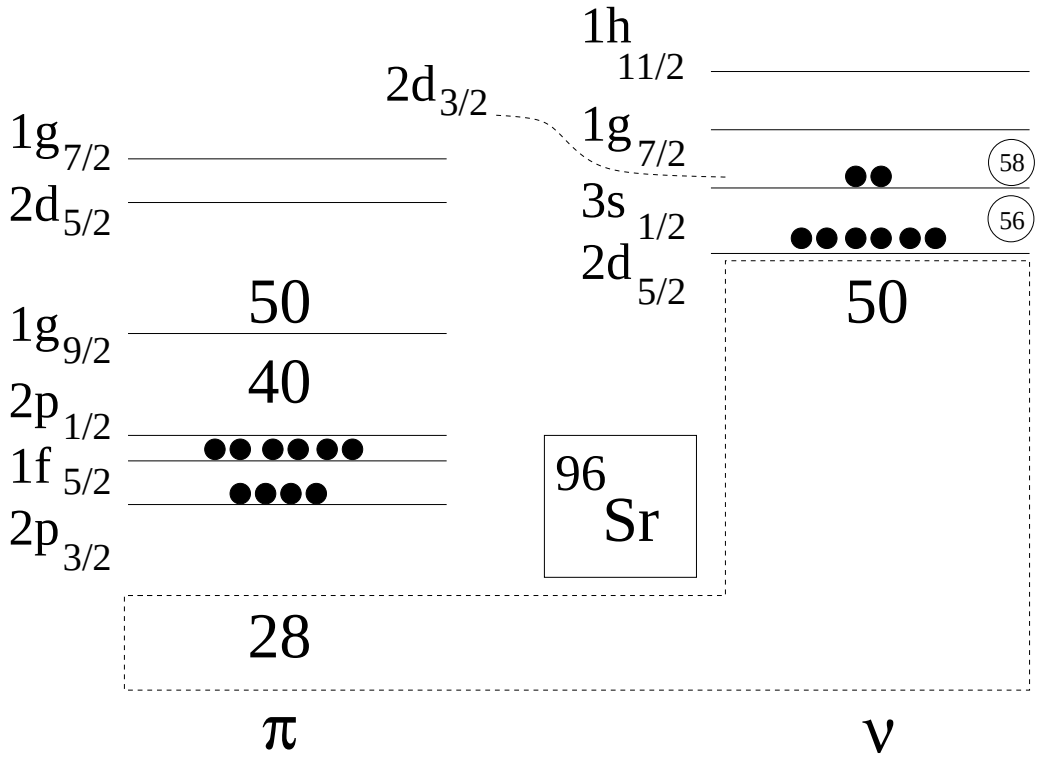

Figure 2.9: Shells involved in the mass A=100 region in the spherical shell model. The position of the $2d_{3/2}$, presented with a dashed line is adopted from the calculations in [58]. The orbitals energy spacing is arbitrary. The microscopical configuration of the spherical ground state of ^{96}Sr is shown.

Even neutron number

For even neutron number, the systematics is shown for ytrium (Z=39). Using spherical Nilsson orbits, the single proton occupies the $2p_{1/2}$ orbit as proven by the confirmed $J^\pi = 1/2^-$ ground state assignment up to neutron number N=58. The onset of deformation is triggered by proton-particle hole excitation across Z=40. The confirmed $J^\pi = 5/2^+$ ground state for $^{99,101}Y$ involves either a single proton into $2d_{5/2}$ lying above the $g_{9/2}$ orbits or a strongly coupled deformed even-even

core and a single proton into the [422]$5/2^+$ Nilsson orbital (prolate deformed $1g_{9/2}$). This second configuration is favoured from both the laser spectroscopy [74] and in-beam γ-rays spectroscopy [75, 76, 77] with a deformation $\beta \simeq 0.4$.

In spherical ytrium isotopes, very long lived isomers have been observed. From laser spectroscopy, a spin/assignment $J^\pi = 9/2^+$ was deduced together with a large spectroscopic quadrupole moment indicating a large *oblate* deformation [70]. This is compatible with a single proton excited into the [404]$9/2^+$ Nilsson orbital (oblate deformed $1g_{9/2}$). In the deformed configuration, one can expect a large fragmentation of the neutron occupancy in the $1\nu g_{7/2}$ and $1\nu h_{11/2}$ orbits.

Beyond N=60, the ground states are highly deformed and no isomeric state has been reported so far.

Even proton number

For even proton number, the systematics is shown for strontium (Z=38) and zirconium (Z=40). In figure 2.8, both at N=57 and N=59, Sr have a confirmed $J^\pi = 1/2^+$ ground state. This spin assignment in the supposed spherical ^{97}Zr and ^{95}Sr (N=57) ground state and is compatible with a single neutron in the $3s_{1/2}$ spherical Nilsson orbit. This assumption is supported by the local maximum of the 2_1^+ excitation energy in ^{96,98}Zr in figure 2.1 corresponding to two neutrons filling the $3s_{1/2}$ spherical Nilsson orbit. With one neutron more in ^{97}Sr (N=59), this spin/parity assignment to $J^\pi = 1/2^+$ is surprising. At N=59, the $3s_{1/2}$ is full and the $\nu 1g_{7/2}$ starts to be filled with one neutron in the conventional spherical Nilsson orbit. In a spherical framework, the $3s_{1/2}$ orbit is the only available low energy J=1/2 level for N=59 nucleus. As mentioned earlier from the proposed $\mathcal{Q}_s$ systematics, the N=59 appears as a transitional region and could present a certain level of deformation. According to MCSM calculations [58], in Zr isotopes, the neutron $2d_{3/2}$ orbit is placed between the $3s_{1/2}$ and the $1g_{7/2}$ and could provide a $J^\pi = 1/2^+$ spin/parity when deformed (1/2[400]). Therefore, the possible weakly deformed ground state at N=59 must be based on a mixture of weakly deformed $s_{1/2}$, $d_{5/2}$, $d_{3/2}$ and $g_{7/2}$ neutron orbits which differ from the large deformation of the ground state beyond N=60.

Isomeric states have drawn a particular attention below N=60 as possible candiate for shape isomers [78, 79, 70]. Long-lived $9/2^{+m}$ states have been identified in several odd Sr and Zr isoropes but unfortunately no spectroscopic quadrupole moment were measured so far. However, rotational bands have been clearly established supporting the deformed character, and therefore shape coexistence, in these isotopes. It is proposed in [79] that the $9/2^{+m}$ isomeric state involves a neutron excitation from the deformed 9/2[404] ($g_{9/2}$)orbit from the ^{78}Ni core into the deformed 3/2[541] ($h_{11/2}$).

In the deformed Nilsson diagram for excited configurations, at N = 59, the odd neutron can be placed either on the 3/2[541] ($h_{11/2}$) orbital, making a $3/2^-$ rotational band, or the 3/2[411] ($g_{7/2}$) orbital, making a $3/2^+$ rotational band. The deformation is larger than at N = 58 but the 9/2[404]($g_{9/2}$) orbital still limits the deformation. The deformed $3/2^+$ and $3/2^-$ excited band heads have been observed experimentally (not shown in the figure, see [78]) and are based on the single neutron occupancy of these deformed orbits.

In the deformed region, at N=61 and 63, laser spectroscopy have established the deformed (prolate) character of ^{101}Zr and ^{101}Sr ground states. Tentative spins and parities are $(3/2^+)$ and $(5/2^-)$ respectively. At N = 61 the situation is analogous to that at N = 59. Two additional deformed bands with the single neutron in the 3/2[411] ($g_{7/2}$) and 5/2[532] ($h_{11/2}$) orbitals are observed. It is worth mentioning that the $9/2^{+m}$ K-isomer rotational band (similar to N=59) still exists at N=61 in the deformed ^{101}Zr. It means that it is not the configuration based on the $\nu 9/2[404]$ excitation which becomes the ground state at N=60. In other words, the deformed ground state beyond N=60 does not involve, from the experimental point of view, an excitation from the ^{78}Ni core. As described later in the section 2.5.2, Monte Carlo Shell Model Calculations lead to the same conclusion and do not involve any neutrons excitation from the ^{78}Ni core to reproduce the large deformation beyond N=60.

2.4.2 Transition probabilities overview

Numerous γ-rays experimental data set exist probing the onset of deformation, from level schemes to B(E2) values by lifetime measurement, which give more indirect proof of the *shape* and microscopical configurations compared to Coulomb excitation experiments. A list of recent relevant works in the last 5 years in which I have been involved is listed below in addition to the Coulomb excitation data presented before.

- B(E2;$2_1^+ \rightarrow 0_1^+$) value in ^{90}Kr [80].
- Abrupt shape transition at neutron number N=60: B(E2) values in ^{94,96,98}Sr from fast γ timing, [81].
- Evolution of nuclear shapes in odd-mass yttrium and niobium isotopes from lifetime measurements following fission reactions, [77].
- Experimental study of the lifetime and phase transition in neutron-rich ^{98,100,102}Zr, [82].
- Evidence for coexisting shapes through lifetime measurements in ^{98}Zr, [8]

As a result, the B(E2;$2_1^+ \rightarrow 0_1^+$) systematics is now completed from N=50 to N=60, ie covering from the neutron shell closure to the shape transition, for Zr, Sr and Kr isotopes. The systematics is presented in figure 2.10 where the B(E2) in W.u. are normalized by the mass A for each isotopes. This representation first proposed by R. F. Casten and N. V. Zamfir [83] illustrates the amount of nucleons participating to the collectivity. If the ratio equals unity, it illustrates that all nucleons participate to the collective behaviour. In a nearly spherical nucleus, this ratio should be close to 0 whereas in highly collective nucleus it should approach 1. In the case of the Sr/Zr isotopes, the onset of collectivity follows the two extremes. Below N=60, the ratio is very close to 0. For ^{96,98}Zr, the local maximum of the 2_1^+ excitation energy (see figure 2.1), reflecting the $\nu s_{1/2}$ occupancy, corresponds to a local minimum in figure 2.10. From N=60, the ratio saturates where all nucleons participate to the collective behaviour suggesting an almost *perfect* rigid rotor.

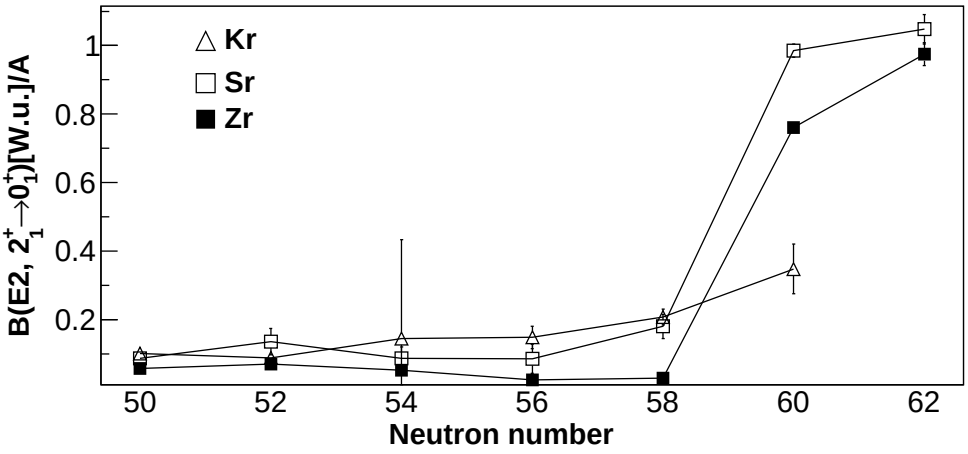

Figure 2.10: Systematics of the B(E2;$2_1^+ \rightarrow 0_1^+$) in W.u. normalized by the mass A as a function of the neutron number for Kr, Sr and Zr isotopes.

2.4.3 Rotational band and configuration mixing

From the collective model of A. Bohr and B. R. Mottelson, in a rotational band, the spectroscopic quadrupole moment, ie the intrinsic moment of the 2_1^+ state, equals the transitional quadrupole moment that one can convert from the B(E2;$2_1^+ \rightarrow 0_1^+$) as follow :

$$\mathcal{Q}_s(I,K) = \frac{3K^2 - I(I+1)}{(I+1)(2I+3)} \cdot \mathcal{Q}_0$$

where $\mathcal{Q}_0$ is the intrinsic quadrupole moment of the I state (ie in the nucleus frame) and $\mathcal{Q}_s$ is the spectroscopic quadrupole moment (ie in the laboratory frame). I is the angular momentum with its projection K. In the rotational model

$$B(E2;(I_i,K) \rightarrow (I_f,K)) = (5/16\pi) \cdot \mathcal{Q}_0^2 \cdot (I_i K 20 | I_f K)^2$$

.

For an even-even rotational nucleus and for its first 2^+, $I = 2$, $K = 0$, the rotor model gives :

$$\mathcal{Q}_s(2,0) = -(2/7) \cdot \mathcal{Q}_0$$

.

Simplifying by $\mathcal{Q}_0$, the asymptote limit is

$$\frac{\mathcal{Q}_s(2,0)}{\sqrt{B(E2;(0,0) \rightarrow (2,0))}} = -0.906$$

In [84], a global survey of the 2_1^+ states collectivity is proposed using a quantity, R_{QB}, defined as :

$$R_{QB} = -\frac{\mathcal{Q}_s(2_1^+)}{\sqrt{B(E2; 0_1^+ \rightarrow 2_1^+)}}$$

In rare-earth elements, known to be excellent rotor, the $E_x(4_1^+)/E_x(2_1^+)$ ratio saturates at 10/3 [83] with the R_{QB} ratio nearly equal to unity. The $E_x(4_1^+)/E_x(2_1^+)$ ratio equals 1.2 (3.0) in ^{96}Sr (^{98}Sr) respectively. The B(E2;$2_1^+ \rightarrow 0_1^+$)/A ratio yields a value of 0.18 (0.98) in ^{96}Sr (^{98}Sr) respectively. This indicates that ^{96}Sr behaves as a spherical vibrator and ^{98}Sr as an almost perfect rotor. From our Coulomb excitation data, spectroscopic quadrupole moments for the 2_1^+ state in ^{96,98}Sr were measured at -22(30) efm^2 and -52(24) efm^2 respectively. The accurate value of the B(E2), leads to $R_{QB}(^{96}Sr) = 0.46(70)$ and $R_{QB}(^{98}Sr) = 0.45(28)$. The large error bars on the experimental $\mathcal{Q}_s$ do not allow drawing final conclusion for ^{96}Sr. However, within the experimental error bars, the value for ^{98}Sr is found far from what one expect for a good rotational nucleus.

As mentioned earlier [10, 68, 11], using the full set of E2 matrix elements, the two-level mixing model was applied in ^{98}Sr. A mixing angle of 0.87(1) was extracted for the 0_1^+ state wave function while the 2^+ states have almost no mixing. *Unperturbated* matrix elements can be extracted from which an *unperturbated* intrinsic quadrupole moment for the band can be deduced, later translated in the laboratory frame. The *unperturbated* matrix elements equals -1.45(2) eb (to be compared to the measured -0.63($^{+0.32}_{-0.28}$) eb for the 2_1^+ state). This leads to an *unperturbated* $\mathcal{Q}_s^{un}$ = -110(3) efm^2. Using $\mathcal{Q}_s^{un}$ in the R_{QB} equation leads to $R_{QB}^{un}(^{98}Sr) = 0.96(2)$, ie in the rotational limit. As a summary, the weak mixing of the 0^+ states wave functions does not influence significantly the rotational behaviour of the excitation energies and B(E2).However, the measured spectroscopic quadrupole moment for the 2_1^+ state shows a clear perturbation from its rotational behaviour. Using the two-levels mixing model, the *unperturbated* moment fits well the rotational behaviour. One must underline that $\mathcal{Q}_s^{un}$ doesn't involve the measured $\mathcal{Q}_s(2_1^+)$ (see [9] for the details). An approximate experimental $\mathcal{Q}_s^{un}$ can be estimated from the average measured $\langle\mathcal{Q}_s^{un}\rangle$ in the 4^+, 6^+ and 8^+ states and equals to -1.6(3) eb [11]. In that case, $R_{QB}^{\langle\mathcal{Q}_s\rangle}(^{98}Sr) = 1.4(5)$, in agreement with the previous observations. As a results, the presented study for ^{98}Sr shows the influence of the mixing in the shape coexistence and how it can be taken into account in collective nuclei. However, the spectroscopic quadrupole moment of the 2_1^+ state is not discussed here and not used in the present R_{QB} calculations. Its value is found smaller than the $\mathcal{Q}_s^{un}$ calculated from mixing model and the average value at higher spins. The difference could be attributed to the mixing of the wave functions. However, from the mixing model, it is found negligible. Therefore, the low value is not attributed to the mixing but to a certain level of triaxility as deduced from the sum rules.

2.4.4 Particle-Core coupling scheme

In the deformed region, one can also underline that lifetime measurements in odd-proton and even-neutron [77] illustrate very well the particle+rotor model (so-called strong coupling between a deformed even-even core and a single particle) [85]. In ^{99}Y, the ground state spin/parity is $5/2^+$. In the particle+rotor model, the ground state can be seen as $5/2^+ = \pi[422]5/2^+ \otimes 0^+(^{98}Sr)$. The proposed $9/2^+$ state at 284 keV in ^{99}Y can be part of the multiplet of the $\pi[422]5/2^+ \otimes 2^+(^{98}Sr)$ configuration. The B(E2; $2^+ \rightarrow 0^+$) established at 0.259(8) e^2b^2 in ^{98}Sr [10] is compatible with the measured B(E2; $9/2^+ \rightarrow 5/2^+$) = 0.25(2)e^2b^2 in ^{99}Y by [77], supporting very well the particle+rotor model.

At N=58, in spherical ^{96}Sr, the 2^+ state excitation energy is 815 keV with a B(E2; $2^+ \rightarrow 0^+$) = 0.045(10) e^2b^2. In the weak coupling scheme, ^{97}Y should present a multiplet of states $(1/2^-)\otimes 2^+(^{96}Sr) = (5/2^-, 3/2^-)$ with a barycentre equal to the excitation energy of the 2^+ state in ^{96}Sr and similar B(E2) to the ground state. A state at 953 keV with proposed spin/parity assignment $(5/2^-, 3/2^-)$ and a lifetime $T_{1/2} \leq 4$ ps is suggested. A more accurate measurement of this lifetime would confirm the spin/parity assignment of the ground state and the weak coupling scheme. In lighter isotopes at N=56, the 2^+ state excitation energy in ^{94}Sr is 837 keV with a corresponding B(E2) = 0.020(8) e^2b^2. In ^{95}Y, two states with confirmed spin/parity at 827 keV $(5/2^-)$ and 685 keV $(3/2^-)$ are the obvious candidates for the $(1/2^-)\otimes 2^+(^{94}Sr)$ multiplet. Unfortunately, the corresponding B(E2) are not measured. If such measurements could confirm the weak coupling scheme, it would bring further indications that the Z=40 is a robust su-shell closure. Indeed such weak-coupling states have been established around large proton shell gap at Z=28, Z=50 and Z=82.

2.4.5 Experimental multi-messenger approach: the ^{96}Sr case

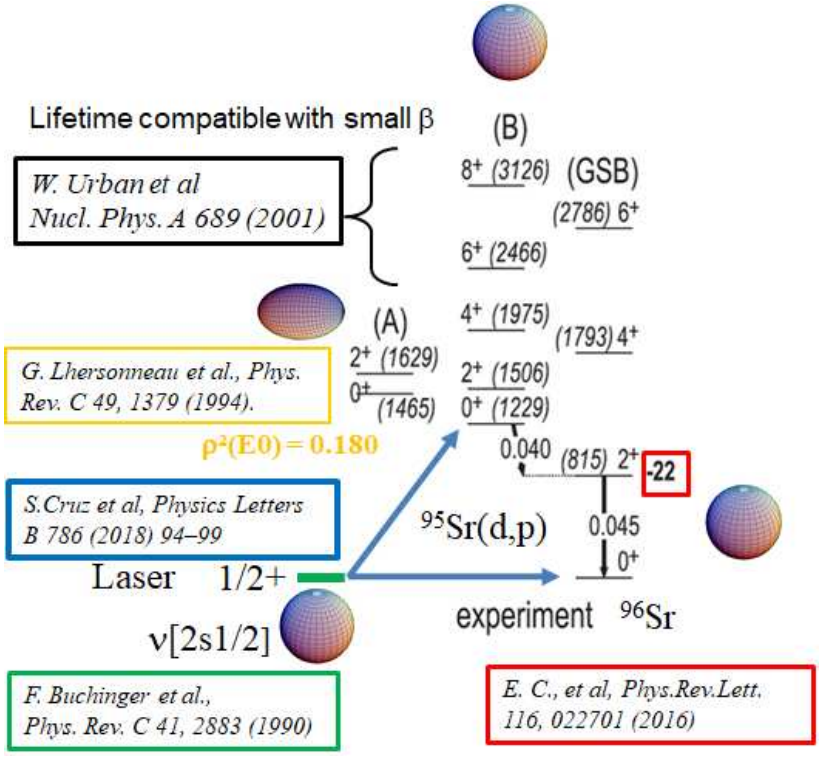

Figure 2.11: Multi-messenger studies of the shape coexistence in ^{96}Sr

Figure 2.11 shows the compilation of several experimental data set for ^{96}Sr. The low spectroscopic quadrupole moment of the 2_1^+ state and relatively large B(E2) indicate its vibrational nature

around a weak deformation [10]. As already mentioned, two 0^+ excited states have been observed at 1229 and 1465 keV. E0 spectroscopy was performed and deduced one of the highest $\rho^2(E0)$ value between the 0_2^+ and 0_3^+ states, indicating a very large difference in deformation and/or large mixing of the wave functions [24]. The E0 branch to the ground state was never established. The 2_2^+ and 2_3^+ states are very close in energy to the 0_2^+ and 0_3^+ states respectively, suggesting a rotational band. The second 4^+, 6^+ and 8^+ states develop a rotational band but it is very unclear to which band head it belongs. The lifetime of the second 6^+ and 8^+ states was measured and suggest a rather weak deformation [78]. The ^{95}Sr ground state is a $1/2^+$ state compatible with the spherical Nilsson orbit $\nu[s1/2]$ [86]. Unfortunately, its spectroscopic quadrupole moment was not measured. The neutron transfer reaction ^{95}Sr(d,p)^{96}Sr was recently performed [13, 87], which favours spherical component of the populated states are favoured in ^{96}Sr. It turned out that the ground state is relatively weakly populated as the main spherical strenght is found in the low lying 0^+ states, suggesting a rather weak deformation of the ground state (compatible with the spectroscopic quadrupole moment extracted from the Coulomb excitation) and a nearly spherical 0_2^+ state which however presents a large mixing with the deformed 0_3^+ state [13, 87]. From the E0 spectroscopy and the large $\rho^2(E0)(0_3^+ \rightarrow 0_2^+)$, the 0_3^+ becomes a natural candidate for the band head of the deformed configuration that becomes the ground state in ^{98}Sr. Such measurement was not performed from ^{97}Zr to ^{98}Zr having also two excited 0^+ states. One could assume a similar scenario and draw a direct comparison between the $0_{1,2,3}^+$ states in ^{96}Sr and ^{98}Zr.

However, different conclusions were drawn in the N=58 ^{98}Zr by [8]. In this work, the B(E2) values in ^{98} Zr have been measured and compared to MCSM calculations. The calculations propose the coexistence of three different structures at low spin: a nearly spherical ground state (0_1^+), a deformed excited 0_2^+ state, and a well-deformed (band-like) structure possibly based on the 0_3^+ state. The calculated proton and neutron occupancies are very similar in both 0_2^+ and 0_3^+ deformed states. Only small differences in the neutron occupancies make the change in deformation. The ^{95}Sr(d,p)^{96}Sr transfer reaction cross sections propose instead nearly spherical 0_1^+ and 0_2^+ states with a well-deformed 0_3^+ state. The angular distributions treated as a single-step process to the 0_2^+ is best fitted for a $l = 0$ angular momentum transfer, thus neutron populating the $\nu 2s_{1/2}$ orbital. According to the previous discussions, a deformed configuration would involve a $l = 2$ ($d_{3/2}$), or $l = 4$ ($g_{7/2}$) or $l = 5$ ($h_{11/2}$) angular momentum transfer. The microscopical configuration of the $0_{2,3}^+$ state at N=58 remains therefore puzzling.

2.5 Theoretical calculations for ^{96,98}Sr

2.5.1 Mean field approach

The sharp transition and magnitude of the deformation at A$\sim$100 remain a challenge for theories. Similarly to the experimental effort, numerous theoretical works have been published (more than 100 theoretical papers since the 70's) on the subject. All nuclear models have been used to reproduce this onset of deformation such as the HFB + the generator coordinate method (GCM), the macroscopic-microscopic method, the shell model, the Monte Carlo shell model, the interacting boson model (IBM) approximation, the VAMPIR model and covariant density functional (DF) theory (PC-PK1). The global comparison of all the models is out of the scope of the present discussion.

In the following, the state-of-the-art of mean-field calculations using the Gogny D1S interaction with GCM-GOA and Monte Carlo Shell Model Calculations will be briefly discussed.

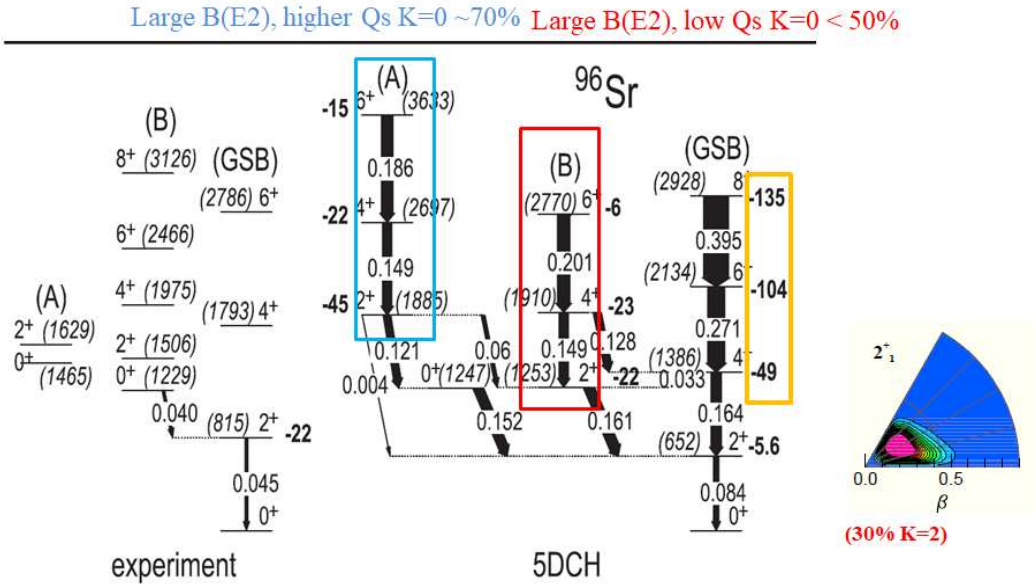

Figure 2.12: Comparison between the experimental and calculated level scheme of ^{96}Sr using the Gogny D1S interaction. The excitation energies are mentioned in brackets. The arrows are proportional to the B(E2) indicated in e^2b^2. The measured and calculated spectroscopic quadrupole moments are given in efm^2 next to each state.

We compared the set of E2 matrix elements with calculations using the Gogny D1S interaction with GCM-GOA. The comparison is presented in [10, 68, 11]. Bands assignment in calculated states is not obvious. We developed a graphical method detailed in [11] to construct theoretical bands. In figure 2.12, the calculated level scheme is compared to the experimental one for ^{96}Sr. As discussed in [10, 11], the Gogny calculations over estimate the collectivity at N=58 and under estimate the deformation at N=60. The calculated ground state band differs from the experimental ones in B(E2) and predict a very fast increase of the $\mathcal{Q}_s$ as a function of spin with a significant contribution of K=2 (30%) for the 2_1^+ state leading to this low $\mathcal{Q}_s$. This is impossible to verify today. The calculations do not predict two 0^+ excited states in contrast to the experimental situation. The (B) band presents large B(E2) associated to low $\mathcal{Q}_s$ with only 50% of K=0 underlying the triaxial character of the state. In the (A) band, large B(E2)'s are associated to large $\mathcal{Q}_s$ with a large contribution of K=0.

Figure 2.13 shows the comparison between the Gogny calculations and the VAMPIR approach [88]. The VAMPIR B(E2) are mentioned in red. The agreement is surprisingly good in spite of the very different approaches used in the calculations.

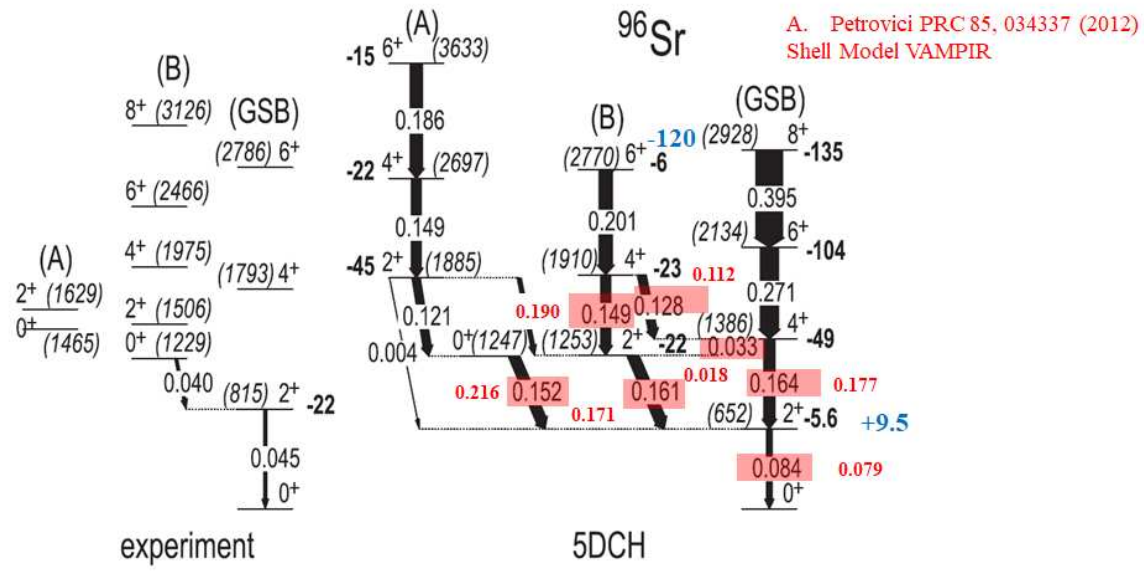

Figure 2.13: Comparison between the experimental and calculated level scheme of ^{96}Sr using the Gogny D1S interaction and the VAMPIR approach

In figure 2.14, the calculated level scheme is compared to the experimental one for ^{98}Sr using the Gogny interaction. In both cases, the ground state band has a large prolate deformation. It is worth mentioning that in spite of the differences in absolute values, the Gogny calculations predict a drop of the $\mathcal{Q}_s$ between the 4_1^+ and the 2_1^+ states as observed experimentally. A K=2 γ-band is predicted very close to the ground state band but not yet observed experimentally. The nearly spherical configuration is assigned as the (A) band based on the similarities in the B(E2) connecting to the ground state band.

A summary of the experimental ρ^2(E0) transition with the calculated ones using Gogny D1S, Excited VAMPIR and 5DCH (PC-PK1) in table 2.2. It must be underlined that discrepancies are huge and prediction not always calculated for all transitions making the comparison difficult.

2.5.2 Shell model approach

In the Sr and Zr isotopic chains, the spherical-to-deformed transition takes place when going from 58 to 60 neutrons, thus when the $\nu g_{7/2}$ orbital is being filled. Shell model calculations were performed for the Zr isotopic chain in an extended model space [89, 5, 58, 8] and pointed to the $\pi - \nu$ interaction between the spin-orbit partners $\pi 0g_{9/2}$ and $\nu 0g_{7/2}$ as the main mechanism for the shape change: as the $\nu 0g_{7/2}$ orbital is being filled, the Z=40 sub-shell gap between the $\pi 0f_{5/2}$ and $\pi 0g_{9/2}$ effective single-particle energies (ESPE) is reduced, giving rise to multiple particle-hole excitations

Table 2.2: Monopole transition strengths $\rho^2(E0)$ between 0^+ states. Experimental results are compared with those calculated within the beyond-mean-field approach with a five-dimensional collective Hamiltonian and the Gogny D1S force (present study) and using the complex excited VAMPIR approach [88].

		experiment ^{96}Sr	5DCH (Gogny)	Excited VAMPIR
			$\rho^2(E0)$ $(\cdot\ 10^3)$	
0_2^+	0_1^+	.	106	66
0_3^+	0_1^+	.	22	
0_3^+	0_2^+	185(50)[24]	95	9
		experiment ^{98}Sr		5DCH (PC-PK1)
0_2^+	0_1^+	53(5)[67]	179	117
0_3^+	0_1^+	.	40	
0_3^+	0_2^+	.	75	

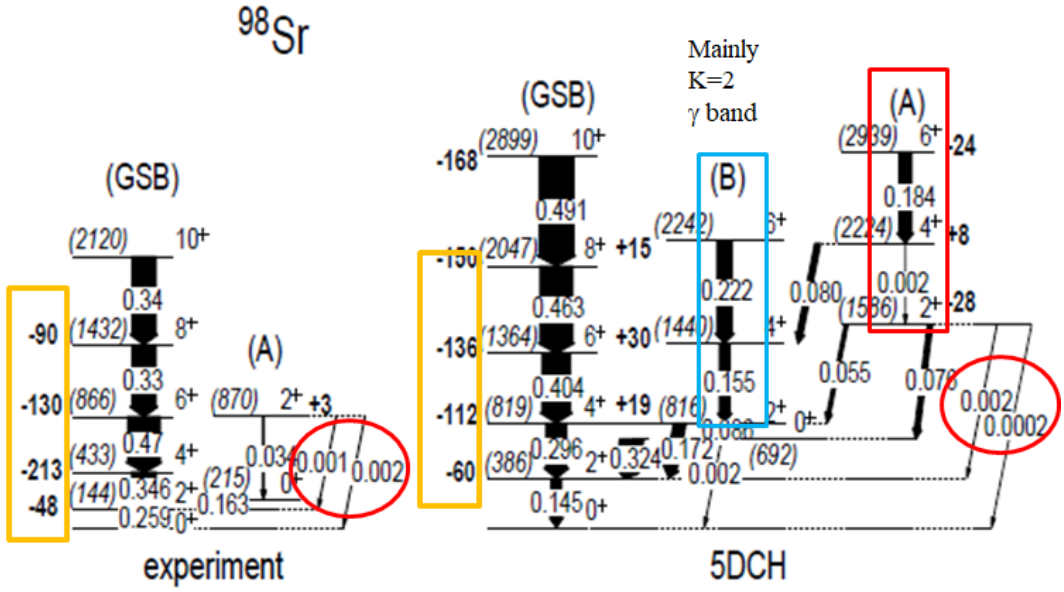

Figure 2.14: Comparison between the experimental and calculated level scheme of ^{98}Sr using the Gogny D1S interaction

across the gap. The most recent calculations [5, 58, 8] using MCSMC show a spectacular agreement with the experimental data in even-even nuclei and become the reference in the mass region. In the calculations [90, 8], the 0_2^+ and 0_3^+ below N=60 result from 2p-2h proton excitations (with a possible 4p-4h contribution) from the pf-shell into the $\pi 0g_{9/2}$ orbital. On the neutron side, the $\nu g_{9/2}$ remains fully filled, ie without excitation from the ^{78}Ni core. The deformed configurations in even-even excited 0^+ does not involve neutron excitation from the N=50 closed shell. This might explain why $(9/2^{+m})$ deformed states still remains beyond N=60 in odd-neutron Sr/Zr isotopes as excited configurations. In the deformed configuration, neutrons are well distributed from the $d_{5/2}$ into the $s_{1/2}$,$d_{3/2}$ and more significantly into the $g_{7/2}$ and $h_{11/2}$ as deduced from the previous studies of odd neutron isotopes. A similar mechanism is known to be responsible for the rapid onset of deformation and shape coexistence in neutron-rich isotopes around N= 8, 20, 28 and 40, with different spin-orbit partners [91, 92, 1, 93, 94].

2.6 Conclusions

For the future, several systematics are needed :

- ^{98}Sr remains a unique case in term of experimental data. More are needed in particular in the N=58 and N=59 to understand the shape evolution along the yrast bands and excited deformed configuration.

- Coulomb excitation of ^{96}Sr, Zr and Kr isotopes are mandatory to determine the shape of the different configuration.
- Following the exploratory work on the ^{95}Sr(d,p) reaction, single and double nucleon transfer experiment are needed to probe both the proton and neutron microscopic configuration.
- The N=59 isotonic line deserves a particular interest in laser and direct nucleon transfer experiment.
- In the spherical isotopes, the weak coupling scheme was not yet studied in details.
- The differences in structure and deformation of the 0_2^+ and 0_3^+ below N=60 in even-even Sr and Zr isotopes must be clarified.
- Laser spectroscopy of long lived isomeric state from N=50 to N=60 must be pursued as well as for ground state beyond N=60.
- In the global survey of the spectroscopic quadrupole moment, the safe Coulomb excitation of ^{102}Mo will make the bridge between the island of large deformation and the triaxial shape region
- Regarding the very large amount of experimental data in the mass region, holistic comparison in theoretical work must be encouraged.

Partie III

Shape coexistence in the neutron rich Ni isotopes

Chapter 3

Shape coexistence at N=40 and Z=28

3.1 Introduction

In isotopes with Z<28 and N=40, a new region of deformation was identified and characterized in the recent years. When removing only two protons from ^{68}Ni to ^{66}Fe, first excited states and reduced transition probabilities have indicated an onset of collectivity. This mass region presents a difference with the two other cases presented in the manuscript. The Z=28 shell closure is a strong shell closure as revealed by the doubly magic character of ^{56}Ni [95] and ^{78}Ni [96, 17] by opposition to the Z=40 sub-shell closure. The corresponding large proton gap implies that, in the scheme of the π particle-hole excitation as standard mechanism leading to shape coexistence, it must involve a substantial gain in $\pi - \nu$ quadrupole correlation energy. Along the Ni isotopic chain, neutrons are added to the $\nu g_{9/2}$ orbital from ^{69}Ni to the doubly magic ^{78}Ni. The experimental level schemes for the yrast band in even-even nuclei show a 8^+ isomeric state arising from the alignment of a broken neutron pair as an example of seniority $\nu = 2$ scheme. The resulting multiplet should be pure neutron states, ie with very low E2 probabilities. In ^{70}Ni, the 8^+ and 6^+ states present such character as the enhanced B(E2) for the 2^+ state was interpreted as an indication that the Z=28 proton shell gap, *near* ^{68}Ni, is relatively weak leading to core polarization [97, 98, 99]. From the B(E2) measurements in Ni, it was proposed that the spin-orbit splitting $\pi f_{7/2} - f_{5/2}$ is reduced when filling the $\nu g_{9/2}$ orbital through the tensor term of the nuclear interaction favouring the development of collectivity and possibly shape coexistence. Already in the 80's, M. Girod et al [100] predicted a low lying deformed 0^{+m} state in ^{68}Ni as a first prediction of shape coexistence at N=40. Deformed states below N=40 would therefore involved the $\nu g_{9/2}$ as intruder orbit.

^{68}Ni is therefore cornerstone of the mass region. The proton shell gap is closed at Z=28 by the $f_{7/2}$ orbits and the next shells are the $p_{3/2}$, $f_{5/2}$ and $p_{1/2}$. On the neutron side, the N=40 gap is defined between the $p_{1/2}$ and the $g_{9/2}$, $d_{3/2}$ orbitals. Experimentally, at N=40, the mass measurements do not show an increase of binding energy [101]. However, ^{68}Ni mimics the characteristics of a doubly magic nucleus with a first 2^+ state at 2 MeV excitation energy, a minimum of the B(E2,

$0^+ \rightarrow 2^+$) and a first excited state being a 0^+ state. Following the scheme of shape coexistence driven by a π p-h excitation, deformed states would consist in promoting a proton from the $f_{7/2}$ to the $p_{3/2}$, $f_{5/2}$ or $p_{1/2}$ orbitals coupled to a $high - j$ neutron intruder orbits (in the present case the $g_{9/2}$). The later should coexist with spherical configuration and even become the ground state when proton are continuously removed from the $\pi f_{7/2}$ orbit. In ^{67}Co, a β-decay isomer was discovered and interpreted as a π(1p-2h) excitation across Z=28 and shape isomer [102]. Using the energy of the intruder π(2p-1h) state in ^{69}Cu and, symmetrically, the π(1p-2h)state in ^{67}Co, which both lie at N=40, D. Pauwels *et al.* have been able to predict a deformed π(2p-2h) state in ^{68}Ni. The predicted energy from this analysis leads to a rather low value of 2.2 MeV excitation energy, which can be understood only with an important gain in binding energy from the $\pi - \nu$ residual interactions between the two proton holes and the active valence neutrons across N=40 [3]. The shape coexistence in ^{68}Ni has been investigated by the observation of low lying 0^+ state as a candidate for the deformed proton configuration.

The systematics of the 2^+ excitation energy of Fe isotopes doesn't show any local maximum at N=40 but a continuous decrease from N=36 to N=58, as an indication of collectivity and therefore deformation. In comparison with N=28, this onset of collectivity occurs closer to the proton shell closure (see figure 3.1). As Ar and S isotopes show a local maximum at N=28, already 2 protons from ^{68}Ni, no increase of the excitation energy is observed. In Co isotopes, similarly to Cu and Zn in which coexist single particle, collective and core-coupled states [103, 104], are states that would be naturally expected in odd-A masses based on the coupling of the single proton hole in the $f_{7/2}$ with even-even cores states. The corresponding multiplet is composed of the $f_{7/2} \otimes 2^+ = (3/2^-, 9/2^-, 11/2^-)$ states.

The systematics of excitation energies and B(E2) values in the Fe, Co and Ni isotopes show that the $9/2^-_1$(Co) and 2^+_1(Ni) excitation energies as well as those of the $3/2^-_1$(Co) and 2^+_1(Fe) states behave similarly. It is therefore tempting to interpret the $9/2^-_1$ state as a proton hole coupled to 2^+_1(Ni) [105] and the $3/2^-_1$ state as a proton particle coupled to the deformed 2^+_1(Fe). The $11/2^-$ states have been recently established and not shown in the figure. Weakly deformed excited states must have all the characteristics of a spherical core-coupled states (weak coupling scheme). The barycentre of the multiplet should equal the 2^+ energy of the even-even Ni core and the B(E2) to the ground state. Deformed states should follow the strong coupling scheme where the intruder neutron orbit $\nu g_{9/2}$ is coupled to the rotational band of the even-even Fe core. The deformed configuration in odd-Co should present a $(2^+ \otimes g_{9/2}) = 11/2^+$, $(4^+ \otimes g_{9/2}) = 13/2^+$ etc ... sequence similar to the 2^+, 4^+ etc ... rotational band in the even-even Fe core. The low energy excited states $9/2^-$, $11/2^-$ and $3/2^-$ states have been identified in ^{63,65,67}Co. In the present study, the core-coupled scheme was tested by the systematic lifetime measurements of relevant excited states leading to reduced transition probabilities and compared to large scale shell model calculations.

3.2 Lifetime measurement and transition probabilities around N=40

The onset of collectivity in the mass region was probed by the measurement of the reduced transition probabilities (B(E2) and B(M1)) from lifetime measurements using the plunger technique. A series of experiments were conducted at the GANIL facility using the EXOGAM and AGATA

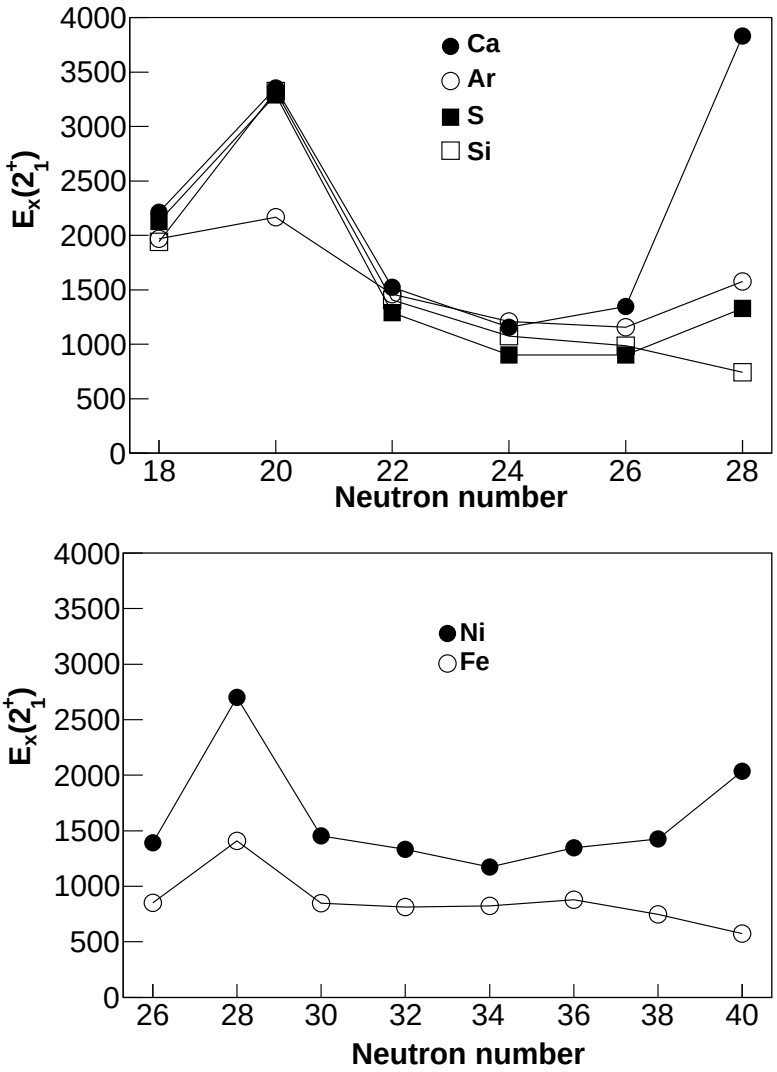

Figure 3.1: Top panel: Systematics of the experimental energies in the even-N Ca, Ar, S and Si isotopes. Bottom panel: Systematics of the experimental energies in the even-N Fe and Ni isotopes.

HPGe arrays, the VAMOS magnetic spectrometer and a plunger device to measure lifetime of excited states in neutron rich Fe and Co isotopes produced by multi-nucleon transfer between heavy ions. Lifetime in ^{62,64}Fe 2^+ and 4^+ states have shown that by comparison with shell model calculations, the $\nu g_{9/2}$ occupancy triggers the onset of collectivity at N=40 as the full amplitude is reproduced when the $\nu d_{5/2}$ is included [106, 107]. The core coupled assumption in the $(3/2^-, 9/2^-, 11/2^-)$ states in Co isotopes was tested by the measurement of their B(E2) to the

ground state (tentatively assigned to J^π=$(7/2^-)$ from the single proton hole in the $f_{7/2}$ orbit) and compared to the E2 transition in the corresponding 2^+ state in the even-even core. In the following a review of the measured values in Co is presented and enriched from measured performed in other facilities.

3.2.1 The $3/2^-_1$ state

The $B(\mathrm{E2}; 3/2^-_1 \rightarrow 7/2^-_1)$ value in ^{63}Co and ^{65}Co have been deduced from the lifetime measurement in [108, 109]. The measured value in ^{63}Co is found well below that of $B(\mathrm{E2}; 2^+_1 \rightarrow 0^+_1)$ in Fe. This indicates that the $N = 40$ gap has not completely collapsed at $Z = 27$ or that the $3/2^-_1$ state has in fact a single-particle character. As shown in [106, 107], the onset of collectivity in Fe is clearly established at $N = 38$. If the $3/2^-_1$ state results from the coupling of a proton to the 2^+_1(Fe) state, then the $B(\mathrm{E2}; 3/2^-_1 \rightarrow 7/2^-_1)$ value should rise at $N = 38$, making the measurement of this quantity in ^{65}Co very important. The $3/2^-$ lifetime was recently measured in ^{65}Co [109] with a value τ=5(5) ps leading also to a B(E2) = 17(16) W.u to be compared to 22(2) W.u for the B(E2, $2^+ \rightarrow 0^+$) in ^{64}Fe and 7(1) W.u in ^{66}Ni making the experimental conclusion elusive. It is however presently proposed that it belongs to the $\pi f^{-1}_{7/2} \otimes 2^+$ Ni state multiplet [109].

3.2.2 The $9/2^-_1$ state

The lifetime to the ground state was measured in ^{63,65}Co in [108]. The $9/2^-_1 \rightarrow 7/2^-_1$ transition probability is even more difficult to interpret since the decay occurs by E2 or M1, and the interpretation depends on the assumed multi-polarity. Presently the E2/M1 mixing ratio is not known. Assuming a pure E2 transition, the $B(\mathrm{E2}; 9/2^-_1 \rightarrow 7/2^-_1)$ value extracted for ^{63}Co is compatible with the $B(\mathrm{E2}; 2^+_1 \rightarrow 0^+_1)$ value in ^{64}Ni. It is proposed that it belongs to the $\pi f^{-1}_{7/2} \otimes 2^+$ Ni state multiplet in [108, 109].

3.2.3 The $11/2^-_1$ state

In [110, 107, 109], the lifetime of $11/2^-$ states at 1664 (1674) (1480) keV in ^{61}Co (^{63}Co) (^{65}Co) respectively have been measured and were interpreted also as a $\pi f^{-1}_{7/2} \otimes 2^+$ Ni state based on the deduced transition strength similar to the B(E2,$2^+ \rightarrow 0^+$) in Ni.

3.2.4 The $1/2^-_1$ state

This state plays a major role in the shape coexistence scenario. In [102], D. Pauwels *et al.* reported the observation of a $J^\pi = (1/2^-)$ β isomeric state at 491 keV in ^{67}Co and interpreted as a deformed proton intruder state 1p-2h across the Z=28 shell gap. A $(1/2^-)$ proton state is proposed at 1095 keV in ^{65}Co [105]. The E2/M1 mixing ratio of the transition to the $3/2^-$ state is unknown [109]. Assuming a pure E2 transition to the $3/2^-_1$ state, the deduced B(E2) from its lifetime is found large, B(E2) = 67(1) W.u. On the contrary, a pure M1 multi-polarity leads to low B(M1). It is presently interpreted as a member of the deformed configuration [109]. This deformed state is not populated in multi-nucleon transfer reaction [108, 111].

Table 3.1: Measured lifetime (τ [ps]) in odd-mass Co isotopes.

		A. Dijon [108]	M. Klintefjord [107]	V. Modamio [110]	B. Olaizola [109]
^{63}Co	$(3/2^-)_{995keV}$	15.4(18)			
	$(9/2^-)_{1383keV}$	0.9(4)			
	$(11/2^-)_{1674keV}$		0.55(19)	1.0(3)	
^{65}Co	$(3/2^-)_{882keV}$				5(5)
	$(9/2^-)_{1480keV}$	$\leq$17.3			
	$(11/2^-)_{1480keV}$	$\leq$17.3		1.3(5)	
	$(1/2^-)_{1095keV}$				1803(28)

Table 3.2: Measured B($\lambda\mu$) [W.u.] in odd-mass Co isotopes and even-even Ni isotopes.

		Assuming Pure E2	Assuming Pure M1
N=36			
^{63}Co	$(3/2^-)_{995keV}$	3.7(4)	-
	$(9/2^-)_{1383keV}$	12(5)	0.013(4)
	$(11/2^-)_{1674keV}$	4(1)	-
^{64}Ni	$2^+_{1345.75keV}$	9.04(28)	-
N=38			
^{65}Co	$(3/2^-)_{882keV}$	17(16)	-
	$(9/2^-)_{1480keV}$	*	*
	$(11/2^-)_{1480keV}$	6(2)	-
^{66}Ni	$2^+_{1424.8keV}$	7.6(13)	-
	$(1/2^-)_{1095keV}$	67(1)	$1.83(3) \times 10^{-3}$

3.2.5 Summary of the experimental results

The measured lifetimes are summarized in table 3.1 and deduced transition probabilities in table 3.2. The experiments in [108, 107, 110] correspond to plunger measurements in multi-nucleon transfer reaction using different heavy beams and targets. Even if the range in sensitivity is similar, they differ in populated states making them complementary. The reference [109] is a fast-timing measurement after β-decay populating different states. From these set of measurements, it is concluded that the $(3/2^-)$, $(9/2^-)$ and $(11/2^-)$ states are part of the $\pi f^{-1}_{7/2} \otimes 2^+$ Ni multiplet based on the similarities in excitation energy and corresponding B(E2) to the ground state. This conclusion is supported by comparison with shell model calculations. However, one could argue that the experimental conclusion is overstated regarding the uncertainties highlighted in table 3.2. First, the B(E2) for the $(9/2^-)$ state in ^{63}Co is not determined accurately since the $\delta(E2/M1)$ mixing ratio is not measured. The $(3/2^-)$ in ^{65}Co has 100% error bar and the relatively precise value for the $(3/2^-)$ and $(11/2^-)$ states in ^{63}Co differ significantly from the B(E2) in ^{64}Ni. Finally, only the $(11/2^-)$ state in ^{65}Co fits well the weak coupling scheme. More precise measurements are there-

fore needed to probe experimentally the coupling scheme and track possible deviation from the model to probe the influence of the deformed configurations. Spins and parities must be uniquely determined and $\delta(E2/M1)$ mixing ratio measured. Finally, higher precision lifetime measurements or Coulomb excitation cross-sections are mandatory to extract with smaller error bar the reduced transition probabilities.

The $(1/2^-)$ is interpreted in comparison with shell model calculation as a deformed proton state involving excitation above the Z=28 gap in [109]. There is, today, no unambiguous experimental data supporting the interpretation. Indeed, the long lifetime measured in [109] arises mainly from the low energy E2 transition to the $(3/2^-)$ state and cannot be used as an argument on its structure since the $\delta(E2/M1)$ mixing ratio is not measured. A $(1/2^-)$ is not part of the $\pi f_{7/2}^{-1} \otimes 2^+$ Ni multiplet and in the interpretation of a large deformation, the $(1/2^-)$ spin parity can be related to a single proton excitation to the $p_{3/2}^1$ $(1/2^-[321])$orbit. One could speculate that when neutron are added to the $g_{9/2}$ orbit, this state could become the ground state as a result of the onset of deformation established in the Fe isotopes. The ground state spin and parity beyond N=40 in Co isotopes remain unknown. The possible spin/parity inversion of the ground state from $7/2^- \rightarrow 1/2^-$, as suggested by the excitation energy systematic, is not yet established.

3.2.6 Theoretical calculations

Calculations from [108] are compared with the data in [108]. It is clear that the inclusion of the $1g_{9/2}$ orbital becomes imperative as the neutron number approaches $N = 40$. This conclusion can be drawn by observing that, towards $N = 40$, excitation energies are overestimated in a pf model space and B(E2) values are underestimated. Nevertheless, even with the *pfg* interaction which includes the $1g_{9/2}$ orbital, the excitation energies of the $3/2_1^-$ and $9/2_1^-$ levels are slightly higher and the B(E2) values of the transitions to the ground state are somewhat smaller in ^{67}Co compared to lighter Co isotopes, indicative of some effect of an $N = 40$ sub-shell closure in the calculation. Our measured $B(\mathrm{E2}; 3/2_1^- \rightarrow 7/2_1^-)$ value in ^{63}Co falls well below the value calculated with *pfg*, which indicates that the shell model overestimates the collectivity of the $3/2_1^-$ state. On the other hand, the calculated $B(\mathrm{E2}; 9/2_1^- \rightarrow 7/2_1^-)$ value in ^{63}Co comes out at 11.1 W.u, in excellent agreement with the experimental value of 11.4 (55) W.u, obtained under the assumption of pure E2. However, although the E2 rate is well reproduced by the shell model, it fails to obtain the correct B(M1) value for this transition. This can be inferred from the lifetime of the $9/2_1^-$ level which is calculated a factor 10 shorter than the measured value of 0.9 (4) ps due to a large calculated $B(\mathrm{M1}; 9/2_1^- \rightarrow 7/2_1^-)$ value of 0.36 W.u, obtained with bare nucleon g factors. This result is not significantly altered if the spin g factors are quenched by a factor 0.7.

To what extent are the simple interpretations, mentioned in the introduction, of a $1\pi f_{7/2}$ particle coupled to a 0_1^+ or 2_1^+ in Fe or a $(1\pi f_{7/2})^{-1}$ hole coupled to a 0_1^+ or 2_1^+ in Ni, borne out by the shell-model calculations? This can be illustrated with the example of the $7/2_1^-$ and $9/2_1^-$ states.

The most important components of these states are

$$\begin{aligned} |7/2_1^-\rangle &\approx 0.62|(1\pi f_{7/2})^{-1} \otimes 0_1^+(\mathrm{Ni}); 7/2\rangle \\ &\pm 0.38|(1\pi f_{7/2})^{-1} \otimes 2_1^+(\mathrm{Ni}); 7/2\rangle + \cdots , \\ |9/2_1^-\rangle &\approx 0.62|(1\pi f_{7/2})^{-1} \otimes 2_1^+(\mathrm{Ni}); 9/2\rangle \\ &\pm 0.31|(1\pi f_{7/2})^{-1} \otimes 4_1^+(\mathrm{Ni}); 9/2\rangle + \cdots . \end{aligned} \tag{3.1}$$

These components represent barely 50% of the total. There is thus considerable fragmentation of the wave function in the shell model and, accordingly, the simple interpretations at best are only qualitatively valid. This fragmentation also explains the large $B(\mathrm{M1}; 9/2_1^- \rightarrow 7/2_1^-)$ value obtained in the shell model. No M1 transition is allowed between the main components in the decomposition (3.1) since they involve different core states (0_1^+ and 2_1^+, respectively). On the other hand, the first component of the $9/2_1^-$ state and the second component of the $7/2_1^-$ state are connected by the proton part of the M1 operator, and this leads to the large calculated $B(\mathrm{M1})$ value. Given that the measured lifetime of the $9/2_1^-$ level implies a small $B(\mathrm{M1}; 9/2_1^- \rightarrow 7/2_1^-)$ value, a tentative conclusion of our analysis is that the shell model using these interaction predicts too much fragmentation. No new recent measurement of the $3/2^-$ (Fe-like) and $9/2^-$ (Ni-like) lifetime have been reported since.

The measured B(E2) were finally compared to state-of-the-art Shell Model calculations using the LNPS interaction [92]. Calculations reproduce well the experimental level scheme [112] and the measured lifetime of the $11/2^-$ states [107]. In [109], the B(E2) are compared to measured values in ^{65}Co and in particular to the proton deformed $(1/2^-)$ state. Experimentally, its B(E2) to the $3/2^-$ is surprisingly high, assuming a pure E2 transition. This large B(E2) is not compatible with the calculated value. This is unexpected since the interaction has reproduced well the spectroscopic data in the mass region. However, it must be underlined that the experiment was not design to measure the M1/E2 mixing ratio. Assuming instead a pure M1 transition, the calculated B(M1) is 6.10^{-3} Wu to be compared to 2.10^{-2} Wu in LNPS which is reasonably close. This is supporting that the transition is dominated by the M1 component and the corresponding B(E2) probably low. To support the dominant M1 contribution, the Weisskopf estimates can be used. The Weisskopf estimates for the 212.7 keV decay to the $(3/2^-)$ state in ^{65}Co are $\tau = 123$ ns for an E2 and $\tau = 3$ ps for an M1. The measured value is τ= 1.80(2) ns. Using the E2 Weisskopf estimates, a mixing ratio $\delta(\mathrm{E2/M1}) \sim 0.01$ is calculated and is supporting a large domination of the M1 component. The $(1/2^-)$ state is interpreted as a deformed proton intruder state. In the even-even Ni core, such intruder appears as a (2p-2h) 0^+ state [102]. The shape isomers will be discussed in the next section but as the collectivity of excited states in Co is discussed, a comparison between the $0^+_{def.} \rightarrow 2^+_1$ in the even-even Ni core and the $(1/2^-) \rightarrow (3/2^-)$ will be discussed in the following.

In ^{66}Ni, the deformed 0_4^+ proton state is located at 2974 kev with a B(E2) to the 2_1^+ state of 0.2 W.u. [113]. In [114], the LNPS calculations leads to a low B(E2)=8.10^{-3} W.u. The MCSMC from [113] predicts a B(E2)= 6.10^{-3} W.u. Both experimental and calculations are coherent with a low B(E2). The $(1/2^-) \rightarrow (3/2^-)$ B(E2) in ^{65}Co is also found small. In ^{68}Ni, the deformed proton state is located at 2511 keV (see next section). According to [115], the B(E2) to the 2_1^+ is 2.3 W.u. The published LNPS calculations are 0.9 W.u [115, 116] in reasonable agreement. The LNPS wave function for the $1/2^-$ state at 1290 keV in ^{65}Co has been published in [109] and has great similarities with the wave function of the 0^+ proton deformed states in ^{66}Ni. The deformed proton

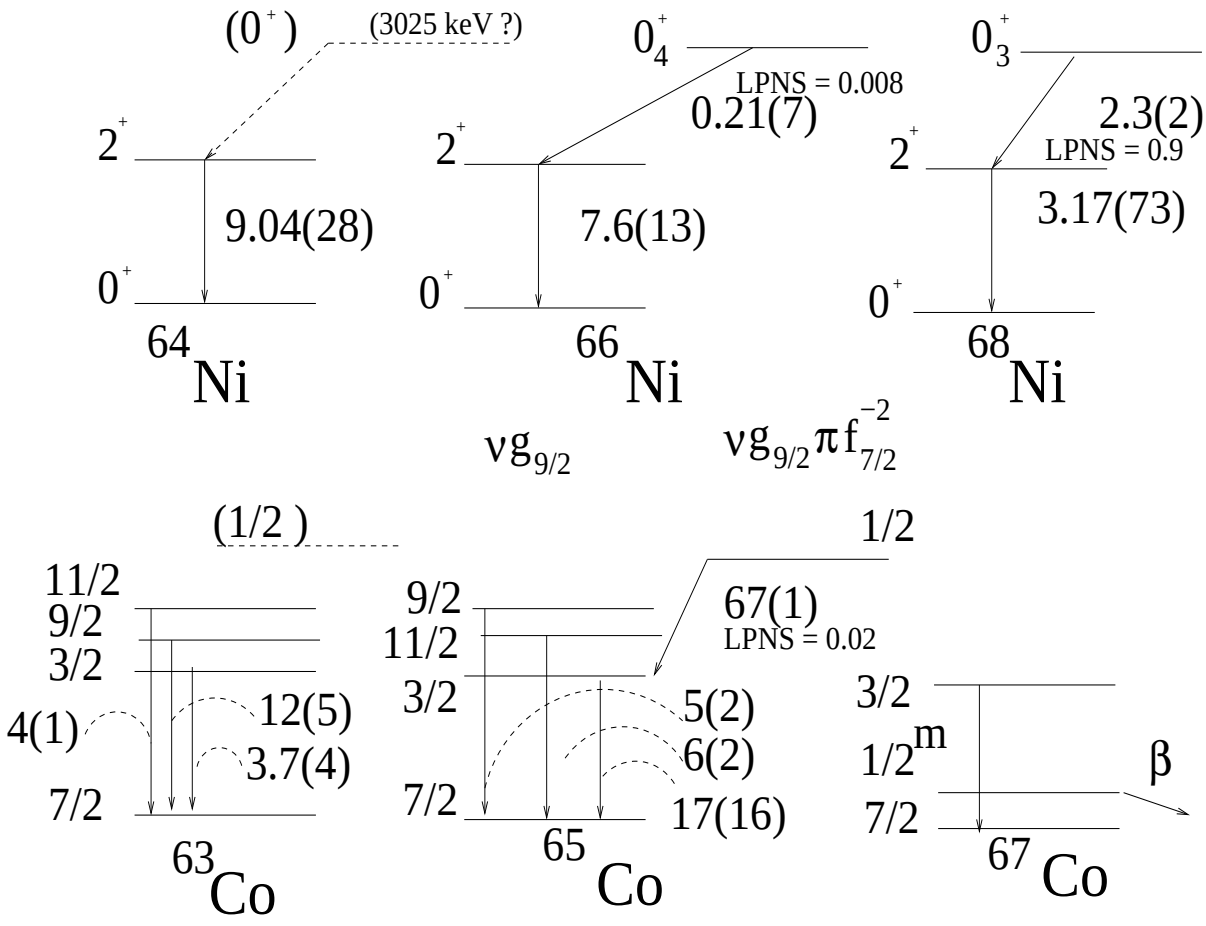

Figure 3.2: Level scheme and B(E2) in W.u for the ^{A}Co and $^{A+1}$Ni isotopes. The member of the $2^+(^{A+1}\text{Ni}) \times \pi f_{7/2}^{-1}$ multiplet and the deformed $1/2^-$ states are shown for the Co isotopes. The first 2^+ and proposed deformed 0^+ state in Ni are shown.

state in Co corresponds to a 1 proton excitation from the $f_{7/2}$ to the $f_{5/2}$ and neutrons excitations from fp to $g_{9/2}$.

3.3 Shape Isomers and deformed state in the vicinity of ^{68}Ni

The quest for a π(2p-2h) 0^+ intruder state in ^{68}Ni is a long story. The first speculation for a shape isomer in this nuclei was published in [117, 100]. Using the ^{70}Zn(^{14}C,^{16}O)^{68}Ni reaction, excited states have been populated in a pure 2 protons transfer. Two excited states at 1.77 MeV and 2.20 MeV have been identified and interpreted by differential cross section to be the 0_2^+ and 2_1^+ states respectively. The 2_1^+ was later proposed at 2033 keV. The presence of a 0^+ state as first excited state triggered discussion on its nature and the mean-field calculations using the Gogny interaction display a spherical minimum, but a second minimum exists at large deformation β = 0.3. This minimum could correspond to the observed 0_2^+ isomeric state. The excitation energy of the 0_2^+ isomeric state has been recently remeasured and placed at an energy of 1604 keV (instead of 1770 keV) based on the direct detection of the $0_2^+ \rightarrow 0_1^+$ E0 transition [118] and was interpreted as a neutron state with 2 particles scattered from the $p_{1/2}$ into the $g_{9/2}$ of moderate oblate deformation ($\beta \sim$0.2) [118, 111]. The ^{66}Ni(t,p)^{68}Ni reaction was performed recently and 2 neutron transfer cross sections have shown a strong population of the 0_1^+ state and a weak population of the 0_2^+ state [119, 120]. This result is consistent with the $\nu g_{9/2}^2$ interpretation of the 0_2^+ state.

Despite the large number of experiments dedicated to ^{68}Ni, no evidence for a 0^+ state based on a proton-pair excitation could be found. In [121], W. F. Mueller et al. proposed a (0^+) state at 2511 keV with a unique γ decay to the 2_1^+ state, populated in the decay of a low spin (3^+) β isomer ($T_{1/2}$=1.6(3) s.) in ^{68}Co. The state in ^{68}Ni was not populated in the β-decay of the (7^-) ground state. The proposed spin/parity for the (3^+) isomer leads to an interpretation of a neutron state based on a pair excitation from the $f_{5/2}$ into the $g_{9/2}$ for the 2511 keV state. In [102], D. Pauwels *et al.* reported the observation of a $J^\pi = (1/2^-)$ β isomeric state at 491 keV in ^{67}Co and interpreted as a deformed proton intruder state (1p-2h) across the Z=28 shell gap. The proposed wave function for the proposed $(1/2^-)$ state is a $\pi(f_{7/2}^{-2}p_{3/2}^{+1})$ deformed configuration with the Nilsson $1/2^-[321]$ orbital. The coupling with neutron excited from the pf to the intruder gd shell give rise to the reduction of the Z=28 effective shell gap and to the low excitation energy of the intruder state. This isomeric state associated to the $7/2^-$ π(2p-1h) in ^{69}Cu at 1711 keV allows the prediction of a π(2p-2h) deformed state at 491+1711 = 2202 keV in ^{68}Ni [3]. In [116], we reported the observation of delayed 168(1) keV γ-ray transition with $T_{1/2} = 216^{+65}_{-50}$ ns in ^{68}Ni populated by the two proton transfer reaction ^{238}U(^{70}Zn,^{68}Ni)^{240}Pu. We proposed as assignment for this E_γ=168(1) keV transition the decay from a new 0_3^+ state at 2202(1) keV to the 2_1^+. Because of the very limited statistics, it was unfortunately not possible to use γ-γ coincidences to build the level scheme. The non-observation of the $2_1^+ \rightarrow 0_1^+$ decay is consistent both with the very low cross-section to populate this new isomer and with the low efficiency at the focal plane at 2 MeV. Weisskopf estimates for the half-life of an E1, E2, M1 and M2 168 keV transition are 0.1 ps, 300 ns, 6 ps and 20 μs respectively. The measured half-life indicates therefore an E2 character. The corresponding very low $B(E2 : 0_3^+ \rightarrow 2_1^+) = 25.3(4)e^2fm^4$ (1.5(2) W.u.) (assuming a pure E2 transition), indicates a single particle character.

The position of the proposed 0_3^+ was in a remarkable agreement with the 2202 keV π(2p-2h) 0^+

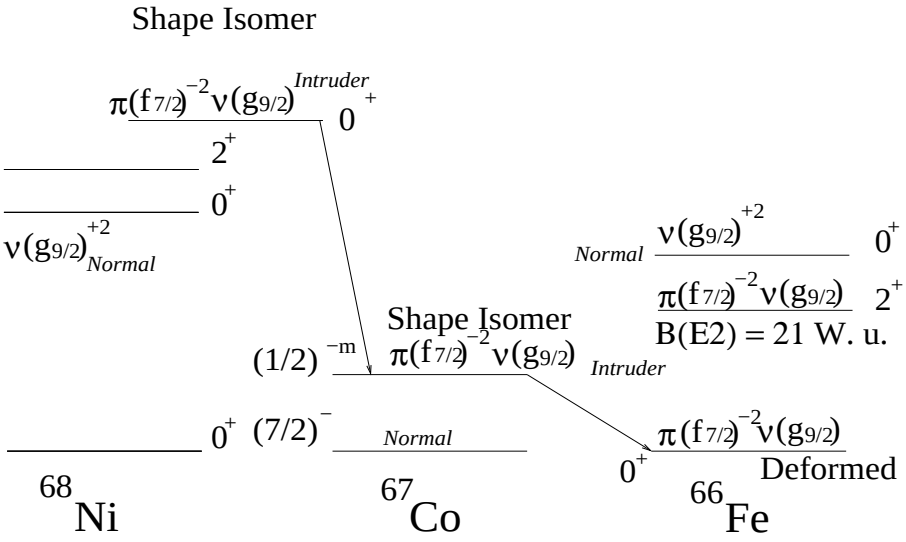

Figure 3.3: Shape coexistence at N=40. Evolution of the 2p-2h proton *intruder* and *normal* $\nu g_{9/2}$ states in ^{68}Ni, ^{67}Co and ^{66}Fe.

intruder state deduced by D. Pauwels *et al.* [3]. In [116], we performed large shell model (LSSM) calculations with the most recent interaction tailored for the mass region (LNPS) and in an extended valence space for ^{68}Ni [92]. In these calculations, a third 0_3^+ state is found at 2.4 MeV for which the dominant configuration is a pure π(2p-2h) i.e. $(f_{7/2})^{-2}$. This *intruder* state has only pure *normal* parity neutron states as neighbours. The 2_1^+ state wave function is calculated to be a pure ν(2p-2h) configuration and hence with a negligible overlap with the proposed state. Therefore the B(E2) is expected to be very small, possibly leading to an isomeric character as observed. The calculations show that the strong deformation in the Cr chain is the result of the proton-neutron correlations between the neutrons populating the $0g_{9/2}$-$1d_{5/2}$ orbitals and the valence protons in the pf shell. The calculated deformation for the $0^+_{1,2,3}$ states are $\beta_2 \simeq 0.18$, 0.24 and 0.4 respectively. The shell model calculations using LNPS published in [116] give for the first time the microscopical description of the deformed intruder proton state. The 0_2^+ is a pure neutron state with 2 neutron in the $g_{9/2}$ from the pf shells. The 0_3^+ is a strict excitation of proton pair from the $f_{7/2}$ into the $f_{5/2}$ with a fragmented neutron wave function in the $pf - g_{9/2}$ orbitals as a signature of large deformation. In the calculations, a fourth 0^+ state compatible with the state observed by W. F. Mueller et al. proposed at 2511 keV [121] is not predicted.

Following the publication, several experiments focussed on the spectroscopy of ^{68}Ni. The new isomer was not confirmed by [122] and a delayed 168 keV γ-ray in coincidence with the 2_1^+ decay was excluded. However, the spin parity assignment of the (0^+) state at 2511 keV proposed by [121] was confirmed by the $0 \rightarrow 2 \rightarrow 0$ angular correlation measurement. Presently, 2 excited 0^+ states are confirmed in ^{68}Ni. The conclusion of [122] is *"Particular attention was devoted to searching for the decay of the proton-2p2h, 2202-keV, 0^+ isomer. No evidence for such an intruder state was observed in the present study. Given the impact such a state would have on understanding the structure of nuclei in the ^{68}Ni region, more conclusive evidence of its location is required."* . The 2511 keV 0_3^+ state is compatible with the shell model prediction for a 2p-2h proton intruder state and the results of the other experiments, even if its shape and microscopical configuration was never measured, support the shape isomer interpretation [116, 111, 118, 123, 115]. It is worth mentioning that the E0 branch from the 0_3^+ decay was not observed [123, 115] but its lifetime was established at $T_{1/2}$=0.57(5) ns. Using upper limit for the E0 branching ratios to the 0_2^+ and 0_1^+ states, small $\rho^2(E0) \leq 5$ m.u and ≤ 25 m.u. respectively were extracted. The low $\rho^2(E0)$ could be interpreted as a signature of small differences in deformation between state or more likely as a signature of a low mixing of the respective wave functions. In [111, 123], a 2_2^+ state at 2742.6 keV is proposed as band member of the 0_3^+ intruder state. Such rotational band with a $E_\gamma(2^+ \rightarrow 0^+)$ = 232 keV in ^{68}Ni leads to an approximated deformation parameter $\beta_2 \sim 0.45$ using the Ramans estimate, compatible with the LNPS calculations.

In the present understanding, the ^{68}Ni ground state configuration has a moderate deformation. The 2_1^+ and 0_2^+ states correspond to a neutron pair scattered into the $g_{9/2}$ orbital. The configuration of the highly deformed intruder 0_3^+ state, with valence protons holes in the pf shell, is very similar to the Fe $(0_1^+/2_1^+)$ states, i.e. with two proton holes in the $\pi f_{7/2}$ orbital. Therefore, the configuration corresponding to the 0_3^+ state in ^{68}Ni migrates down to 491 keV excitation energy in ^{67}Co (the $(1/2^-)$ isomer) and becomes the ground state in ^{66}Fe when removing protons to the Z=28 shell closure. The *normal* configuration, by opposition to the *intruder* one, might then appear as a low-lying 0^+ state in ^{66}Fe. In [124, 125, 114], a 0_2^+ state at 1414 keV was identified in the

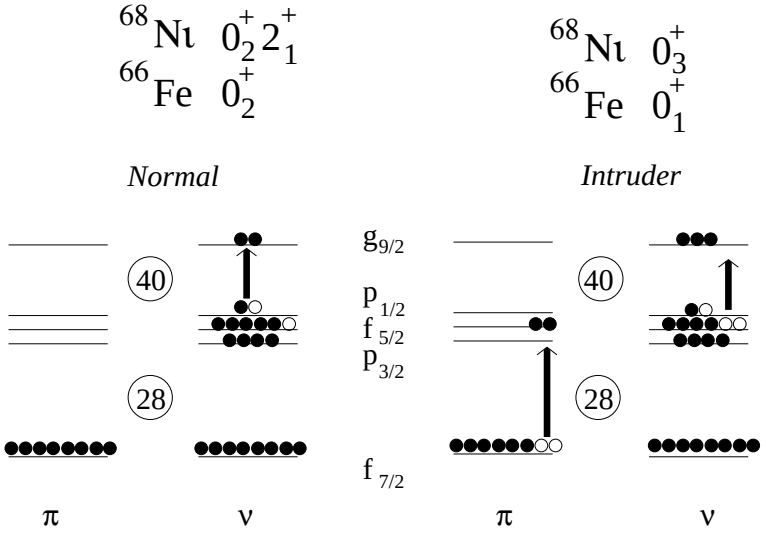

Figure 3.4: Shape coexistence at N=40. Microscopical configuration illustration.

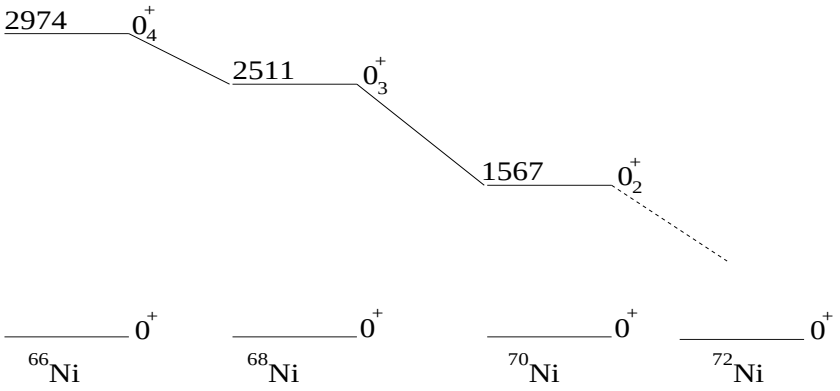

Figure 3.5: Systematics of proton deformed excited 0^+ state in Ni isotopes.

β-decay of ^{66}Mn. The shell model calculations predict such a state at the proper energy with a *normal* configuration $\pi f^5_{7/2}(p_{3/2}f_{5/2}p_{1/2})^1\ \nu p^4_{3/2}f^4_{5/2}p^2_{1/2}g^2_{9/2}$ similar to the $(0^+_2/2^+_1)$ states in ^{68}Ni [124]. As a summary, this shape coexistence scenario is illustrated in figures 3.4 and 3.3.

Recent large scale shell model calculations have provided wave function description of the 0^+ states in ^{68}Ni. The LNPS [116, 123] and MCSMC [126], state-of-the-art, are compared in figure 3.6. Even if the approaches are slightly different, the proposed configurations are very similar for the 0^+_3 state with a pair excitation of proton from the $f_{7/2}$ into the $f_{5/2}$ and fragmented neutron wave function with significant increase of the $g_{9/2}$ occupancy. The p-n interaction between the $\pi f^{-2}_{7/2}$ and $\nu g^3_{9/2}$ gives rise to the deformed configuration.

It is worth mentioning that since this intense experimental work on ^{68}Ni, similar proton deformed configurations have been proposed in ^{66}Ni [113, 114, 127] and in ^{70}Ni [128, 129, 130] giving rise to a triple shape coexistence scenario evolution between ^{66}Ni and ^{70}Ni. The question of low lying deformed 0^+ state in the neutron mid-shell in ^{72,74}Ni is therefore opened. From [113], four 0^+ states have been identified in ^{66}Ni. How these 3 excited 0^+ states evolve in ^{68}Ni leaves room for a possible explanation to the 168 keV delayed γ-ray transition.

Even if the experimental data show consistency in even-even nuclei, the β-decay chain for the mass A=68 deserves some attention since the spin parity of the β-isomer in ^{68}Co plays a major role in the possible constraint of the microscopic configuration of the proton 2p-2h intruder state in ^{68}Ni. After the discovery of the short lived β-isomer in ^{68}Co [121], several spin/parity assignments were proposed in the light of the populated excited states in ^{68}Ni. The claim for a proton 0^+ 2p-2h state at 2511 keV in ^{68}Ni should make a coherent β-decay chain for A=68. This review is proposed below. The list of the different assumptions for the spins and parities assignement is chronological.

- *(7^-) high spin ground state β-decay.* In [121], the high spin ground state $T_{1/2}$=0.23(3) s. is proposed as a 7^- state with the $\pi f^{-1}_{7/2} \otimes \nu g^{+1}_{9/2}$ configuration. The decay of this state doesn't populate the 0^+_3 state in ^{68}Ni but only pure neutron states. Indeed, the $\nu f_{5/2} \rightarrow \pi f_{7/2}$ Gamow-Teller is favoured and populates closed proton shell in ^{68}Ni with neutron states having the $\nu f^{-1}_{5/2}g^{+1}_{9/2}$ configuration compatible with the (6^-, 7^-) states assumptions.
- *(3^+) low spin isomer assumption.* In [121], the low spin isomer $T_{1/2}$=1.6(3)s. state is proposed

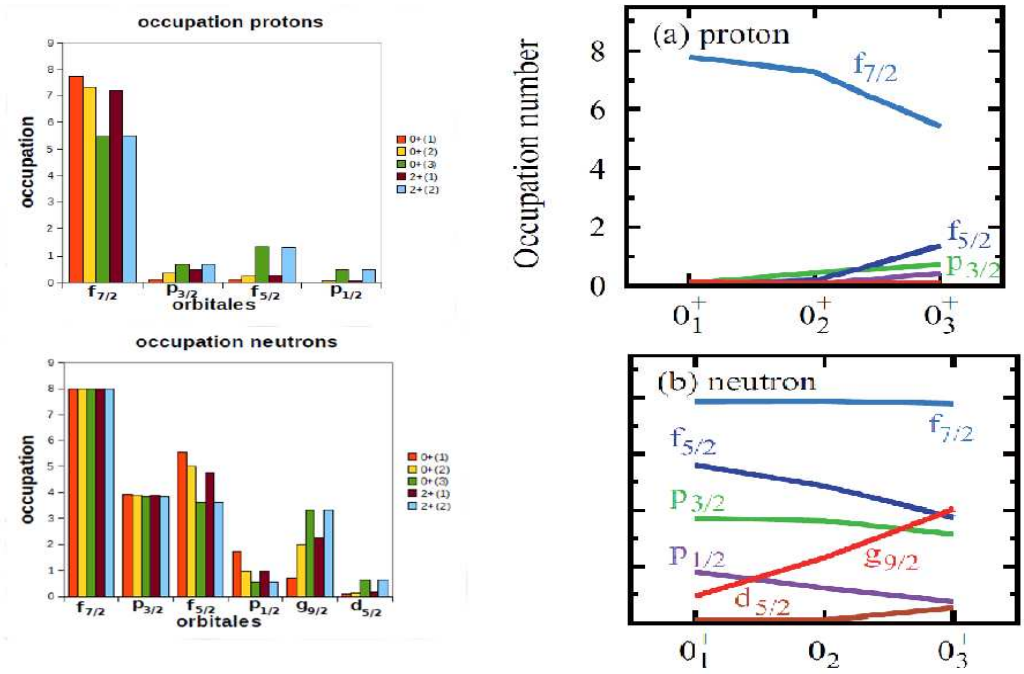

Figure 3.6: Proton and neutron occupancy for the 0^+ states in ^{68}Ni for (left) LNPS from [116, 123] and (right) MCSMC from [126]

as a (3^+) state with the $\pi f_{7/2}^{-1} \otimes \nu g_{9/2}^{+2} p_{1/2}^{-1}$ configuration. The decay of this state shows a weak population of the 0_3^+ state in ^{68}Ni. Similarly to the (7^-) ground state, a (3^+) would favour a $\nu f_{5/2} \rightarrow \pi f_{7/2}$ Gamow-Teller, populating pure neutron states having the $\nu p_{1/2}^{-1} f_{5/2}^{-1} g_{9/2}^{+2}$ configuration. According to shell model calculations, this is the exact configuration of the 0_2^+ and 2_1^+ states in ^{68}Ni. The decay of the 0_2^+ was not observed in [121] but the branching ratio to the 2_1^+ is the largest ($\leq$39(8)%). Proton states at 5 MeV in ^{68}Ni are also populated indicating that there is a significant $\nu p_{1/2} \rightarrow \pi p_{3/2}$ Gamow-Teller strength leading to proton states with the $\pi f_{7/2}^{-1} p_{3/2}^{+1} \otimes \nu p_{1/2}^{-2} g_{9/2}^{+2}$ configuration. Without the gain in pairing energy, such 1p-1h π states lies at higher excitation energy than a 2p-2h state. The weak population of the proposed 2p-2h proton state in ^{68}Ni would involve the combination of a $f_{5/2} \rightarrow \pi f_{5/2}$ Gamow-Teller with a $f_{7/2} \rightarrow f_{5/2}$ proton excitation. This could be compatible with the low branching ration to the 0_3^+ assuming the 2p-2h proton configuration.

- *(1^+) low spin isomer assumption.* In [131], ^{68}Co was populated from the ^{68}Fe ground state favouring the low spin isomer. It is proposed a new (1^+) spin/parity assignment for the isomer fed by an E1 transition from a state at 45 keV above, thus a 2^- or 1^- state. The (1^+) assignment suggests a proton excitation into the deformed intruder orbital coupled to two neutrons in the $g_{9/2}$, ie the $\pi f_{7/2}^{-2} p_{3/2}^{+1} \otimes \nu p_{1/2}^{1} g_{9/2}^{+2}$ configuration. The $\nu p_{1/2} \rightarrow \pi p_{3/2}$ Gamow-Teller should be favoured and populates states with the $\pi f_{7/2}^{-2} p_{3/2}^{+2} \otimes \nu p_{1/2}^{0} g_{9/2}^{+2}$ configuration, ie a proton pair excitation above the Z=28 gap into the $p_{3/2}$ orbital. This configuration is not the exact configuration expected for the two proton intruder at low excitation energy since, according to calculations, the proton pair is predicted into the $\pi f_{5/2}$ (the gain in pairing energy is more important). But proton state should be anyhow favoured. Instead, the β-feeding shows a large feeding of the neutron states in ^{68}Ni. As a result, the proposed (1^+) ground state is very unlikely. The decay by an E1 transition at 45 keV could instead lead to the population of a 1^+ state that decays to a $(2^-, 1^-)$ isomeric state, ie a reverse assignment to the one proposed in [131]. This $(2^-, 1^-)$ state assignment leads to a $\nu(p_{1/2}^{-2} g_{9/2}^{3}) \otimes \pi(f_{7/2}^{-1})$ or $(f_{7/2}^{-2} p_{3/2}^{+1})$ configuration. Such configuration with a fully depopulated $\nu p_{1/2}$ will favour the $\nu f_{5/2} \rightarrow \pi f_{7/2}$ Gamow-Teller and populate pure neutron states as experimentally observed.

- *(2^-) low spin isomer assumption.* In [123], the (2^-) spin/parity assignment is finally favoured. But the proposed configuration is a low-lying deformed $[321]1/2^-$ proton configuration coupled to the down-sloping $[431]3/2^+$ and $[440]1/2^+$ neutron orbitals originating from the spherical $g_{9/2}$ orbital, thus one of the previously proposed configuration $\nu(f_{5/2}^{6} p_{1/2}^{-2} g_{9/2}^{3}) \otimes \pi(f_{7/2}^{-2} p_{3/2}^{+1})$. Such configuration will favour the $\nu f_{5/2} \rightarrow \pi f_{7/2}$ Gamow-Teller transition. The populated states will be $\nu(f_{5/2}^{5} p_{1/2}^{-2} g_{9/2}^{3}) \otimes \pi(f_{7/2}^{-1} p_{3/2}^{+1})$. It means proton single particle state as observed in [121] and to some extend if the excited proton in the $p_{3/2}$ decays to the $f_{7/2}$, the 0_2^+ and 2_1^+ neutron states in ^{68}Ni as experimentally observed. This excludes a strong population of the proton 2p-2h state by β-decay into the ^{68}Ni.

As a summary, neither the direct (t,p) reaction [120] or β-decay from the low or high spin states in ^{68}Co can strongly populate the 2p-2h deformed proton intruder state in ^{68}Ni. From this compilation, the (1^+) assignment for the low spin isomer is very unlikely. The (3^+) and (2^+) assumptions are compatible with the current interpretation of the 0_3^+ state in ^{68}Ni. Figure 3.7 illustrates the compilation of the data used in this review. If possible, the $(^3He, n)$ reaction from the deformed ^{66}Fe or α-transfer from ^{64}Fe would favour the population of the deformed state in

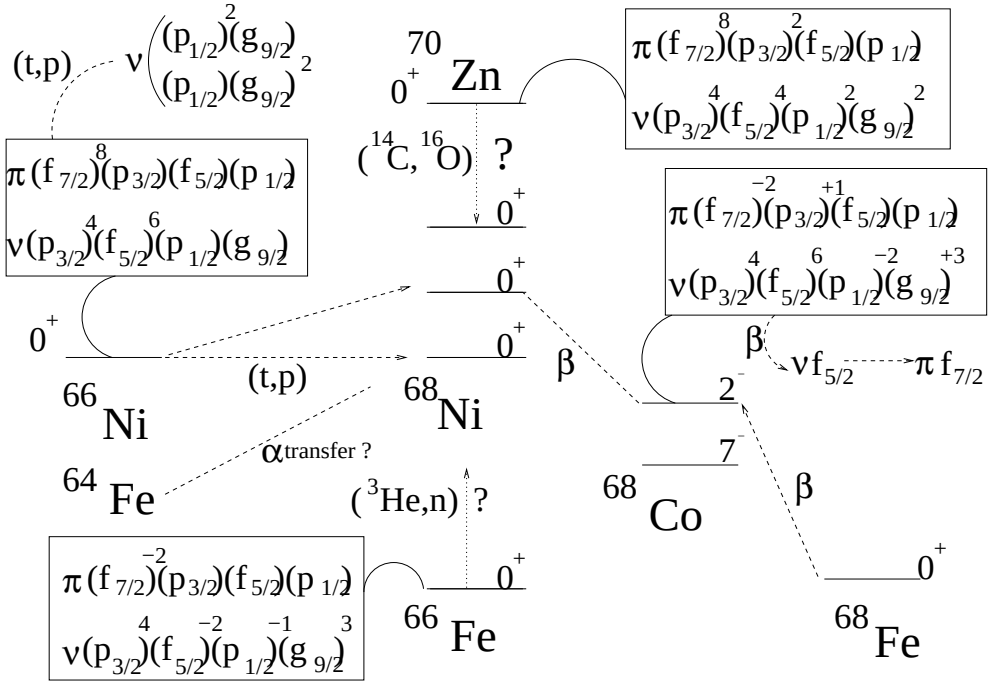

Figure 3.7: Multi-messenger approach for the 0^+ states in ^{68}Ni

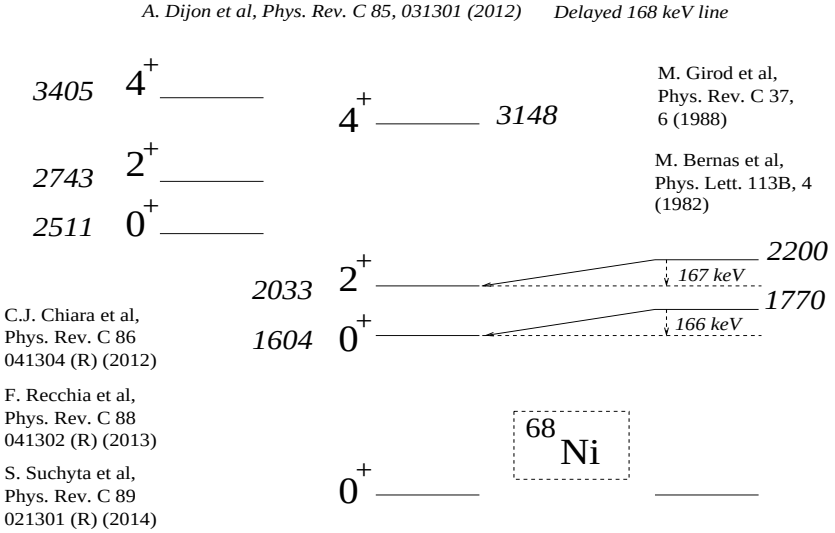

Figure 3.8: The 168 keV transition mystery

^{68}Ni.

The coherence with the $^{70}Zn(^{14}C,^{16}O)^{68}Ni$ data remains puzzling. In the two experiments by [100] and [117], the 0_2^+ and 2_1^+ states were proposed first at 1770 and 2200 keV respectively. Later measurements, as mentioned before, corrected the respective values at 1604 and 2033 keV. The two corrections are 166 and 167 keV respectively (see figure 3.8), very close to the proposed delayed line at 168 keV which was never confirmed later. **This systematic shift of 167(1) keV is disturbing and gives room for a possible explanation for the 168 keV γ-ray observed in [116].**

The microscopical structure of ^{70}Zn would reveal the possibility to populate the proper state in a strict 2 proton transfer. It is proposed to discuss, from the constrained theoretical wave functions of ^{70}Zn, the probability to populate the deformed proton state in ^{68}Ni. For this purpose, we use, as constrain, the B(E2, $2^+ \rightarrow 0^+$) measured using different experimental methods. The compilation of the measured B(E2,$2_1^+ \rightarrow 0_1^+$) in ^{70}Zn is presented in figure 3.9 and compared to Shell Model calculations using the LNPS and JUN45 interactions [132, 104, 133]. The contributions to the ground state configurations using the JUN45 interaction are listed in table 3.3. The JUN45 calculations for the B(E2) is shown in figure 3.9 and reproduces well the experimental average value with a close Z=28 proton shell, indicating that the wave function doesn't involve any excitation from the ^{56}Ni core. The two main contributions are : $\pi(p^2_{3/2}f^0_{5/2})\otimes\nu(f^4_{5/2}p^2_{1/2}g^2_{9/2})$ and $\pi(p^2_{3/2}f^0_{5/2})\otimes\nu(f^6_{5/2}p^2_{1/2}g^0_{9/2})$. The feeding of the proton deformed state in ^{68}Ni in a 2 protons stripping reaction is excluded in the second configuration since the neutron $g_{9/2}$ orbital is not occupied.

The configurations with the highest amplitude involve several neutrons scattered into the $g_{9/2}$ orbital and two protons in the $p_{3/2}$ orbital. The amplitude corresponding to an occupied $f_{5/2}$ proton orbital (**) account for 7% of the wave function. Other theoretical calculations [134] propose a wave function for the ^{70}Zn ground state as $\pi(f^{7.4}_{7/2}p^{1.2}_{3/2}f^{0.7}_{5/2}) \otimes \nu(f^{3.7}_{5/2}p^{0.7}_{1/2}g^{3.3}_{9/2})$, ie with scattered

Table 3.3: Calculated wave function for the ground state of ^{70}Zn using the JUN45 interaction. The configurations indicated with (**) are compatible with the population of the deformed proton state in ^{68}Ni by a 2 proton stripping from ^{70}Zn.

Amplitude	^{70}Zn
0.1456	$\nu(p^4_{3/2}f^4_{5/2}p^2_{1/2}g^2_{9/2})\pi(p^2_{3/2}f^0_{5/2})$
0.1275	$\nu(p^4_{3/2}f^6_{5/2}p^2_{1/2}g^0_{9/2})\pi(p^2_{3/2}f^0_{5/2})$
0.0941	$\nu(p^4_{3/2}f^6_{5/2}p^0_{1/2}g^2_{9/2})\pi(p^2_{3/2}f^0_{5/2})$
0.0677	$\nu(p^2_{3/2}f^6_{5/2}p^2_{1/2}g^2_{9/2})\pi(p^2_{3/2}f^0_{5/2})$
0.0564	$\nu(p^4_{3/2}f^4_{5/2}p^0_{1/2}g^4_{9/2})\pi(p^2_{3/2}f^0_{5/2})$
0.0451	$\nu(p^2_{3/2}f^4_{5/2}p^2_{1/2}g^4_{9/2})\pi(p^2_{3/2}f^0_{5/2})$
0.0221	$\nu(p^4_{3/2}f^4_{5/2}p^0_{1/2}g^4_{9/2})\pi(p^0_{3/2}f^2_{5/2})$ **
0.0212	$\nu(p^2_{3/2}f^6_{5/2}p^0_{1/2}g^4_{9/2})\pi(p^2_{3/2}f^0_{5/2})$
0.0203	$\nu(p^4_{3/2}f^4_{5/2}p^2_{1/2}g^2_{9/2})\pi(p^0_{3/2}f^2_{5/2})$**
0.0200	$\nu(p^4_{3/2}f^2_{5/2}p^2_{1/2}g^4_{9/2})\pi(p^2_{3/2}f^0_{5/2})$
0.0167	$\nu(p^3_{3/2}f^6_{5/2}p^1_{1/2}g^2_{9/2})\pi(p^2_{3/2}f^0_{5/2})$
0.0149	$\nu(p^4_{3/2}f^5_{5/2}p^1_{1/2}g^2_{9/2})\pi(p^2_{3/2}f^0_{5/2})$
0.0141	$\nu(p^4_{3/2}f^6_{5/2}p^0_{1/2}g^2_{9/2})\pi(p^0_{3/2}f^2_{5/2})$**
0.0130	$\nu(p^2_{3/2}f^4_{5/2}p^2_{1/2}g^4_{9/2})\pi(p^0_{3/2}f^2_{5/2})$**

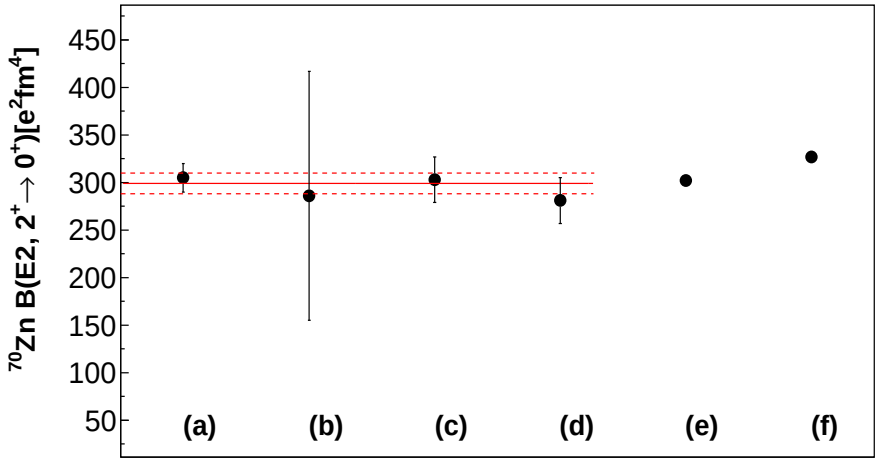

Figure 3.9: Systematics of the measured B(E2,$2_1^+ \rightarrow 0_1^+$) in ^{70}Zn. Experimental data (a) [135], (b) [136], (c) [132], (d) [137], (e) SM JUN45, (f) SM LNPS. The average value is 299(11) e^2fm^4 to be compared to 302 and 327 for the JUN45 and LNPS calculations respectively.

neutron in the $g_{9/2}$ and also with a very low occupancy of the proton $f_{5/2}$.

The ^{14}C beam has a $p_{1/2}^{-2}$ proton configuration considering a ^{16}O core. Therefore, the pair transfer should favour Δl=0, and the removal of the two protons in ^{70}Zn from the $p_{3/2}^2$ would be favoured. The two protons stripping from the occupied $p_{3/2}$ or $f_{5/2}$ proton orbital will give rise to the wave function of the 0_1^+ and (0_2^+ and 2_1^+) neutron states in ^{68}Ni according to the proposed calculations. Therefore, the main feeding in ^{68}Ni should populate neutron states. The remaining four configurations with two protons in the $f_{5/2}$ orbital could populate the deformed proton state if protons are removed from the $f_{7/2}$ core with a Δl=2 transfer, ie giving a similar 2 hole proton configuration into the $f_{7/2}$. This transfer would correspond to a very low cross section. As a conclusion, based on the present discussion on the ^{70}Zn ground state wave function, it is very unlikely that the experiments performed in [100] and [117] have populated the proton deformed state in ^{68}Ni. In these experiments, the ground state is populated with the highest cross section, indicating that the second calculated wave function, with empty neutron $g_{9/2}$ orbital, should be the dominant configuration in ^{70}Zn. The 0_2^+ and 2_1^+ states are populated with two orders of magnitude less giving a very weak chance to observe the low cross section to the proton deformed state.

One could propose two reactions compatible with the population of the proton state in ^{68}Ni. Obviously, starting from a deformed configuration will increase the cross section. Both ^{64}Fe and ^{66}Fe ground state have a proton $(f_{5/2})^{-2}$ configuration and the lifetime measurements show that both neutron $g_{9/2}$ and $d_{5/2}$ orbitals are already populated in ^{64}Fe [106]. Therefore the ^{64}Fe(^{7}Li,t)^{68}Ni (α transfer) or ^{66}Fe(^{3}He,n)^{68}Ni reactions could favor the population of the proton deformed state.

3.4 $\mathcal{Q}_s$ systematics

Contrary to the two previous mass regions, experimental spectroscopic quadrupole moments have not been measured in the vicinity of ^{68}Ni (last measured is ^{64}Ni), in Co (last measured is ^{60}Co), Fe (last measured is ^{61}Fe) and Mn (last measured is ^{56}Mn) isotopes. Therefore, the large overview of spectroscopic quadrupole moments presented in the N=Z and A=100 mass region cannot be produced. This underlines the lack of experimental data in the mass region. Ni, Co, Fe and Mn elements have chemical properties making these elements difficult to extract from an ISOL target. Nuclei lying below ^{68}Ni are not populated by fission of heavy elements and being neutron rich are not populated in fusion-evaporation of heavy ions. These isotopes are populated by high energy heavy ions fragmentation or Multi-nucleon transfer reaction around the Coulomb barrier using heavy ions. Such area remains a Terra incognita for such techniques.

3.5 Conclusions

A shape coexistence scenario emerges around N=40 in Ni, Co, Fe and Cr isotopes. An important experimental effort in the last five years have clarified the level schemes and spin/parity assignments. Very few relevant transition probabilities have been measured and no experimental data have been published on the direct determination of the shape (ie spectroscopic quadrupole moment) or possible constrains on the microscopical configuration of the intruder state. Presently, the direct proof for a 2p-2h proton excitation would a be milestone in the mass region.
In Co isotopes, unknown E2/M1 mixing prevent from a direct B(E2)/B(M1) comparison. In addition, based on the unique multi-polarity, the overlap between the B(E2) in Co and Ni is not as unambiguous as expected from the weak coupling model. The systematic in excitation energy of the $(1/2^-)$ deformed state suggests an inversion beyond N=40 with the ground state. This has never been proven.

In ^{68}Ni isotope, one should remember that so far the E0 transition from the 0^+_3 was not observed and the spin assignment comes from the angular correlation $0\rightarrow\ 2\ \rightarrow 0$. The shape of this state is not confirmed by a spectroscopic quadrupole moment and no B(E2) connecting to a possible rotational 2^+ state is measured. The safe Coulomb excitation of a high intense ^{68}Ni beam would be a milestone in the present discussion.

In the last section, an analysis of the different path to reach the 2p-2h proton state by β-decay and nucleon transfer is proposed. It shows that indeed, with its proposed configuration, these direct reactions cannot strongly populate such configuration. The consistency between proton, neutron transfer and β-decay is proven. The consistency between the 2 protons transfer from ^{14}C and the delayed 168 keV line is not obvious. One could speculated that, instead, a third excited 0^+ state, of neutron nature, similar to the one in ^{66}Ni, was populated.

Partie IV

Shape coexistence around N=Z=40

Chapter 4

Shape coexistence around N=Z=40

4.1 Introduction

The neutron deficient isotopes, close to the N=Z line, between Ge and Zr, are a long standing area of shape coexistence. Stable Ge isotopes have shown a competition between a spherical excited configuration and a deformed ground state. As these isotopes are stable, they have been studied by safe Coulomb excitation and spectroscopic quadrupole moment for the first 2^+ states were extracted. Low lying 0^{+m} states have been identified as evidence of shape coexistence. However, shape parameter of states built on top of this proposed shape isomers are not yet experimentally measured.

For heavier elements, from Se to Zr, Wood-Saxon calculations including a spin-orbit term [138, 139] and more elaborated mean field calculations using the Skyrme interaction [140, 141] or the Gogny interaction [142, 143, 144, 145, 146, 147] have predicted a shape coexistence between prolate and oblate configurations. Low-lying 0^{+m} states have been identified in ^{72,74,76}Se, ^{72,74,76}Kr and ^{80}Sr as first evidence. A specificity of the mass region is that several spectroscopic observations point to a strong mixing of the wave functions corresponding to the two configurations. In Kr isotopes, a perturbation of the ground state band moment of inertia at low spin was observed. Similarly, the reduced transition probabilities is showing a reduction of the collectivity at low spin as a result of the possible shape mixing (see figure 4.1). Combining the excitation energy of both the 2_1^+ and 4_1^+ states and the B(E2, $2_1^+ \rightarrow 0_1^+$), the correlation between the $R_{42}=4_1^+/2_1^+$ excitation energy ratio and the B(E2)[W.u.].A^{-1} shows that these N$\sim$Z nuclei are located far from the systematics of all other nuclei in the nuclear chart as shown in [148]. These off-systematics points are understood as the result of the mixing.

The perturbation of the 0^+ ground state and 0^{+m} isomeric state excitation energy with respect to the higher spins extrapolation was used to quantify for the first time the wave function mixing using the two levels mixing model [22]. In the case of the neutron deficient Kr isotopes, a mixing of 27% of the wave function is extracted for the ^{76}Kr ground state. This mixing reaches a maximum

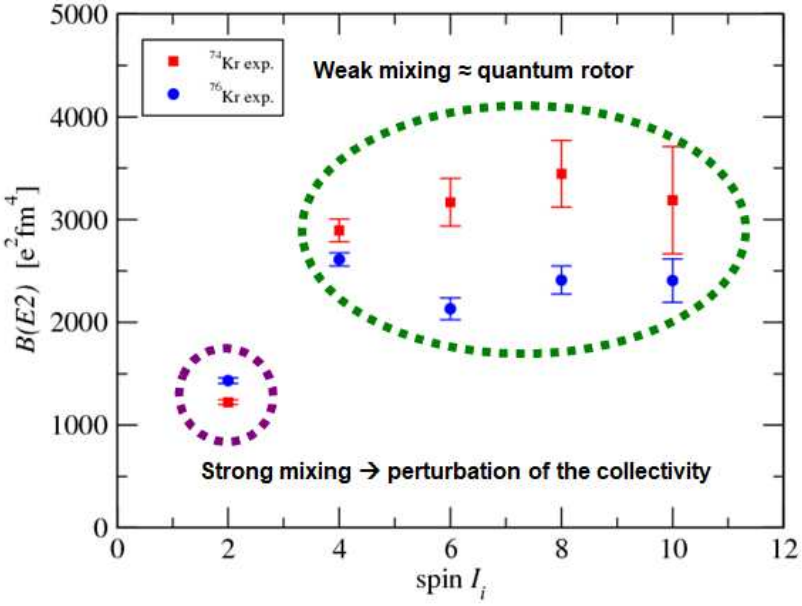

Figure 4.1: Experimental B(E2↓) in the ground state band of ^{74,76}Kr from lifetime measurement.

of 50% in ^{74}Kr deduced from the maximum value of $\rho(E0)$ and minimum excitation energy of the 0^{+m}. In ^{72}Kr, the 0^{+m} excitation energy increases with a reduced $\rho^2(E0)$ leading to a mixing of 10% [22]. This parabolic trend suggests an inversion of shape from ^{78}Kr to ^{72}Kr with a crossing at ^{74}Kr where both configurations are almost degenerated [22]. So far, the evaluation of the sign of the deformation, i.e. prolate or oblate, was derived from comparison with theoretical models. For instance, using a comparison between measured B(E2; $2^+ \rightarrow 0^+$) and theoretical values, Iwasaki et al [149] proposed that the first 2^+ state in ^{72}Kr is compatible with an oblate shape and therefore suggesting a prolate shape for heavier isotopes.

All these experimental probes gave rise to *indirect* evidence of the shape coexistence. Laser spectroscopy is an experimental technique from which spectroscopic quadrupole moment in odd-mass nuclei ground state can be measured as well as for long-lived isomers. Unfortunately such systematic is rather scarce close to the N=Z line and does not involve the isotopes of interest as it will be more detailed in section 4.3.

4.2 Coulomb excitation experiment results

Direct evidence of the shape coexistence in this mass region came from the safe Coulomb excitation of radioactive beams. The Coulomb excitation cross section, via the second order effect of the reorientation [39, 40, 72], is sensitive to the E2 diagonal matrix element from which a spectroscopic quadrupole moment can be deduced. The very first safe multi-step coulomb excitation of a post-accelerated radioactive beam was performed for the neutron deficient Kr isotopes at the SPIRAL1 facility, GANIL in the framework of my PhD thesis work. Post-accelerated beams of ^{74}Kr and ^{76}Kr were delivered to the EXOGAM setup and bombarded a ^{208}Pb target just below the Coulomb barrier. A charged particle detector covered scattering angles ensuring "safe" Coulomb excitation according to Cline's criteria [39]. As a result of my analysis, the first ever spectroscopic quadrupole moments in short lived excited states in unstable isotopes were measured [9]. This work represents the first direct experimental proof of the proposed shape coexistence scenario in neutron deficient Krypton isotopes, and the reorientation effect has been exploited for the first time with a radioactive ion beam. The details of the analysis and discussion can be found in [9]. To summarize the output of this rich set of E2 matrix elements both transitional (leading to B(E2)) and diagonal (leading to spectroscopic quadrupole moment) :

- 16(13) E2 transitional matrix elements have been measured in ^{76}Kr (^{74}Kr) respectively.
- The measurement has shown an inconsistent value of the 4_1^+ state lifetime in ^{74}Kr later confirmed and corrected by a dedicated plunger measurement [32]
- 5(5) E2 diagonal matrix elements have been measured in ^{76}Kr (^{74}Kr) respectively for the first time.
- The transition strengths from the Coulomb excitation measurement are in good agreement with the results of the lifetime measurement.
- Using the precise lifetimes as additional input in the analysis of the Coulomb excitation data enhanced the sensitivity to the reorientation effect and allowed extracting spectroscopic quadrupole moments for several excited states.
- The negative diagonal matrix elements of the states in the ground-state bands of both isotopes prove their prolate character
- The excited 2_2^+ and 2_3^+ states are interpreted as γ-vibrational and oblate rotational states, respectively.
- However, a clear classification of the states is difficult due to the mixing of prolate and oblate configurations, on one hand, and K = 0 and K = 2 configurations, on the other hand.
- The matrix elements were interpreted in a phenomenological two-band mixing model. The results confirm the earlier finding of maximum mixing between prolate and oblate configurations in the wave functions of the 0^+ states in ^{74}Kr. In ^{76}Kr, the mixing of the ground state is 31(4)% whereas it was measured at 27(1)% from the E0 spectroscopy. In ^{74}Kr, the mixing is found equal (52%) in both experiment.

- The purity of the wave functions increases rapidly with spin, explaining the increase in the transition strength and at the same time the very strong inter-band transitions between the different 2^+ and 0^+ states (see figure 4.1).
- The two level mixing model fails to describe consistently the band mixing in ^{76}Kr, probably due to the strong coupling with the presumed γ-vibrational band.
- The quadrupole sum rule formalism was applied to derive shape parameters for the 0^+ states.
- The first rotational invariant, Q^2 (similar to $|\beta_2|$), is found large for both states in both isotopes confirming their deformed character
- The second rotational invariant, $cos3\delta$ (similar to γ) shows that the ^{76,74}Kr ground state are axially prolate. The 0_2^+ state in ^{76}Kr is oblate with a large triaxial contribution. The second 0^+ state in ^{74}Kr reaches a maximum of triaxility.
- The transition strengths and quadrupole moments were compared to theoretical calculations going beyond the static mean-field approach using the Gogny D1S interaction and the Skyrme SLy6 interaction. The present SLy6 interaction is limited to axial symmetry. The comparison emphasize the importance of including the triaxial degree of freedom to describe the shape coexistence in the light krypton isotopes.

4.3 $\mathcal{Q}_s$ systematics

The diagonal $E2$ matrix elements extracted from the Coulomb excitation analysis can be translated into spectroscopic quadrupole moments and compared to the ground states quadrupole moment in odd-mass neighbouring nuclei. Data used for this comparison are compiled from [70, 46] and completed by quadrupole moments of the 2_1^+ states in ^{70,72}Se[150, 149, 151] and ^{72}Ge [152].

In figure 4.2,the compilation of the absolute deformation amplitude ($|\beta_2|$) is restricted to Z>31 and N<50. First, it is worth mentioning that such measurement did not yet reach the N=Z line above the Ni chain and are far from ^{100}Sn.

From the Z=32, a clear onset of deformation is observed between Ge and Se isotopes, i.e. when the proton $f_{5/2}$ is populated and with at least four neutrons holes in the $g_{9/2}$. From this systematics in neutron number, the shell closure at nucleon number 40 does not present a stabilizing effect toward spherical shape and the maximum of deformation is reached at Z$\simeq$N$\simeq$38-39.

In figure 4.3, the algebraic deformation is deduced (β_2). The blue (green) squares indicate a prolate (oblate) deformations respectively. The first matrix shows the deformation for the ground states in odd-nucleon isotopes and for the 2_1^+ state in even-even isotopes. Beyond Se, deformation are large and prolate. Approaching the N=Z line, a prolate to oblate transition occurs in ^{70}Se. No other shape inversion as a function of the neutron number was proven so far. The second panel highlights the shape coexistence scenario. This matrix shows the same algebraic deformation (β_2) measured for isomers, which are living long-enough to allow a laser spectroscopy, and for $2_{2,3}^+$ states built above a low-lying 0_2^+ from safe Coulomb excitation measurements. The 2_2^+ state is not chosen by default. Indeed, in this mass region, K=2 γ-band are frequent at low excitation energy. Therefore, for the compilation, the 2_2^+ or 2_3^+ state is chosen from the largest B(E2) value to the

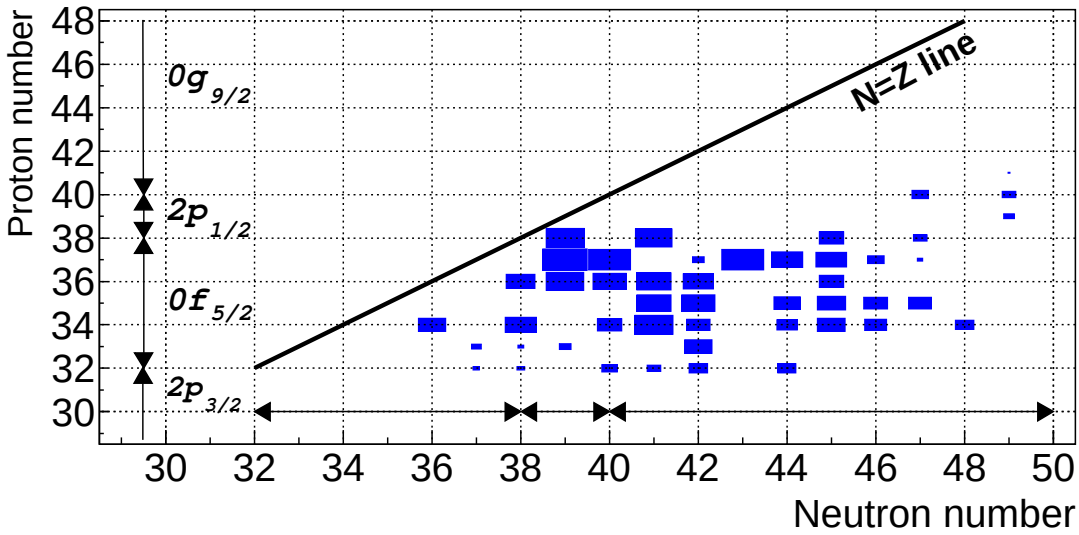

Figure 4.2: Absolute deformation amplitude ($|\beta_2|$) in the (N,Z) plan from measured spectroscopic quadrupole moments. The spherical Nilsson orbitals are indicated. the blue squares size are proportional to the absolute deformation amplitude ($|\beta_2|$) for ground state in odd-nucleon isotopes and for the 2_1^+ state for even-even isotopes.

0_2^+ state.

The comparison between the two matrices illustrates the shape coexistence in a given isotope. In Ge isotopes, the ground state presents a very small deformation and the 2_3^+ state has a large one illustrating the shape coexistence between a spherical ground state and a deformed excited configuration. So far, the shape change in Ge isotopes was not proven. In light odd-mass Kr, the $\mathcal{Q}_s$ in long-lived isomers are not established. Large systematics also exists for the Rb isotopes (Z=37). The ground states have large prolate deformation. The isomers have an oblate or prolate character. Beyond Rb, available data are almost non-existing.

4.4 Probing the deformation from the first excited states in even-even isotopes

In ^{68}Se, the systematics of the momentum of inertia suggests that the ground state band is oblate as the band built on top of the 2_2^+ at 1594 keV has a prolate character (see figure 4.4) [153]. The B(E2, $2_1^+ \rightarrow 0_1^+$) was first measured during my PhD [154] and later with more precision by [155]. The value is found compatible with theoretical prediction of an oblate, γ-unstable, deformed state. The spectroscopic quadrupole moment remains un-measured.

In ^{70}Se, the systematics of the momentum of inertia suggests that the ground state band at low

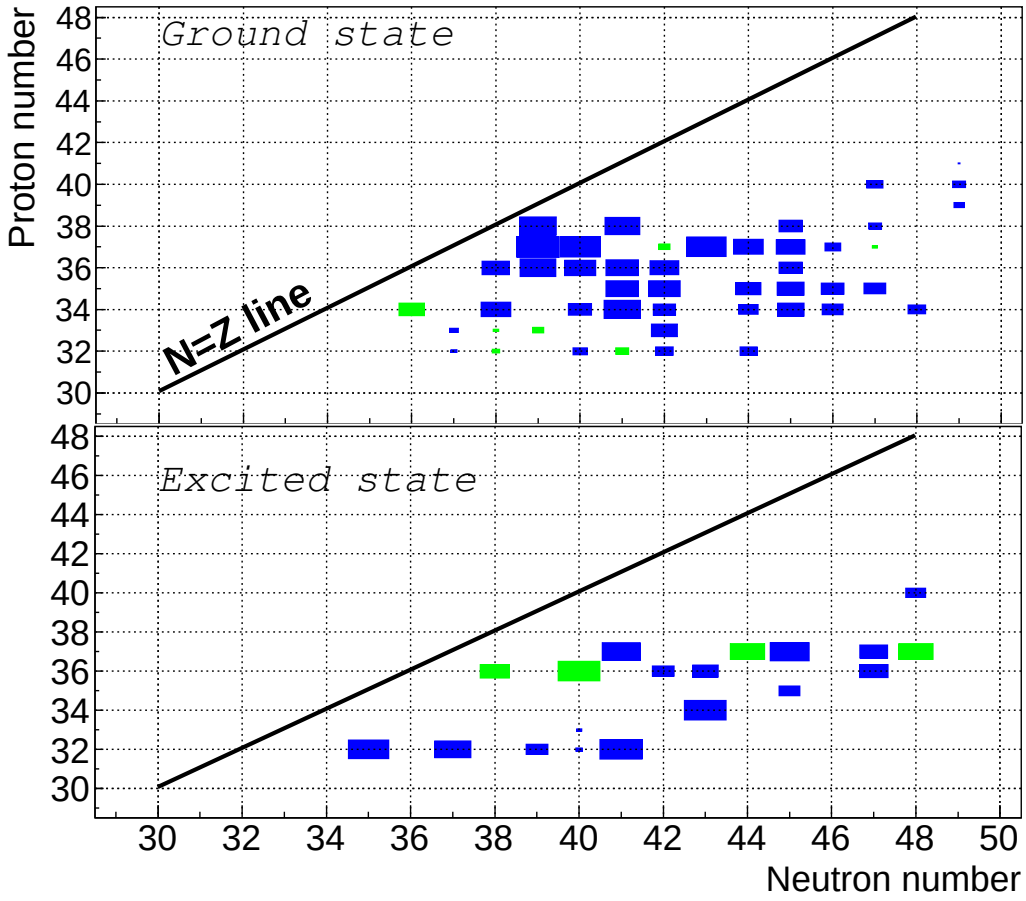

Figure 4.3: Algebraic deformation amplitude (β_2) in the (N,Z) plan from measured spectroscopic quadrupole moments. *Top*: for ground or 2_1^+ states. *Bottom*: for isomers or $2_{2,3}^+$ states

spin is oblate and turn to be prolate at higher spin [156]. Combined Safe Coulomb excitation using post-accelerated beams by A. Hurst [150] and high precision lifetime measurement by J. Ljungvall [149] have proven the oblate character of the 2_1^+ state. Finally, J. Henderson performed the safe Coulomb excitation of ^{72}Se [151]. A negative spectroscopic quadrupole moment for the 2_1^+ state was measured, supporting its prolate character [151]. Previous measurements in stable Se isotopes by [157, 158] have also proved a prolate 2_1^+ state. There is therefore a shape change for the 2^+ from prolate to oblate in ^{70}Se. No spectroscopic quadrupole moment are known beyond the 2_1^+ state.

Recently, the first spectroscopy of ^{70}Kr was performed and suggests, by comparison with theoretical calculations, a shape coexistence scenario [159]. In ^{72}Kr, using a comparison between measured B(E2; $2^+ \rightarrow 0^+$) and theoretical values, Iwasaki et al [149] proposed that the first 2^+ state in ^{72}Kr is compatible with an oblate shape. The safe Coulomb excitation of ^{74,76}Kr provides the first evidence for a shape coexistence scenario with a prolate ground state band and an oblate

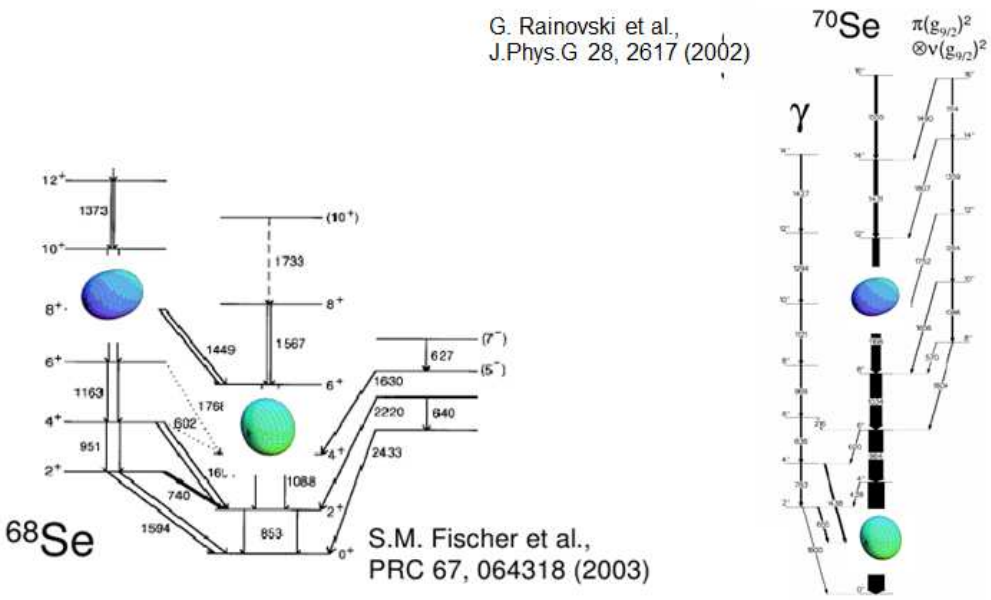

Figure 4.4: Proposed shape assignment in neutron deficient Se isotopes

excited configuration with large mixing of the wave functions. Finally, the safe Coulomb excitation of ^{78}Kr was performed in [160]. The prolate character of the 2_1^+ is established as for the 2_2^+ and 2_3^+ state triaxial prolate and oblate deformation are determined.

Experimental data are even more scarce in Sr isotopes. Its chemical properties makes Sr element very difficult to extract from an ISOL target. In addition, the N $\sim$Z ^{76}Sr isotopes becomes very exotic and produced with very low cross section. Neutron deficient Sr isotopes have a large deformation as deduced from the observation of rather regular rotational ground states band and corresponding large B(E2). In [148], A. Lemasson et al., have proposed a low mixing between the configurations from the measured B(E2, $2^+ \rightarrow 0^+$) placed in the systematics of the correlation between the $R_{42}=4_1^+/2_1^+$ excitation energy ratio and the B(E2)[W.u.].A^{-1}. Even if the experimental point follows the systematics of the Kr isotopes, assuming that the R_{42} is perturbed by the mixing, a unique feature of ^{76}Sr arises. Indeed, with a typical mixing strength of 0.2 MeV and a 0_2^+ excitation energy at around 1 MeV, a mixing of 5% is extracted. This apparent contradiction between weak mixing and perturbation of the collectivity calls for more detailed spectroscopic data as the search for the 0_2^+ state and related electromagnetic strength.

The systematics of the 2_1^+ excitation energy and B(E2) for N=Z nuclei are presented in figure 4.5 extracted from [148]. The systematics show a clear onset of collectivity between ^{72}Kr and ^{76}Sr at the N=Z line. It is proposed, at the mean-field level, that an increase of axiallity explains the onset of collectivity [155]. A similar systematics of spectroscopic quadrupole moment and quadrupole invariant would confirm the proposed symmetry effect.

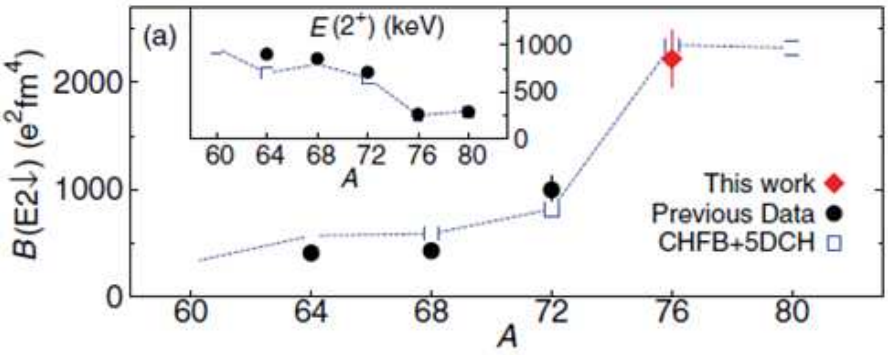

Figure 4.5: B(E2;$2_1^+ \rightarrow 0+_1$) systematics at the N=Z line. Figure from [148].

4.5 Probing the role of the $g_{9/2}$ from laser spectroscopy

One could expect that this increase of collectivity as a function of the proton number could be related to an increase of the $g_{9/2}$ occupancy acting as an intruder. Its role can be evaluated from the experimental point of view from the systematics of the spin and parity of the ground states. In figure 4.6, the spin and parity measured for the ground states of odd-masses by laser spectroscopy is presented from Se to Sr. The most probable Nilsson orbital is indicated with the spherical orbit parentage. The deformation character is extracted from laser spectroscopy or deduced from neighbouring even-even nuclei using Coulomb excitation experiment.

In ^{69}Se (Z=34, N=35), an oblate (from ^{70}Se shape) $1/2^-$ spin/parity is assigned. It is proposed that the configuration is dominated by the deformed $1f_{5/2}$ orbit with the 1/2[310] oblate orbital. In ^{73}Se, the $9/2^+$ assignment suggests the 9/2[404] orbits, i.e. an oblate deformation, with a $g_{9/2}$ orbital acting as an intruder. From Coulomb excitation measurement, ^{72}Se has a prolate character and the shape inversion to oblate occurs for ^{70}Se. Therefore, one could assume that ^{73}Se has a prolate deformation and the local oblate character is surprising. At N=41, the $g_{9/2}$ is naturally populated and the $5/2^+$ spin/parity is compatible with the deformed 5/2[422] orbital. In Br isotopes, with a spin parity $1/2^-$ and $3/2^-$ assigned to the 1/2[310] and 3/2[301] deformed $f_{5/2}$ orbital, the proton $g_{9/2}$ is not yet involved. In Kr isotopes, ^{73}Kr with a spin/parity $3/2^-$ points again to the $f_{5/2}$ orbital, hence suggesting an oblate shape. Beyond, at N=39 and 41 with a proposed prolate shape as for N=38 and N=40, the $5/2^+$ spin/parity supports the occupation of the prolate deformed $g_{9/2}$ similarly to the Se isotopes. At Z= 37, ^{75,77}Rb favour also the proton $f_{5/2}$ orbital. In Sr isotopes, at N=39, similarly to the Se and Kr isotopes, the ground state suggests the occupation of the neutron deformed $g_{9/2}$. Surprisingly, ^{79}Sr would correspond to a ground state involving the $\nu f_{5/2}$ orbital.

From the present systematics, the odd-proton isotopes do not point for the occupation of the $\pi g_{9/2}$ as in intruder, at least until Z=37, and underline the role of the deformed $\pi f_{5/2}$ orbitals. In even-proton isotopes, similarly, until N=37, the deformed neutron $f_{5/2}$ is favoured. From N=39,

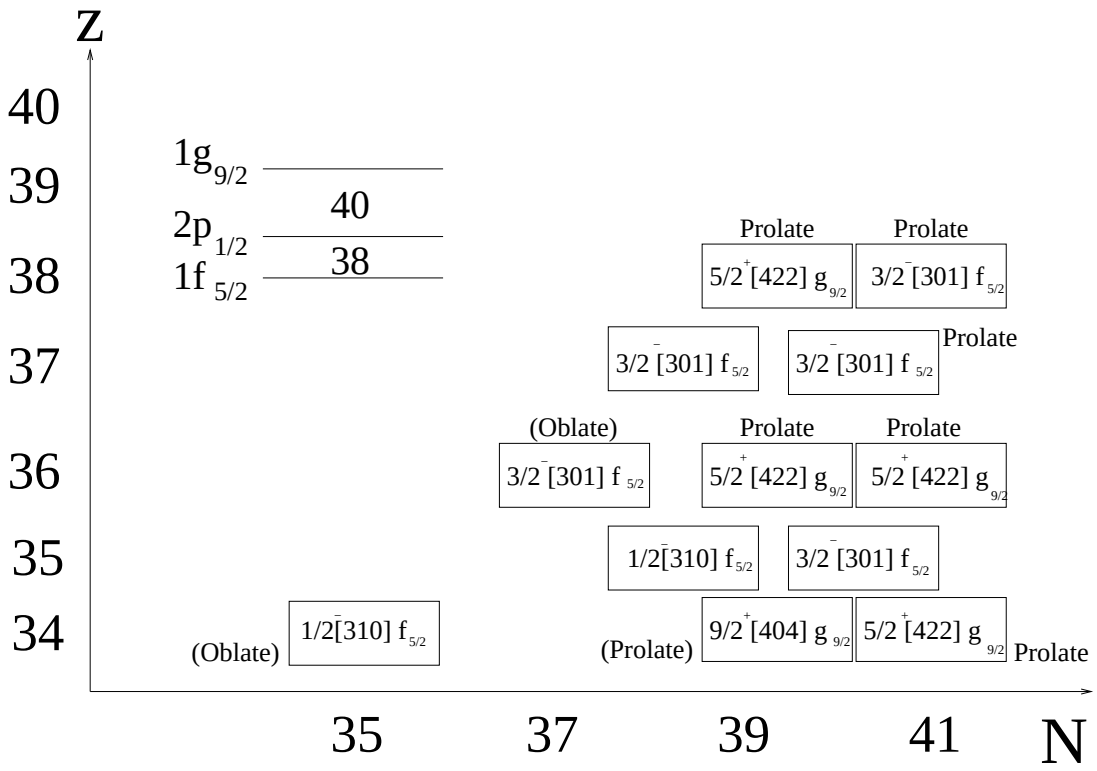

Figure 4.6: *Top* : Systematics of spin/parity assignment from laser spectroscopy in N∼Z nuclei. The shape mentioned next to the configuration is determined from measured $\mathcal{Q}_s$.

the neutron $g_{9/2}$ orbital appears as an intruder. But its role in the increase of collectivity when the proton number increases is not established from this systematics. For the Se and Kr isotopic chains, the transition from prolate to oblate deformation when approaching the N=Z line seems to be correlated to the change from the neutron $g_{9/2}$ to $f_{5/2}$ occupation. ^{77}Sr and ^{79}Sr remain prolate with however a change of the neutron orbit. The systematics underline that the shape coexistence, before N=Z, from Se to Sr, seems to be dominated by the competition between the deformed gaps at 34, 36 and 38 in the pf shells.

4.6 Short overview of the theoretical approaches

4.6.1 Mean Field calculations in Se, Kr, Sr and Zr isotopes

In this section, spectroscopic data such as B(E2) and excitation energy of the first excited states are compared to mean-field calculations using the Gogny D1S or Skyrme SLy6 interactions. This formalism is expected to perform well in these deformed nuclei having complex mixing of configurations.

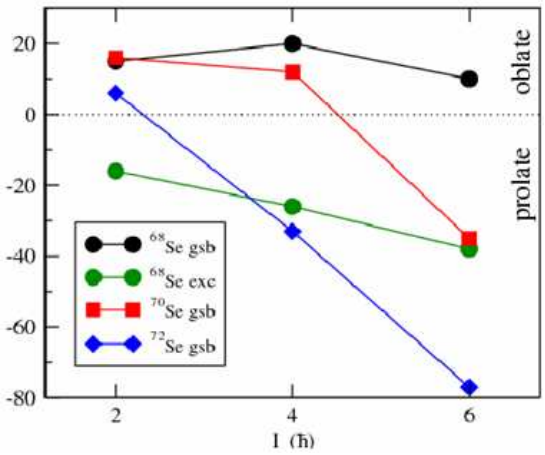

Figure 4.7: Calculated shape evolution in Se isotopes. Picture from [161].

The Se isotopes have been investigated using the Gogny D1S interaction in the mean-field framework in [161]. The known B(E2) are in good agreement with theoretical calculations for the first excited states. These calculations predict a shape change for both ^{70,72}Se from oblate to prolate at spin 4 and 6 respectively as ^{68}Se remains oblate as illustrated in figure 4.7. Unfortunately the spin evolution was not probed so far experimentally. Low lying 0_2^+ states are calculated at high excitation energy ($\geq$ 1 MeV). All three ^{68,70,72}Se are predicted oblate in the 2_1^+ state by the Gogny D1S interaction as a shape change occurs experimentally between ^{72}Se and ^{70}Se from prolate to oblate deformation.

In Kr isotopes, the experimental B(E2) and Q_s were then compared to mean field calculations using the Gogny D1S or Skyrme SLy6 interactions in [9]. In the publication, the later is restricted to axial symmetry. Along the rotational prolate and oblate bands, both calculations reproduce the trend as a function of angular momentum as illustrated in figure 4.8. The Skyrme calculation slightly overestimates the collectivity while the Gogny calculations reproduce well the collectivity as a results of the restriction to axial symmetry in the Skyrme calculation. We proposed that the large overlap between K=0 bands and K=2 γ-band, reflected by large inter-bands B(E2), leads to triaxility and reduces in-band B(E2) and $\mathcal{Q}_s$.

In figure 4.9, the experimental level scheme is compared to the Skyrme calculations. As they are restricted to axial symmetry, no K=2 states are calculated. The oblate configuration is predicted to be the ground state by opposition to the experimental conclusions. Finally, inter-band B(E2) are underestimated. Using the Gogny D1S interaction, the agreement is remarkable for excitation energy and matrix elements (see figure 4.10). The K=0 prolate band is predicted to the ground state band as the 0_2^+ and 2_3^+ are part of the oblate rotational band. A K=2 γ band is predicted with a 2_2^+ band head located below the 2_3^+ as experimentally proposed. A strong mixing of K=0 and K=2 components for the 2_2^+ and 2_3^+ states is obtained, as strong indication of triaxility. E0 transition strengths, $\rho^2(E0)$, are also compared (see figure 4.11). Calculated values are far from

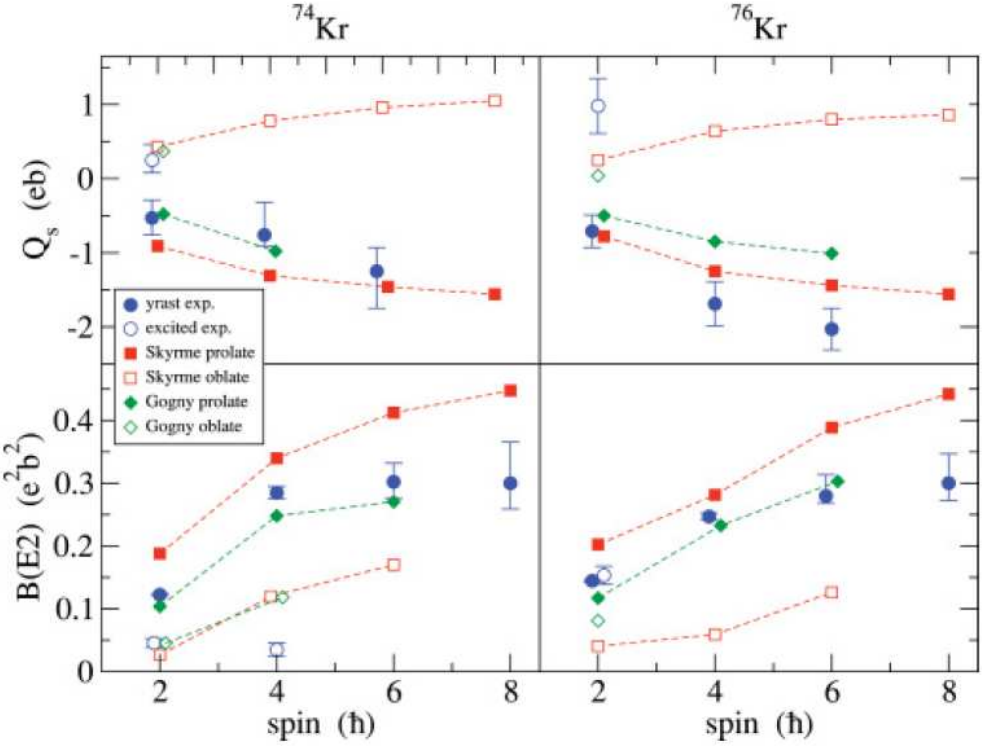

Figure 4.8: Experimental B(E2,↓) and $\mathcal{Q}_s$ compared to both Gogny D1S or Skyrme SLy6 calculations.

the experimental one. The reason is not yet established.

In [162], potential energy surfaces were published in details following the convincing comparison with the experimental spectroscopic data. As it can be seen, the potential energy surfaces using the Gogny GCM+GOA approach show two minima for prolate and oblate deformation. The J^π=0_1^+ projection shows a prolate minima in ^{76}Kr with an increased spread into the γ triaxial degree of freedom in ^{74}Kr and more axial oblate ground state in ^{72}Kr. It was therefore proposed a shape inversion at ^{74}Kr with a maximum triaxiality as suggested by the experimental data even if the oblate character of the ground state of ^{72}Kr is not yet firmly established. In the calculations, increasing the angular momentum leads to a narrow minimum in the wave function distribution with less γ-spread and increased axiality. This increased of axiality in the wave function is correlated to the increase of the measured B(E2) therefore reflecting a weaker mixing as proposed from the experimental data. One can finally notice that there is a shape change between spin 2 and 6 in ^{72}Kr which remains to be proven experimentally. Triaxility seems to be the key ingredient to reproduce the shape coexistence in Kr isotopes. Later on, the Skyrme calculations were developed. Mean-field states generated by triaxial quadrupole constraints that are projected on particle number and angular momentum and mixed by the generator coordinate method on the quadrupole moment were

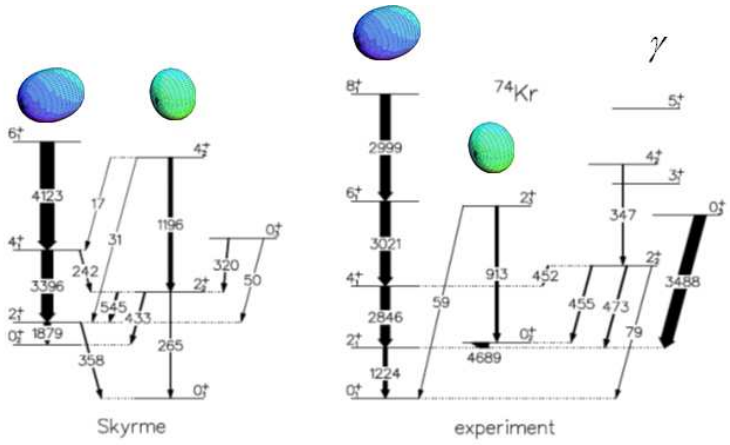

Figure 4.9: Level Scheme comparison between experimental data and Skyrme SLy6 calculations

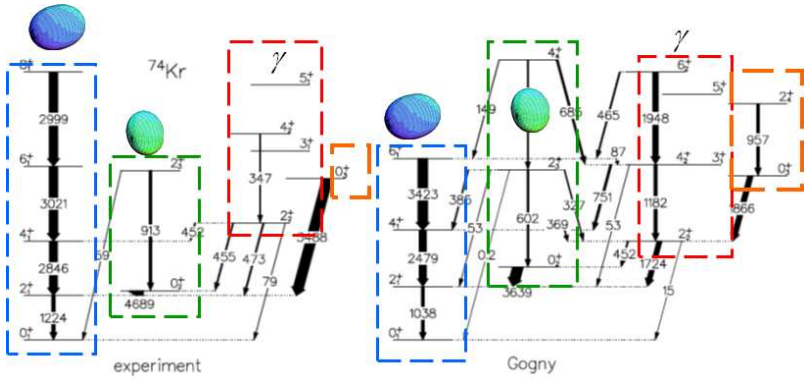

Figure 4.10: Level Scheme comparison between experimental data and Gogny D1S calculations

proposed in [163]. This method is equivalent to a seven-dimensional GCM calculations, mixing all five degrees of freedom of the quadrupole operator and the gauge angles for protons and neutrons. The deduced level schemes cancel the previous disagreement. When triaxiality is not authorized, the same results than the axial Skyrme are obtained suggesting that triaxiality seems to be the key to describe prolate-oblate shape coexistence in this region.

Large systematics for the Sr isotopes are not yet available due to the lack of experimental data. The B(E2) and excitation energy of the first 2^+ state are well reproduced by the calculations using the Gogny D1S interaction.

Along the N=Z, the calculations reproduce well the onset of collectivity between ^{68}Se and ^{76}Sr as shown in figure 4.5. The corresponding potential energy surfaces are also systematically calcu-

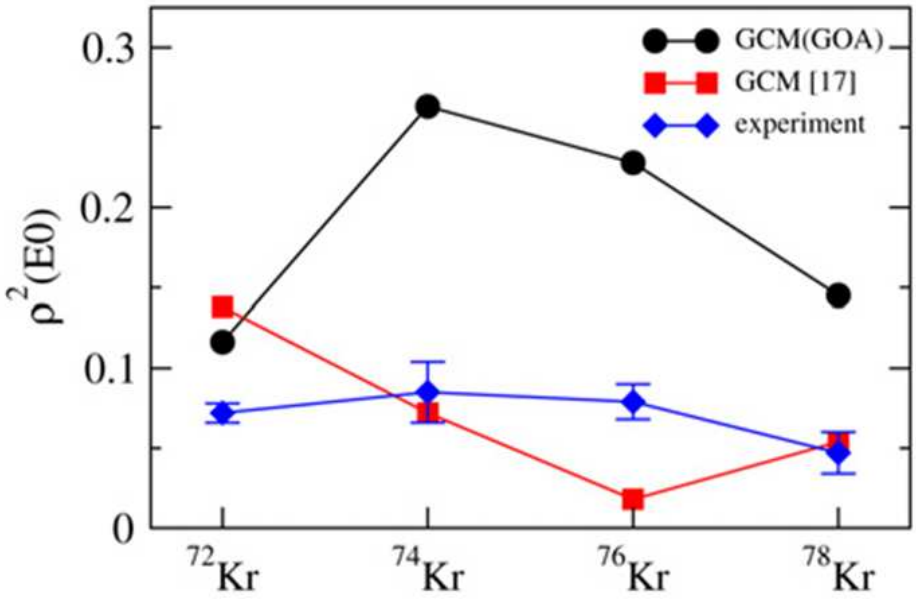

Figure 4.11: Theoretical (Gogny) and experimental E0 systematics. Figure from [162].

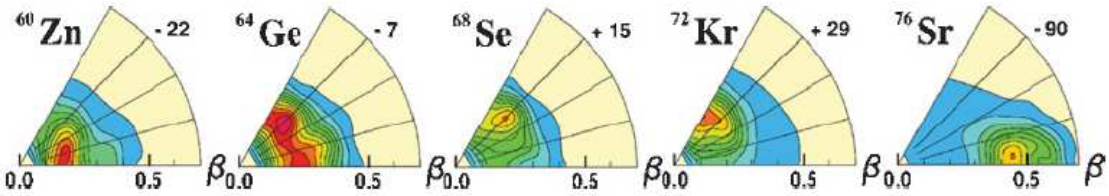

Figure 4.12: HFB potential energy surface for N=Z isotopes. Figure from [162].

lated for N=Z nuclei from ^{60}Zn to ^{76}Sr in the (β, γ) plan in [162]. Figure 4.12 shows an increased of axiallity toward the heaviest masses with a very triaxial and γ-soft minima for ^{64}Ge, a γ-soft oblate minima in ^{68}Se, more axial in ^{72}Kr as the ground state in ^{76}Sr has a large and axial prolate deformation. This increase of axialilty is associated to the increase of B(E2) experimentally observed and emphasizes the role of the degree of freedom in the mass region [148].

4.6.2 Shell Model calculations in Se, Kr, Sr and Zr isotopes

Mean field calculations have shown a remarkable agreement with experimental data. However, they do not provide a microscopical description. One could wonder for instance, if this clear onset of collectivity associated to axiality between Se and Sr is related to an increase in occupancy of a specific orbital for both proton and neutron. Shell model calculations can provide a more fundamental basis or quantitative influence of a specific orbital or valence space. However, there are severe limitations due to the large valence space needed for such calculations. Monte-Carlo Shell Model Calculations (MCSMC) could in principle be applied like in mass A=100 [8, 58], in the Ni chain [6] or in the light Hg isotopes [7]. However, this has never been done for N=Z nuclei.

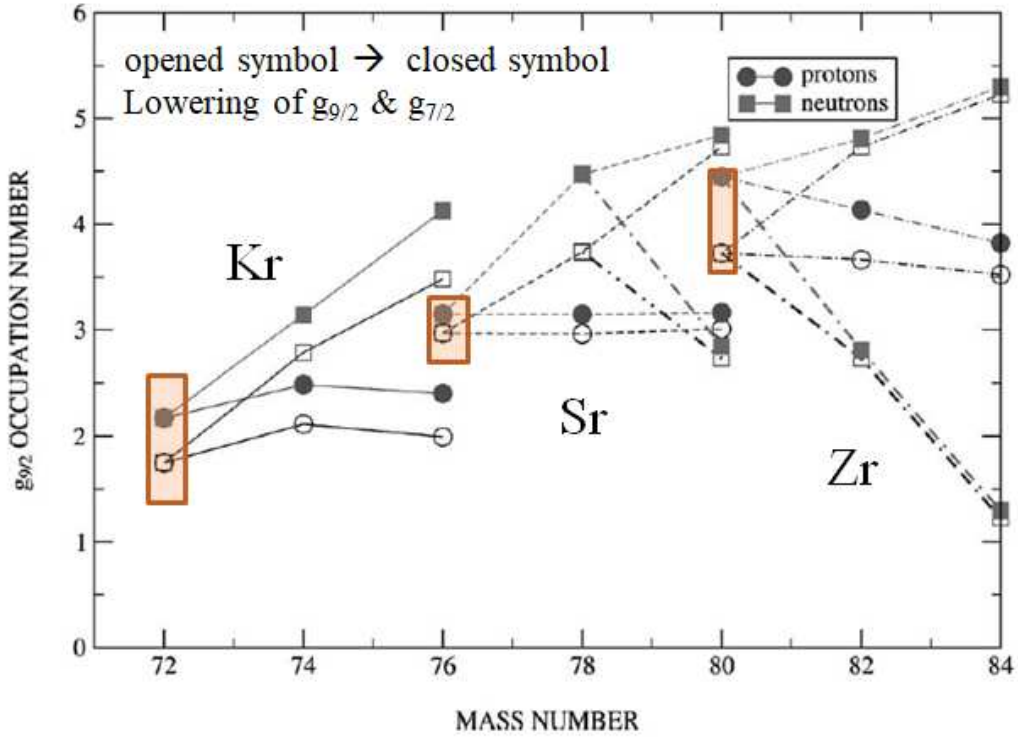

Figure 4.13: Theoretical $g_{9/2}$ occupancy systematics for Kr, Sr, and Zr isotopes. Figure from [164]

Few exact shell model calculations have been performed in truncated valence space and compared to experimental spectroscopic data. Shell model calculations have been performed by K. Langanke et al. with a complete $0f1p0g1d2s$ model space for Kr, Sr and Zr isotopes [164]. Only experimental B(E2; $2_1^+ \rightarrow 0_1^+$) are compared with the calculations and do not reproduce the onset of collectivity between ^{72}Kr and ^{76}Sr. In figure 4.13 taken from [164], the $g_{9/2}$ occupancy is shown for proton and neutron separately. N=Z nuclei are highlighted with brown squares. The increase of collectivity, in the calculations, from Kr to Zr, is correlated to an increase of the $g_{9/2}$ occupancy

for both proton and neutron. In the Kr chain, the neutron $g_{9/2}$ occupancy increases with mass as expected with a calculated shape change between ^{72}Kr and ^{76}Kr. The increased number of neutron in the $g_{9/2}$ favours the prolate deformation.

Later, M. Hasegawa et al. have performed calculations in a truncated $f_{5/2}p_{1/2}g_{9/2}d_{5/2}$ valence space (ie no active $p_{3/2}$) [165]. A strong p-n correlation is proposed since they occupy similar orbitals. Calculations are only available for N=Z nuclei. For the ground state bands, the level schemes are rather well reproduced for ^{68}Se and ^{72}Kr but the calculations underestimate the onset of collectivity in ^{76}Sr.

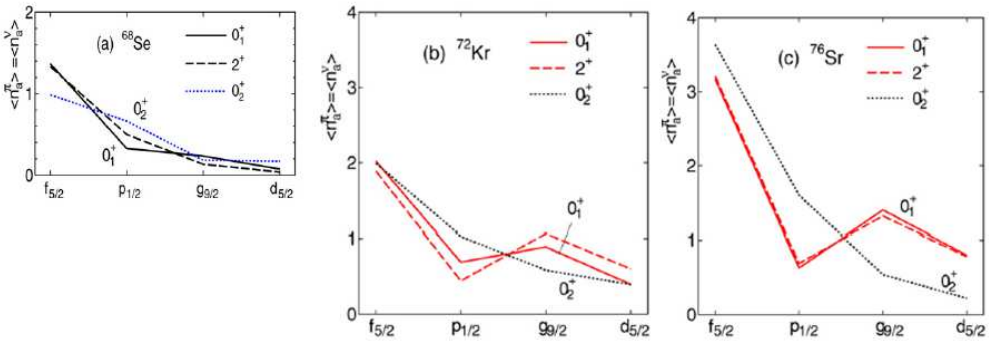

Figure 4.14: Theoretical N=Z isotopes orbits occupancies from [165]

The $f_{5/2}p_{1/2}g_{9/2}d_{5/2}$ occupancies, assuming that there are equal for proton and neutron, are shown for ^{68}Se, ^{72}Kr and ^{76}Sr in figure 4.14. It is known experimentally that ^{68}Se has a lower collectivity [154, 155]. In the calculations for ^{68}Se, the $g_{9/2}d_{5/2}$ occupancy is very low (~ 0.2) for the $0^+_{1,2}$ and 2^+_1 states, ie equivalent for both ground states band and excited configuration. One could speculate that this similarity favours large mixing and consequently lower collectivity. For ^{72}Kr and ^{76}Sr, the $f_{5/2}$ occupancy increases as expected. The $g_{9/2}d_{5/2}$ occupancy increases between ^{68}Se and (^{72}Kr,^{76}Sr) but remains still low (~ 1 particle) for the ground state band and ~ 0.5 particle for the 0^+_2. Contrary to ^{68}Se, there is a clear difference between the ground states band and the excited configuration which could reduce the mixing inducing a more clear shape coexistence scenario with two 0^+ states. The increase by a factor 2 of the experimental B(E2)'s between ^{68}Se and ^{72}Kr is reproduced supporting the contribution of the $g_{9/2}$ orbital. Experimentally, there is a second step by a factor 2 between ^{72}Kr and ^{76}Sr in B(E2) which is also reproduced in the calculation associated to a small increase of the $g_{9/2}$ occupation (~ 0.5 particle).

More recent shell model calculations using the JUN45 and the LNPS interactions have been performed by B. Bounthong in [166]. In the calculations, the B(E2; $2^+_1 \rightarrow 0^+_1$) increases by only 20% between ^{72}Kr and ^{76}Sr as the $g_{9/2}$ occupation remains almost identical, supporting again the role of this orbital in the collectivity of the N=Z nuclei.

In summary, some shell model calculations have investigated the 2^+ state in N=Z nuclei and in the Kr, Sr and Zr chain leading to incomplete conclusions. The Kr chain remains the case where

lot of experimental informations are known (energies, B(E2)'s, g-factors, Qs) and should be an ideal case for SM-like calculations to investigate the microscopical origin of the shape evolution in this mass region. Mean-field calculations work well but only highlight the role of the triaxial degree of freedom. Shell model calculations which should provide a more microscopical description are scare and very limited in their comparison with experimental data but highlight the role of the $g_{9/2}$ orbital.

4.7 Conclusions

For the future, several systematics are needed :

- The Kr case remains unique a decade after the publication of the present results. Post-accelerated radioactive beam of Se, Sr and possibly Zr are of great interest. Especially $^{74-70}$Se, ^{72}Kr and $^{76-80}$Sr beams must be Coulomb excited to provide similar set of E2 matrix element as for the Kr case. These will provide a systematic of the shape evolution and mixing along the N=Z line.
- 0_2^+ states remain unknown in $^{68-70}$Se, ^{76,78}Sr.
- Yrast band's B(E2) have been measured at very low spin up to ^{72}Kr, ^{68}Se, ^{76}Sr.
- no non-yrast E2 matrix elements is known in these isotopes.
- There is a lack of spectroscopic quadrupole moment in the ground state beyond Sr and long-lived isomeric states (particularly $9/2^{+m}$ state) in odd-masses by laser spectroscopy.

The electromagnetic probe provides a shape description and possible link between them. However, it does not provide any direct experimental contribution to the microscopical description in particular the role of the $g_{9/2}$ orbit. Direct nucleon transfer reactions are the standard technique to identify effective single particle energy and occupancy number. Direct reaction such as (d,p) or (d,^3He) to probe neutron and proton orbits were never attempted in these isotopes. Furthermore, similarly to the A$\sim$100 region (see chapter II), two nucleon transfer to probe pair excitation origin across the gap 40 are not yet reachable. Two proton transfer from Mo or Zr isotopes to probe the multi pair excitation across Z=40 would have a significant impact in the shape coexistence scenario description. However, the shape identification (prolate or oblate) in the daughter nuclei must be identified first by safe Coulomb excitation. Two neutrons transfer from ^{74}Kr to ^{72}Kr would also give more insight in the shape inversion. Single nucleon transfer would be the cornerstone of these studies to tentatively match the shape inversion and mixing with a microscopical description.

Partie V

Conclusion

Conclusion

The study of the shape coexistence at the 40 sub-shell closure was revolutionized in the last decade thanks to the availability of new instruments, new accelerators, the re-born of relevant experimental techniques and the Monte-Carlo Shell Model Calculations. Shape coexistence remains a spectacular effect in nuclear structure involving strong proton-neutron quadrupole correlation and pairing against the sub-shells gap. The cross comparison between experimental data from in-beam data and laser spectroscopy brings the pieces for a global understanding. Comparison with theoretical calculations remains today partial. Around the 40 sub-shell closure, large set of experimental data can be used as benchmark for large scale comparisons.

In this manuscript, I have reviewed the state-of-the-art of the shape coexistence phenomena involving the sub-shell closure 40 in three mass regions with N=40 around ^{68}Ni, with Z$\sim$40 in neutron rich isotopes with A$\sim$100 and in self-conjugated nuclei with N$\sim$Z$\sim$40. The two later have benefited in the recent years of experimental results using post-accelerated radioactive ions beam for Coulomb excitation and single nucleon transfer. The Coulomb excitation technique gives access to the spectroscopic quadrupole moment. This is a major step in the description of the shape coexistence in these mass region and reinforces the relevance of the comparison with the most advanced theoretical models. In this manuscript, a particular care was taken in bringing together the different probes such as spin/parity and spectroscopic quadrupole moment from laser spectroscopy in the ground state and the isomers, Coulomb excitation, lifetime measurements, nucleon transfer, E0 spectroscopy and β-decay. The three mass regions have very different level of description.

It is clear that the A$\sim$100 region is characterized by a large amount of experimental data with all techniques showing a clear coherence. Nothing unexpected arise so far. The MCSMC have described for the first time the microscopical mechanism. However, few questions remain. The N=59 isotone evolution as a function of the proton number from Ru to Kr would highlight the role of pairing and proton occupancy. The microscopical description of the Kr isotopes should explain why the offset of deformation is delayed and smoother. Even if the agreement between the MCSMC and some experimental data is remarkable, a global comparison with all spectroscopy data would push forward the constrains to the models. The microscopical description reproduces well the data but this particle-hole scheme coupled to intruder orbital is not experimentally verified. Contrary to the N$\sim$Z nuclei, the agreement between the mean-field calculations and the experimental data is not as good.

In the N$\sim$Z nuclei, large set of experimental data are available for excited states until the Kr isotopes. Clearly, there is a lack of experimental data in the elements from Sr and for all elements in the ground state using laser spectroscopy to draw a global experimental picture. In addition,

these nuclei have never been investigated by direct reaction. The agreement between spectroscopic data and the mean-field calculation is remarkable. Microscopical description using conventional or MCSMC have not reached the level of accuracy obtained in the A∼100 region. Further studies using shell models calculations are the next millestone.

Around ^{68}Ni, the level scheme have been recently clarified. Shell model calculations using conventional approached (LNPS) or Monte-Carlo give a remarkable agreement with the proposed level scheme and first B(E2). The lack of experimental data such spectroscopic quadrupole moments in excited or ground states limits the comparison. The absence of data using laser spectroscopy is evidenced. Similarly to the A∼100 region, the proposed microscopical description is not experimentally verified and systematics studies by direct reaction are needed.

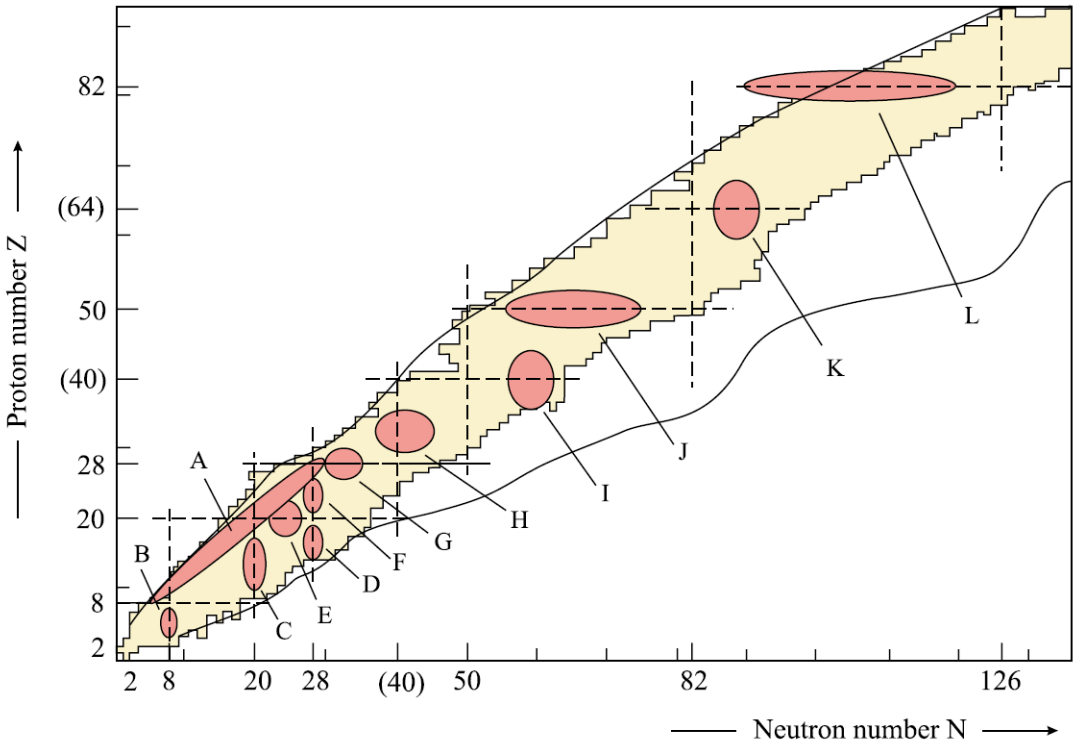

Figure 4.15: Experimentally established area of shape coexistence. Figure from [1]

In figure 4.15, the archipelago of experimentally proven shape coexistence area is shown. In many aspects, the shape coexistence in A∼100 and around ^{68}Ni follow the mechanism proposed by K. Heyde and collaborators without any surprises. All new experimental data are successfully compared to state-to-the-art calculations which reinforce the statements of [1]. So far, along the nuclear chart, the shape coexistence area can be characterized by this mechanism and experimen-

tally proven shape coexistence close to closed shells which do not follow this picture are scarce (see for instance ^{80}Ge [15]). However, the N∼Z nuclei around mass A=80 should draw a particular attention. Indeed, as discussed in this manuscript, they do not really follow this description and should attract the future experimental and theoretical works.

This universal mechanism was never used to predict new area of shape coexistence. Global calculations in the mean-field approach are available and can be used to predict the next area of shape coexistence. In [167], P. Möller proposed a global survey of the phenomena. In figure 4.16 from [167], the number of minima in the potential energy surface is shown for a given nucleus as soon as the depth is greater than 200 keV and its excitation energy lower than 2 MeV. Beyond Z=20, areas with a second minimum overlap very well the figure 4.15. New areas of shape coexistence are predicted in very neutron rich Sn isotopes around N=100 and in super heavy elements around Z=100.

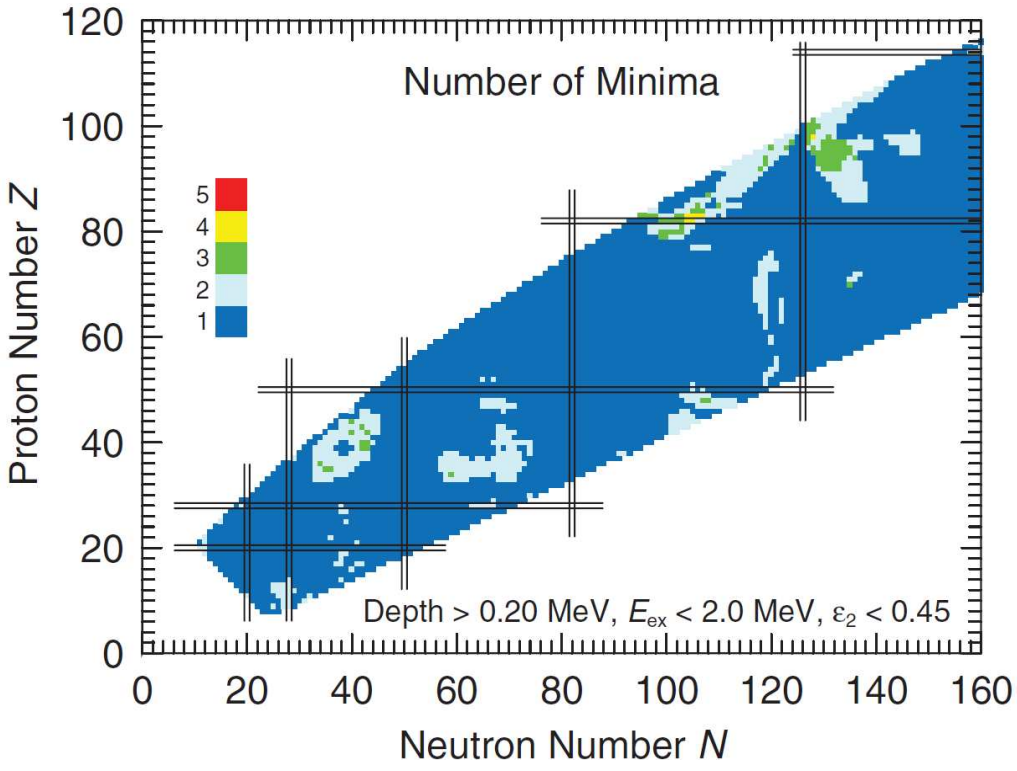

Figure 4.16: The shape coexistence archipelo: calculated number of minima in the potential energy surface of even-even nuclei. Figure from [167].

Similar comparison can be done using the Gogny D1S interaction using the published calculations from [168]. In figure 4.17, stable nuclei are represented with large blue squares. Nuclei indicated with a brown square have a second 0^+ state with an excitation energy below 1.0 MeV and a degree of triaxiality lower than $\gamma = 30$ degrees. Below Z=28, 0_2^+ states are calculated close to

2 MeV. From Ni isotopes, the calculations overlap very well the figure 4.15. Similarly, next area of shape coexistence in the vicinity of the closed Z=50 and Z=82 proton shells are predicted for very neutron rich isotopes. In the Sn isotopes, 0_2^+ at about 0.9 MeV excitation energy are expected in $^{146-150}$Sn. In Pb isotopes, shape isomer at 0.5 MeV excitation energy are predicted in $^{224-230}$Pb. Finally, several areas are anticipated in the super heavy elements in very neutron rich Fm-No isotopes. In the scheme proposed by K. Heyde, the Sn and Pb isotopes can be anticipated. Indeed, the N=100 shell closure lies between the $1h_{9/2}$ and $2f_{5/2}$ neutron orbital. With proton promoted from the $1g_{9/2}$ to $1g_{7/2}$, the p-n interaction is similar to the mass A$\sim$100 region.
One can also notice than both calculations do not predict an area of shape coexistence near ^{78}Ni as proposed in ^{80}Ge [15].

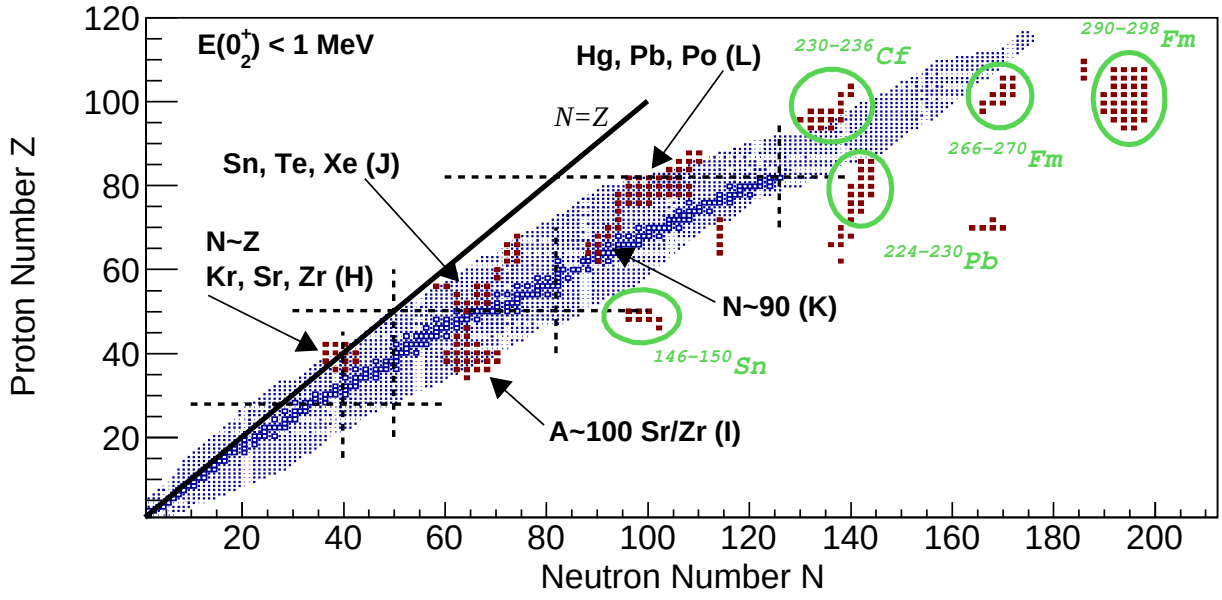

Figure 4.17: The shape coexistence archipelo: calculated low lying 0^+ states in even-even nuclei. Figure from[168].

So far the shape coexistence in atomic nuclei was theoretically investigated by effective theories. In a longer perspectives, with the development of $Ab-Initio$ calculations, one could wonder if the phenomenom and its present effective description emerge naturally from the $first-principles$?

Bibliography

[1] Kris Heyde and John L. Wood. Shape coexistence in atomic nuclei. *Rev. Mod. Phys.*, 83:1467–1521, Nov 2011.

[2] E. Caurier, F. Nowacki, and A. Poves. The shell closure; from to the neutron drip line. *Nuclear Physics A*, 742:14 – 26, 2004.

[3] D. Pauwels et al. Pairing-excitation versus intruder states in ^{68}Ni and ^{90}Zr. *Phys. Rev. C*, 82:027304, Aug 2010.

[4] W. Nazarewicz. Variety of shapes in the mercury and lead isotopes. *Physics Letters B*, 305(3):195 – 201, 1993.

[5] T. Togashi, Y. Tsunoda, T. Otsuka, and N. Shimizu. Quantum phase transition in the shape of zr isotopes. *arXiv:1606.09056 [nucl-th]*, 2016.

[6] Y. Tsunoda, T. Otsuka, N. Shimizu, M. Honma, and Y. Utsuno. Novel shape evolution in exotic ni isotopes and configuration-dependent shell structure. *Phys.Rev. C*, 89:031301, 2014.

[7] B. Marsh et al. Characterization of the shape-staggering effect in mercury nuclei. *Nature Physics*, 2018.

[8] Purnima Singh, W. Korten, T. W. Hagen, A. Görgen, L. Grente, M.-D. Salsac, F. Farget, E. Clément, G. de France, T. Braunroth, B. Bruyneel, I. Celikovic, O. Delaune, A. Dewald, A. Dijon, J.-P. Delaroche, M. Girod, M. Hackstein, B. Jacquot, J. Libert, J. Litzinger, J. Ljungvall, C. Louchart, A. Gottardo, C. Michelagnoli, C. Müller-Gatermann, D. R. Napoli, T. Otsuka, N. Pillet, F. Recchia, W. Rother, E. Sahin, S. Siem, B. Sulignano, T. Togashi, Y. Tsunoda, Ch. Theisen, and J. J. Valiente-Dobon. Evidence for coexisting shapes through lifetime measurements in ^{98}Zr. *Phys. Rev. Lett.*, 121:192501, Nov 2018.

[9] E. Clément et al. Shape coexistence in neutron-deficient krypton isotopes. *Phys. Rev. C*, 75:054313, May 2007.

[10] E. Clément et al. Spectroscopic quadrupole moments in ^{96,98}Sr: Evidence for shape coexistence in neutron-rich strontium isotopes at $n = 60$. *Phys. Rev. Lett.*, 116:022701, Jan 2016.

[11] E. Clément, M. Zielińska, S. Péru, H. Goutte, S. Hilaire, A. Görgen, W. Korten, D. T. Doherty, B. Bastin, C. Bauer, A. Blazhev, N. Bree, B. Bruyneel, P. A. Butler, J. Butterworth, J. Cederkäll, P. Delahaye, A. Dijon, A. Ekström, C. Fitzpatrick, C. Fransen, G. Georgiev,

R. Gernhäuser, H. Hess, J. Iwanicki, D. G. Jenkins, A. C. Larsen, J. Ljungvall, R. Lutter, P. Marley, K. Moschner, P. J. Napiorkowski, J. Pakarinen, A. Petts, P. Reiter, T. Renstrøm, M. Seidlitz, B. Siebeck, S. Siem, C. Sotty, J. Srebrny, I. Stefanescu, G. M. Tveten, J. Van de Walle, M. Vermeulen, D. Voulot, N. Warr, F. Wenander, A. Wiens, H. De Witte, and K. Wrzosek-Lipska. Low-energy coulomb excitation of ^{96,98}Sr beams. *Phys. Rev. C*, 94:054326, Nov 2016.

[12] N. Bree et al. Shape coexistence in the neutron-deficient even-even $^{182-188}hg$ isotopes studied via coulomb excitation. *Phys. Rev. Lett.*, 112:162701, Apr 2014.

[13] S. Cruz, P.C. Bender, R. Krcken, K. Wimmer, F. Ames, C. Andreoiu, R.A.E. Austin, C.S. Bancroft, R. Braid, T. Bruhn, W.N. Catford, A. Cheeseman, A. Chester, D.S. Cross, C.Aa. Diget, T. Drake, A.B. Garnsworthy, G. Hackman, R. Kanungo, A. Knapton, W. Korten, K. Kuhn, J. Lassen, R. Laxdal, M. Marchetto, A. Matta, D. Miller, M. Moukaddam, N.A. Orr, N. Sachmpazidi, A. Sanetullaev, C.E. Svensson, N. Terpstra, C. Unsworth, and P.J. Voss. Shape coexistence and mixing of low-lying 0+ states in 96sr. *Physics Letters B*, 786:94 – 99, 2018.

[14] K. Hadyńska-Klęk, P. J. Napiorkowski, M. Zielińska, J. Srebrny, A. Maj, F. Azaiez, J. J. Valiente Dobón, M. Kici ńska Habior, F. Nowacki, H. Naïdja, B. Bounthong, T. R. Rodríguez, G. de Angelis, T. Abraham, G. Anil Kumar, D. Bazzacco, M. Bellato, D. Bortolato, P. Bednarczyk, G. Benzoni, L. Berti, B. Birkenbach, B. Bruyneel, S. Brambilla, F. Camera, J. Chavas, B. Cederwall, L. Charles, M. Ciemała, P. Cocconi, P. Coleman-Smith, A. Colombo, A. Corsi, F. C. L. Crespi, D. M. Cullen, A. Czermak, P. Désesquelles, D. T. Doherty, B. Dulny, J. Eberth, E. Farnea, B. Fornal, S. Franchoo, A. Gadea, A. Giaz, A. Gottardo, X. Grave, J. Grębosz, A. Görgen, M. Gulmini, T. Habermann, H. Hess, R. Isocrate, J. Iwanicki, G. Jaworski, D. S. Judson, A. Jungclaus, N. Karkour, M. Kmiecik, D. Karpiński, M. Kisieliński, N. Kondratyev, A. Korichi, M. Komorowska, M. Kowalczyk, W. Korten, M. Krzysiek, G. Lehaut, S. Leoni, J. Ljungvall, A. Lopez-Martens, S. Lunardi, G. Maron, K. Mazurek, R. Menegazzo, D. Mengoni, E. Merchán, W. Męczyński, C. Michelagnoli, B. Million, S. Myalski, D. R. Napoli, M. Niikura, A. Obertelli, S. F. Özmen, M. Palacz, L. Próchniak, A. Pullia, B. Quintana, G. Rampazzo, F. Recchia, N. Redon, P. Reiter, D. Rosso, K. Rusek, E. Sahin, M.-D. Salsac, P.-A. Söderström, I. Stefan, O. Stézowski, J. Styczeń, Ch. Theisen, N. Toniolo, C. A. Ur, R. Wadsworth, B. Wasilewska, A. Wiens, J. L. Wood, K. Wrzosek-Lipska, and M. Zięblíński. Quadrupole collectivity in ^{42}Ca from low-energy coulomb excitation with agata. *Phys. Rev. C*, 97:024326, Feb 2018.

[15] A. Gottardo, D. Verney, C. Delafosse, F. Ibrahim, B. Roussière, C. Sotty, S. Roccia, C. Andreoiu, C. Costache, M.-C. Delattre, I. Deloncle, A. Etilé, S. Franchoo, C. Gaulard, J. Guillot, M. Lebois, M. MacCormick, N. Marginean, R. Marginean, I. Matea, C. Mihai, I. Mitu, L. Olivier, C. Portail, L. Qi, L. Stan, D. Testov, J. Wilson, and D. T. Yordanov. First evidence of shape coexistence in the ^{78}Ni region: Intruder 0_2^+ state in ^{80}Ge. *Phys. Rev. Lett.*, 116:182501, May 2016.

[16] D. Rudolph, C. Baktash, M. J. Brinkman, E. Caurier, D. J. Dean, M. Devlin, J. Dobaczewski, P.-H. Heenen, H.-Q. Jin, D. R. LaFosse, W. Nazarewicz, F. Nowacki, A. Poves, L. L. Riedinger, D. G. Sarantites, W. Satuła, and C.-H. Yu. Rotational bands in the doubly magic nucleus ^{56}ni. *Phys. Rev. Lett.*, 82:3763–3766, May 1999.

[17] R. Taniuchi et al. 78ni revealed as a doubly magic stronghold against nuclear deformation. *Nature*, 569:53–58, 2019.

[18] T. Kühl, P. Dabkiewicz, C. Duke, H. Fischer, H. J. Kluge, H. Kremmling, and E. W. Otten. Nuclear shape staggering in very neutron-deficient hg isotopes detected by laser spectroscopy. *Phys. Rev. Lett.*, 39:180–183, Jul 1977.

[19] J. Bonn, G. Huber, H.-J. Kluge, L. Kugler, and E.W. Otten. Sudden change in the nuclear charge distribution of very light mercury isotopes. *Physics Letters B*, 38(5):308 – 311, 1972.

[20] A. N Andreyev et al. A triplet of differently shaped spin-zero states in the atomic nucleus 186pb. *Nature*, 405:430.

[21] P. Van Duppen, E. Coenen, K. Deneffe, M. Huyse, K. Heyde, and P. Van Isacker. Observation of low-lying $J^\pi = 0^+$ states in the single-closed-shell nuclei $^{192-198}$Pb. *Phys. Rev. Lett.*, 52:1974–1977, May 1984.

[22] E. Bouchez et al. New shape isomer in the self-conjugate nucleus ^{72}Kr. *Phys. Rev. Lett.*, 90:082502, Feb 2003.

[23] K. Kawade et al. Excited 0+-levels in98zr. *Zeitschrift für Physik A Atoms and Nuclei*, 304(4):293–299, 1982.

[24] G. Lhersonneau et al. Evolution of deformation in the neutron-rich zr region from excited intruder state to the ground state. *Phys. Rev. C*, 49:1379–1390, Mar 1994.

[25] F. Schussler et al. Discovery of a very low-lying 0+ state in 98sr and shape coexistence implication in 98sr. *Nucl. Phys. A*, 339(3):415 – 428, 1980.

[26] K. Heyde and R. A. Meyer. Monopole strength as a measure of nuclear shape mixing. *Phys. Rev. C*, 37:2170–2175, May 1988.

[27] R. Bengtsson. Some results from potential energy surface calculations for nuclei in the mass 70–80 region. In Jürgen Eberth, Richard A. Meyer, and Kornelius Sistemich, editors, *Nuclear Structure of the Zirconium Region*, pages 17–25, Berlin, Heidelberg, 1988. Springer Berlin Heidelberg.

[28] N.S. Kelsall *et al. Phys. Rev. C*, **64**:024309, 2001.

[29] A. Algora *et al. Phys. Rev. C*, **61**:031303(R), 2000.

[30] J. Döring *et al. Phys. Rev. C*, **52**:R2284, 1995.

[31] H. Sun *et al. Phys. Rev. C*, **59**:655, 1999.

[32] A. Görgen, E. Clément, A. Chatillon, A. Dewald, W. Korten, Y. Le Coz, N. Mărginean, B. Melon, R. Menegazzo, O. Möller, Ch. Theisen, D. Tonev, C. A. Ur, and K. O. Zell. Lifetime measurement in 74kr and 76kr. *The European Physical Journal A - Hadrons and Nuclei*, 26(2):153–157, Nov 2005.

[33] J. Simpson, F. Azaiez, G. DeFrance, J. Fouan, J. Gerl, R. Julin, W. Korten, P. J. Nolan, B. Nyakó, G. Sletten, and P. M. Walker. The exogam array: A radioactive beam gamma-ray spectrometer. *Acta Physica Hungarica, Series A: Heavy Ion Physics*, 11(1-2):159–188, 2000.

[34] N. Warr, J. Van de Walle, M. Albers, F. Ames, B. Bastin, C. Bauer, V. Bildstein, A. Blazhev, S. Bönig, N. Bree, B. Bruyneel, P. A. Butler, J. Cederkäll, E. Clément, T. E. Cocolios, T. Davinson, H. De Witte, P. Delahaye, D. D. DiJulio, J. Diriken, J. Eberth, A. Ekström, J. Elseviers, S. Emhofer, D. V. Fedorov, V. N. Fedosseev, S. Franchoo, C. Fransen, L. P. Gaffney, J. Gerl, G. Georgiev, R. Gernhäuser, T. Grahn, D. Habs, H. Hess, A. M. Hurst, M. Huyse, O. Ivanov, J. Iwanicki, D. G. Jenkins, J. Jolie, N. Kesteloot, O. Kester, U. Köster, M. Krauth, T. Kröll, R. Krücken, M. Lauer, J. Leske, K. P. Lieb, R. Lutter, L. Maier, B. A. Marsh, D. Mücher, M. Münch, O. Niedermaier, J. Pakarinen, M. Pantea, G. Pascovici, N. Patronis, D. Pauwels, A. Petts, N. Pietralla, R. Raabe, E. Rapisarda, P. Reiter, A. Richter, O. Schaile, M. Scheck, H. Scheit, G. Schrieder, D. Schwalm, M. Seidlitz, M. Seliverstov, T. Sieber, H. Simon, K. H. Speidel, C. Stahl, I. Stefanescu, P. G. Thirolf, H. G. Thomas, M. Thürauf, P. Van Duppen, D. Voulot, R. Wadsworth, G. Walter, D. Weißhaar, F. Wenander, A. Wiens, K. Wimmer, B. H. Wolf, P. J. Woods, K. Wrzosek-Lipska, and K. O. Zell. The miniball spectrometer. *The European Physical Journal A*, 49(3):40, Mar 2013.

[35] C.E. Svensson, G. Hackman, C.J. Pearson, M.A. Schumaker, H.C. Scraggs, M.B. Smith, C. Andreoiu, A. Andreyev, R.A.E. Austin, G.C. Ball, A.J. Boston, R.S. Chakrawarthy, R. Churchman, N. Cowan, T.E. Drake, P. Finlay, P.E. Garrett, G.F. Grinyer, B. Hyland, B. Jones, J.P. Martin, A.C. Morton, A.A. Phillips, R. Roy, F. Sarazin, N. Starinsky, J.J. Valiente-Dobn, J.C. Waddington, and L.M. Watters. Position sensitivity of the tigress 32-fold segmented hpge clover detector. *Nuclear Instruments and Methods in Physics Research Section A: Accelerators, Spectrometers, Detectors and Associated Equipment*, 540(2):348 – 360, 2005.

[36] K. Alder and A. Winther. The theory of coulomb excitation of nuclei. *Phys. Rev.*, 91:1578–1579, Sep 1953.

[37] K. Alder and A. Winther. Theory of coulomb excitation. *Phys. Rev.*, 96:237–238, Oct 1954.

[38] K. Alder and A. Winter. *Theory of Coulomb excitation with Heavy ions.* North Holland, Amsterdam, 1974.

[39] Douglas Cline. Nuclear shapes studied by coulomb excitation. *Ann. Rev. of Nucl. and Part. Sc.*, 36:683–716, 1986.

[40] T. Czosnyka, D. Cline, and C. Y. Wu. *Bull. Am. Phys. Soc.*, 28:745, 1983.

[41] M. Zielińska, L. P. Gaffney, K. Wrzosek-Lipska, E. Clément, T. Grahn, N. Kesteloot, P. Napiorkowski, J. Pakarinen, P. Van Duppen, and N. Warr. Analysis methods of safe coulomb-excitation experiments with radioactive ion beams using the gosia code. *The European Physical Journal A*, 52(4):1–14, 2016.

[42] K. Heyde, J. Jolie, J. Moreau, J. Ryckebusch, M. Waroquier, P. Van Duppen, M. Huyse, and J.L. Wood. A shell-model description of 0+ intruder states in even-even nuclei. *Nuclear Physics A*, 466(2):189 – 226, 1987.

[43] A. P. Zuker, J. Retamosa, A. Poves, and E. Caurier. *Phys. Rev. C*, 52:R1741–R1745, Oct 1995.

[44] A. P. Zuker, A. Poves, F. Nowacki, and S. M. Lenzi. *Phys. Rev. C*, 92:024320, Aug 2015.

[45] A. Dewald et al. The differential plunger and the differential decay curve method for the analysis of recoil distance doppler-shift data. *Zeitschrift für Physik A Atomic Nuclei*, 334(2):163–175, 1989.

[46] P. Campbell, I.D. Moore, and M.R. Pearson. Laser spectroscopy for nuclear structure physics. *Progress in Particle and Nuclear Physics*, 86:127 – 180, 2016.

[47] Emmanuel Clément. *Shape coexistence in neutron-deficient Krypton and Selenium isotopes studied by low-energy Coulomb excitation of radioactive ion beams.* Theses, Université Paris Sud - Paris XI, June 2006.

[48] Aurore Dijon. *Evolution of the Collectivity around 68Ni : role of intruder states.* Theses, Université de Caen, July 2012.

[49] Igor Celikovic. *Nuclear structure around doubly-magic nuclei : lifetime measurements in the vicinity of 68Ni and search for isomers around 100Sn.* Theses, Université de Caen, July 2013.

[50] E. Clément et al. Conceptual design of the agata 1$\breve{0}$3c0 array at ganil. *Nucl. Inst. Meth. Phys. Res. A*, 855:1 – 12, 2017.

[51] S. Akkoyun et al. Agata advanced {GAmma} tracking array. *Nucl. Inst. Meth. Phys. Res. A*, 668:26 – 58, 2012.

[52] Sven A.E. Johansson. Gamma de-excitation of fission fragments: (ii). delayed radiation. *Nuclear Physics*, 64(1):147 – 160, 1965.

[53] G. Audi et al. The ame2012 atomic mass evaluation. *Chinese Physics C*, 36(12):1287, 2012.

[54] S. Naimi et al. Critical-point boundary for the nuclear quantum phase transition near a=100 from mass measurements of 96,97kr. *Phys. Rev. Lett.*, 105:032502, Jul 2010.

[55] M. Albers et al. Evidence for a smooth onset of deformation in the neutron-rich kr isotopes. *Phys. Rev. Lett.*, 108:062701, Feb 2012.

[56] F. Flavigny, P. Doornenbal, A. Obertelli, J.-P. Delaroche, M. Girod, J. Libert, T. R. Rodriguez, G. Authelet, H. Baba, D. Calvet, F. Château, S. Chen, A. Corsi, A. Delbart, J.-M. Gheller, A. Giganon, A. Gillibert, V. Lapoux, T. Motobayashi, M. Niikura, N. Paul, J.-Y. Roussé, H. Sakurai, C. Santamaria, D. Steppenbeck, R. Taniuchi, T. Uesaka, T. Ando, T. Arici, A. Blazhev, F. Browne, A. Bruce, R. Carroll, L. X. Chung, M. L. Cortés, M. Dewald, B. Ding, S. Franchoo, M. Górska, A. Gottardo, A. Jungclaus, J. Lee, M. Lettmann, B. D. Linh, J. Liu, Z. Liu, C. Lizarazo, S. Momiyama, K. Moschner, S. Nagamine, N. Nakatsuka, C. Nita, C. R. Nobs, L. Olivier, R. Orlandi, Z. Patel, Zs. Podolyák, M. Rudigier, T. Saito, C. Shand, P. A. Söderström, I. Stefan, V. Vaquero, V. Werner, K. Wimmer, and Z. Xu. Shape evolution in neutron-rich krypton isotopes beyond $n = 60$: First spectroscopy of ^{98,100}Kr. *Phys. Rev. Lett.*, 118:242501, Jun 2017.

[57] J. Dudouet, A. Lemasson, G. Duchêne, M. Rejmund, E. Clément, C. Michelagnoli, F. Didierjean, A. Korichi, G. Maquart, O. Stezowski, C. Lizarazo, R. M. Pérez-Vidal, C. Andreoiu, G. de Angelis, A. Astier, C. Delafosse, I. Deloncle, Z. Dombradi, G. de France,

A. Gadea, A. Gottardo, B. Jacquot, P. Jones, T. Konstantinopoulos, I. Kuti, F. Le Blanc, S. M. Lenzi, G. Li, R. Lozeva, B. Million, D. R. Napoli, A. Navin, C. M. Petrache, N. Pietralla, D. Ralet, M. Ramdhane, N. Redon, C. Schmitt, D. Sohler, D. Verney, D. Barrientos, B. Birkenbach, I. Burrows, L. Charles, J. Collado, D. M. Cullen, P. Désesquelles, C. Domingo Pardo, V. González, L. Harkness-Brennan, H. Hess, D. S. Judson, M. Karolak, W. Korten, M. Labiche, J. Ljungvall, R. Menegazzo, D. Mengoni, A. Pullia, F. Recchia, P. Reiter, M. D. Salsac, E. Sanchis, Ch. Theisen, J. J. Valiente-Dobón, and M. Zielińska. $^{96}_{36}\mathrm{Kr}_{60}$–low-$z$ boundary of the island of deformation at $n = 60$. *Phys. Rev. Lett.*, 118:162501, Apr 2017.

[58] Tomoaki Togashi, Yusuke Tsunoda, Takaharu Otsuka, and Noritaka Shimizu. Quantum phase transition in the shape of zr isotopes. *Phys. Rev. Lett.*, 117:172502, Oct 2016.

[59] H. Mach et al. Retardation of b(e2; 01+ 21+) rates in 9096sr and strong subshell closure effects in the a 100 region. *Nucl. Phys. A*, 523(2):197 – 227, 1991.

[60] G. Jung et al. Gamma-gamma angular correlations of transitions in sr94 and sr96. *Phys. Rev. C*, 22:252–263, Jul 1980.

[61] H. Mach et al. Deformation and shape coexistence of 0+ states in 98sr and 100zr. *Phy. Lett. B*, 230:21 – 26, 1989.

[62] H. Ohm et al. The ground-state deformation of ^{98}sr. *Z.Phys.*, A327:483, 1987.

[63] H. Mach et al. A method for picosecond lifetime measurements for neutron-rich nuclei: (1) outline of the method. *Nucl. Inst. and Meth. A*, 280(1):49 – 72, 1989.

[64] G. Lhersonneau et al. A k=3 two-quasiparticle isomer in 98sr. *Phys. Rev. C*, 65:024318, Jan 2002.

[65] A. G. Smith et al. Spin-dependent triaxial deformation in neutron-rich mo isotopes. *Phys. Rev. Lett.*, 77:1711–1714, Aug 1996.

[66] A. G. Smith et al. Lifetime measurements and nuclear deformation in the a≈100 region. *Phys. Rev. C*, 86:014321, Jul 2012.

[67] J. Park et al. Shape coexistence and evolution in ^{98}Sr. *Phys. Rev. C*, 93:014315, Jan 2016.

[68] E. Clément, M. Zielińska, A. Görgen, W. Korten, S. Péru, J. Libert, H. Goutte, S. Hilaire, B. Bastin, C. Bauer, A. Blazhev, N. Bree, B. Bruyneel, P. A. Butler, J. Butterworth, P. Delahaye, A. Dijon, D. T. Doherty, A. Ekström, C. Fitzpatrick, C. Fransen, G. Georgiev, R. Gernhäuser, H. Hess, J. Iwanicki, D. G. Jenkins, A. C. Larsen, J. Ljungvall, R. Lutter, P. Marley, K. Moschner, P. J. Napiorkowski, J. Pakarinen, A. Petts, P. Reiter, T. Renstrøm, M. Seidlitz, B. Siebeck, S. Siem, C. Sotty, J. Srebrny, I. Stefanescu, G. M. Tveten, J. Van de Walle, M. Vermeulen, D. Voulot, N. Warr, F. Wenander, A. Wiens, H. De Witte, and K. Wrzosek-Lipska. Erratum: Spectroscopic quadrupole moments in ^{96,98}Sr: Evidence for shape coexistence in neutron-rich strontium isotopes at $n = 60$ [phys. rev. lett. **116** , 022701 (2016)]. *Phys. Rev. Lett.*, 117:099902, Aug 2016.

[69] K. Wrzosek-Lipska et al. Electromagnetic properties of 100mo: Experimental results and theoretical description of quadrupole degrees of freedom. *Phys. Rev. C*, 86:064305, Dec 2012.

[70] N.J. Stone. Table of nuclear electric quadrupole moments. *Atomic Data and Nuclear Data Tables*, 111-112:1 – 28, 2016.

[71] M. Albers et al. Shape dynamics in neutron-rich kr isotopes: Coulomb excitation of 92kr, 94kr and 96kr. *Nucl. Phys. A*, 899(0):1 – 28, 2013.

[72] M. Zielińska, L. P. Gaffney, K. Wrzosek-Lipska, E. Clément, T. Grahn, N. Kesteloot, P. Napiorkowski, J. Pakarinen, P. Van Duppen, and N. Warr. Analysis methods of safe coulomb-excitation experiments with radioactive ion beams using the gosia code. *The European Physical Journal A*, 52(4):99, Apr 2016.

[73] J. Srebrny et al. *Nuclear Physics A*, 766:25 – 51, 2006.

[74] B. Cheal, M.D. Gardner, M. Avgoulea, J. Billowes, M.L. Bissell, P. Campbell, T. Eronen, K.T. Flanagan, D.H. Forest, J. Huikari, A. Jokinen, B.A. Marsh, I.D. Moore, A. Nieminen, H. Penttil, S. Rinta-Antila, B. Tordoff, G. Tungate, and J. yst. The shape transition in the neutron-rich yttrium isotopes and isomers. *Physics Letters B*, 645(2):133 – 137, 2007.

[75] E. Monnand, J. A. Pinston, F. Schussler, B. Pfeiffer, H. Lawin, G. Battistuzzi, K. Shizuma, and K. Sistemich. Evidence for a rotational band in99y. *Zeitschrift für Physik A Atoms and Nuclei*, 306(2):183–184, Jun 1982.

[76] F. K. Wohn, John C. Hill, R. F. Petry, H. Dejbakhsh, Z. Berant, and R. L. Gill. Rotational structure and nilsson orbitals for highly deformed odd-a nuclei in the $a \sim 100$ region. *Phys. Rev. Lett.*, 51:873–876, Sep 1983.

[77] T. W. Hagen, A. Görgen, W. Korten, L. Grente, M.-D. Salsac, F. Farget, I. Ragnarsson, T. Braunroth, B. Bruyneel, I. Celikovic, E. Clément, G. de France, O. Delaune, A. Dewald, A. Dijon, M. Hackstein, B. Jacquot, J. Litzinger, J. Ljungvall, C. Louchart, C. Michelagnoli, D. R. Napoli, F. Recchia, W. Rother, E. Sahin, S. Siem, B. Sulignano, Ch. Theisen, and J. J. Valiente-Dobon. Evolution of nuclear shapes in odd-mass yttrium and niobium isotopes from lifetime measurements following fission reactions. *Phys. Rev. C*, 95:034302, Mar 2017.

[78] W. Urban et al. Medium-spin structure of 96,97sr and 98,99zr nuclei and the onset of deformation in the a100 region. *Nucl. Phys. A*, 689(34):605 – 630, 2001.

[79] W. Urban, J. A. Pinston, J. Genevey, T. Rzaca-Urban, A. Złomaniec, G. Simpson, J. L. Durell, W. R. Phillips, A. G. Smith, B. J. Varley, I. Ahmad, and N. Schulz. The $\nu 9/2[404]$ orbital and the deformation in the a 100 region. *The European Physical Journal A - Hadrons and Nuclei*, 22(2):241–252, Nov 2004.

[80] J.-M. Régis, J. Jolie, N. Saed-Samii, N. Warr, M. Pfeiffer, A. Blanc, M. Jentschel, U. Köster, P. Mutti, T. Soldner, G. S. Simpson, F. Drouet, A. Vancraeyenest, G. de France, E. Clément, O. Stezowski, C. A. Ur, W. Urban, P. H. Regan, Zs. Podolyák, C. Larijani, C. Townsley, R. Carroll, E. Wilson, L. M. Fraile, H. Mach, V. Paziy, B. Olaizola, V. Vedia, A. M. Bruce, O. J. Roberts, J. F. Smith, T. Kröll, A.-L. Hartig, A. Ignatov, S. Ilieva, M. Thürauf, S. Lalkovski, D. Ivanova, S. Kisyov, W. Korten, M.-D. Salsac, M. Zielińska, N. Mărginean, D. G. Ghită, R. Lică, C. M. Petrache, A. Astier, and R. Leguillon. $b(e2; 2_1^+ \to 0_1^+)$ value in ^{90}Kr. *Phys. Rev. C*, 90:067301, Dec 2014.

[81] J.-M. Régis, J. Jolie, N. Saed-Samii, N. Warr, M. Pfeiffer, A. Blanc, M. Jentschel, U. Köster, P. Mutti, T. Soldner, G. S. Simpson, F. Drouet, A. Vancraeyenest, G. de France, E. Clément, O. Stezowski, C. A. Ur, W. Urban, P. H. Regan, Zs. Podolyák, C. Larijani, C. Townsley, R. Carroll, E. Wilson, L. M. Fraile, H. Mach, V. Paziy, B. Olaizola, V. Vedia, A. M. Bruce, O. J. Roberts, J. F. Smith, M. Scheck, T. Kröll, A.-L. Hartig, A. Ignatov, S. Ilieva, S. Lalkovski, W. Korten, N. Mărginean, T. Otsuka, N. Shimizu, T. Togashi, and Y. Tsunoda. Abrupt shape transition at neutron number $n = 60$: $b(e2)$ values in ^{94,96,98}**Sr** from fast $\gamma - \gamma$ timing. *Phys. Rev. C*, 95:054319, May 2017.

[82] S. Ansari, J.-M. Régis, J. Jolie, N. Saed-Samii, N. Warr, W. Korten, M. Zielińska, M.-D. Salsac, A. Blanc, M. Jentschel, U. Köster, P. Mutti, T. Soldner, G. S. Simpson, F. Drouet, A. Vancraeyenest, G. de France, E. Clément, O. Stezowski, C. A. Ur, W. Urban, P. H. Regan, Zs. Podolyák, C. Larijani, C. Townsley, R. Carroll, E. Wilson, H. Mach, L. M. Fraile, V. Paziy, B. Olaizola, V. Vedia, A. M. Bruce, O. J. Roberts, J. F. Smith, M. Scheck, T. Kröll, A.-L. Hartig, A. Ignatov, S. Ilieva, S. Lalkovski, N. Mărginean, T. Otsuka, N. Shimizu, T. Togashi, and Y. Tsunoda. Experimental study of the lifetime and phase transition in neutron-rich ^{98,100,102}Zr. *Phys. Rev. C*, 96:054323, Nov 2017.

[83] R. F. Casten and N. V. Zamfir. Valence correlation schemes and signatures of nuclear structure: A simple global phenomenology for b(e2:$2_1^+ \rightarrow 0_1^+$) values. *Phys. Rev. Lett.*, 70:402–405, Jan 1993.

[84] Y.Y. Sharon, N. Benczer-Koller, G.J. Kumbartzki, L. Zamick, and R.F. Casten. Systematics of the ratio of electric quadrupole moments q(21+) to the square root of the reduced transition probabilities b(e2;01+??21+) in even??even nuclei. *Nuclear Physics A*, 980:131 – 142, 2018.

[85] A. Shalit and I. Talmi. *Nuclear Shell Theory.* Courier Dover Publications, 1967.

[86] F. Buchinger, E. B. Ramsay, E. Arnold, W. Neu, R. Neugart, K. Wendt, R. E. Silverans, P. Lievens, L. Vermeeren, D. Berdichevsky, R. Fleming, D. W. L. Sprung, and G. Ulm. Systematics of nuclear ground state properties in $^{78--100}$Sr by laser spectroscopy. *Phys. Rev. C*, 41:2883–2897, Jun 1990.

[87] S. Cruz, K. Wimmer, P. C. Bender, R. Krücken, G. Hackman, F. Ames, C. Andreoiu, R. A. E. Austin, C. S. Bancroft, R. Braid, T. Bruhn, W. N. Catford, A. Cheeseman, A. Chester, D. S. Cross, C. Aa. Diget, T. Drake, A. B. Garnsworthy, R. Kanungo, A. Knapton, W. Korten, K. Kuhn, J. Lassen, R. Laxdal, M. Marchetto, A. Matta, D. Miller, M. Moukaddam, N. A. Orr, N. Sachmpazidi, A. Sanetullaev, C. E. Svensson, N. Terpstra, C. Unsworth, and P. J. Voss. Single-particle structure of neutron-rich sr isotopes via ^{2}H(^{94,95,96}Sr, p) reactions. *Phys. Rev. C*, 100:054321, Nov 2019.

[88] A. Petrovici. Triple shape coexistence and shape evolution in the $n = 58$ sr and zr isotopes. *Phys. Rev. C*, 85:034337, Mar 2012.

[89] K. Sieja, F. Nowacki, K. Langanke, and G. Martinez-Pinedo. Shell model description of zirconium isotopes. *Phys. Rev. C*, 79:064310, Jun 2009.

[90] C. Kremer et al. First measurement of collectivity of coexisting shapes based on type ii shell evolution: The case of 96zr. *arXiv:1606.09057 [nucl-ex]*, 2016.

[91] O. Sorlin and M.-G. Porquet. Nuclear magic numbers: New features far from stability. *Progress in Particle and Nuclear Physics*, 61(2):602 – 673, 2008.

[92] S. M. Lenzi et al. Island of inversion around cr64. *Phys. Rev. C*, 82:054301, Nov 2010.

[93] E. Caurier, G. Martínez-Pinedo, F. Nowacki, A. Poves, and A. P. Zuker. *Rev. Mod. Phys.*, 77:427–488, Jun 2005.

[94] B.A. Brown. *Progress in Particle and Nuclear Physics*, 47(2):517 – 599, 2001.

[95] K. L. Yurkewicz, D. Bazin, B. A. Brown, C. M. Campbell, J. A. Church, D. C. Dinca, A. Gade, T. Glasmacher, M. Honma, T. Mizusaki, W. F. Mueller, H. Olliver, T. Otsuka, L. A. Riley, and J. R. Terry. Nuclear structure in the vicinity of $n = z = 28$ ^{56}Ni. *Phys. Rev. C*, 70:054319, Nov 2004.

[96] Z. Y. Xu, S. Nishimura, G. Lorusso, F. Browne, P. Doornenbal, G. Gey, H.-S. Jung, Z. Li, M. Niikura, P.-A. Söderström, T. Sumikama, J. Taprogge, Zs. Vajta, H. Watanabe, J. Wu, A. Yagi, K. Yoshinaga, H. Baba, S. Franchoo, T. Isobe, P. R. John, I. Kojouharov, S. Kubono, N. Kurz, I. Matea, K. Matsui, D. Mengoni, P. Morfouace, D. R. Napoli, F. Naqvi, H. Nishibata, A. Odahara, E. Şahin, H. Sakurai, H. Schaffner, I. G. Stefan, D. Suzuki, R. Taniuchi, and V. Werner. β-decay half-lives of ^{76,77}Co, ^{79,80}Ni, and ^{81}Cu: Experimental indication of a doubly magic ^{78}Ni. *Phys. Rev. Lett.*, 113:032505, Jul 2014.

[97] R. Grzywacz, R. Béraud, C. Borcea, A. Emsallem, M. Glogowski, H. Grawe, D. Guillemaud-Mueller, M. Hjorth-Jensen, M. Houry, M. Lewitowicz, A. C. Mueller, A. Nowak, A. Płochocki, M. Pfützner, K. Rykaczewski, M. G. Saint-Laurent, J. E. Sauvestre, M. Schaefer, O. Sorlin, J. Szerypo, W. Trinder, S. Viteritti, and J. Winfield. New island of μs isomers in neutron-rich nuclei around the shell closures. *Phys. Rev. Lett.*, 81:766–769, Jul 1998.

[98] O. Perru, O. Sorlin, S. Franchoo, F. Azaiez, E. Bouchez, C. Bourgeois, A. Chatillon, J. M. Daugas, Z. Dlouhy, Zs. Dombrádi, C. Donzaud, L. Gaudefroy, H. Grawe, S. Grévy, D. Guillemaud-Mueller, F. Hammache, F. Ibrahim, Y. Le Coz, S. M. Lukyanov, I. Matea, J. Mrazek, F. Nowacki, Yu.-E. Penionzhkevich, F. de Oliveira Santos, F. Pougheon, M. G. Saint-Laurent, G. Sletten, M. Stanoiu, C. Stodel, Ch. Theisen, and D. Verney. Enhanced core polarization in ^{70}Ni and ^{74}Zn. *Phys. Rev. Lett.*, 96:232501, Jun 2006.

[99] A. F. Lisetskiy, B. A. Brown, M. Horoi, and H. Grawe. New $t = 1$ effective interactions for the fpg model space: Implications for valence-mirror symmetry and seniority isomers. *Phys. Rev. C*, 70:044314, Oct 2004.

[100] M. Girod, Ph. Dessagne, M. Bernas, M. Langevin, F. Pougheon, and P. Roussel. Spectroscopy of neutron-rich nickel isotopes: Experimental results and microscopic interpretation. *Phys. Rev. C*, 37:2600–2612, Jun 1988.

[101] G. Audi;F.G. Kondev;M. Wang;;B. Pfeiffer;X. Sun;J. Blachot;M. MacCormick. The nubase2012 evaluation of nuclear properties. *Chinese physics C*, 36(12):1157, 2012.

[102] D. Pauwels, O. Ivanov, N. Bree, J. Büscher, T. E. Cocolios, J. Gentens, M. Huyse, A. Korgul, Yu. Kudryavtsev, R. Raabe, M. Sawicka, I. Stefanescu, J. Van de Walle, P. Van den Bergh, P. Van Duppen, and W. B. Walters. Shape isomerism at $n = 40$: Discovery of a proton intruder state in ^{67}Co. *Phys. Rev. C*, 78:041307, Oct 2008.

[103] I. Stefanescu, G. Georgiev, D. L. Balabanski, N. Blasi, A. Blazhev, N. Bree, J. Cederkäll, T. E. Cocolios, T. Davinson, J. Diriken, J. Eberth, A. Ekström, D. Fedorov, V. N. Fedosseev, L. M. Fraile, S. Franchoo, K. Gladnishki, M. Huyse, O. Ivanov, V. Ivanov, J. Iwanicki, J. Jolie, T. Konstantinopoulos, Th. Kröll, R. Krücken, U. Köster, A. Lagoyannis, G. Lo Bianco, P. Maierbeck, B. A. Marsh, P. Napiorkowski, N. Patronis, D. Pauwels, G. Rainovski, P. Reiter, K. Riisager, M. Seliverstov, G. Sletten, J. Van de Walle, P. Van Duppen, D. Voulot, N. Warr, F. Wenander, and K. Wrzosek. Interplay between single-particle and collective effects in the odd-a cu isotopes beyond $n = 40$. *Phys. Rev. Lett.*, 100:112502, Mar 2008.

[104] I. C˘elikovi´c, A. Dijon, E. Clément, G. de France, P. Van Isacker, J. Ljungvall, A. Dewald, C. Fransen, G. Georgiev, A. Görgen, A. Gottardo, M. Hackstein, T. W. Hagen, C. Louchart, P. Napiorkowski, A. Obertelli, F. Recchia, W. Rother, S. Siem, B. Sulignano, P. Ujić, J. J. Valiente-Dobón, and M. Zielińska. Probing collectivity in zn isotopes with one particle or hole outside the $n = 40$ subshell closure. *Phys. Rev. C*, 91:044311, Apr 2015.

[105] D. Pauwels, O. Ivanov, N. Bree, J. Büscher, T. E. Cocolios, M. Huyse, Yu. Kudryavtsev, R. Raabe, M. Sawicka, J. Van de Walle, P. Van Duppen, A. Korgul, I. Stefanescu, A. A. Hecht, N. Hoteling, A. Wöhr, W. B. Walters, R. Broda, B. Fornal, W. Krolas, T. Pawlat, J. Wrzesinski, M. P. Carpenter, R. V. F. Janssens, T. Lauritsen, D. Seweryniak, S. Zhu, J. R. Stone, and X. Wang. Structure of ^{65,67}Co studied through the β decay of ^{65,67}Fe and a deep-inelastic reaction. *Phys. Rev. C*, 79:044309, Apr 2009.

[106] J. Ljungvall, A. Görgen, A. Obertelli, W. Korten, E. Clément, G. de France, A. Bürger, J.-P. Delaroche, A. Dewald, A. Gadea, L. Gaudefroy, M. Girod, M. Hackstein, J. Libert, D. Mengoni, F. Nowacki, T. Pissulla, A. Poves, F. Recchia, M. Rejmund, W. Rother, E. Sahin, C. Schmitt, A. Shrivastava, K. Sieja, J. J. Valiente-Dobón, K. O. Zell, and M. Zielińska. Onset of collectivity in neutron-rich fe isotopes: Toward a new island of inversion? *Phys. Rev. C*, 81:061301, Jun 2010.

[107] M. Klintefjord, J. Ljungvall, A. Görgen, S. M. Lenzi, F. L. Bello Garrote, A. Blazhev, E. Clément, G. de France, J.-P. Delaroche, P. Désesquelles, A. Dewald, D. T. Doherty, C. Fransen, A. Gengelbach, G. Georgiev, M. Girod, A. Goasduff, A. Gottardo, K. Hadyńska-Klęk, B. Jacquot, T. Konstantinopoulos, A. Korichi, A. Lemasson, J. Libert, A. Lopez-Martens, C. Michelagnoli, A. Navin, J. Nyberg, R. M. Pérez-Vidal, S. Roccia, E. Sahin, I. Stefan, A. E. Stuchbery, M. Zielińska, D. Barrientos, B. Birkenbach, A. Boston, L. Charles, M. Ciemala, J. Dudouet, J. Eberth, A. Gadea, V. González, L. Harkness-Brennan, H. Hess, A. Jungclaus, W. Korten, R. Menegazzo, D. Mengoni, B. Million, A. Pullia, D. Ralet, F. Recchia, P. Reiter, M. D. Salsac, E. Sanchis, O. Stezowski, Ch. Theisen, and J. J. Valiente Dobon. Measurement of lifetimes in ^{62,64}Fe,^{61,63} Co, and ^{59}Mn. *Phys. Rev. C*, 95:024312, Feb 2017.

[108] A. Dijon, E. Clément, G. de France, P. Van Isacker, J. Ljungvall, A. Görgen, A. Obertelli, W. Korten, A. Dewald, A. Gadea, L. Gaudefroy, M. Hackstein, D. Mengoni, Th. Pissulla, F. Recchia, M. Rejmund, W. Rother, E. Sahin, C. Schmitt, A. Shrivastava, J. J. Valiente-Dobón, K. O. Zell, and M. Zielińska. Lifetime measurements in ^{63}Co and ^{65}Co. *Phys. Rev. C*, 83:064321, Jun 2011.

[109] B. Olaizola, L. M. Fraile, H. Mach, F. Nowacki, A. Poves, A. Aprahamian, J. A. Briz, J. Cal-González, D. Ghiţa, U. Köster, W. Kurcewicz, S. R. Lesher, D. Pauwels, E. Picado,

D. Radulov, G. S. Simpson, and J. M. Udías. Properties of low-lying states in ^{65}Co from lifetime measurements. *Phys. Rev. C*, 99:024321, Feb 2019.

[110] V. Modamio, J. J. Valiente-Dobón, S. Lunardi, S. M. Lenzi, A. Gadea, D. Mengoni, D. Bazzacco, A. Algora, P. Bednarczyk, G. Benzoni, B. Birkenbach, A. Bracco, B. Bruyneel, A. Bürger, J. Chavas, L. Corradi, F. C. L. Crespi, G. de Angelis, P. Désesquelles, G. de France, R. Depalo, A. Dewald, M. Doncel, M. N. Erduran, E. Farnea, E. Fioretto, Ch. Fransen, K. Geibel, A. Gottardo, A. Görgen, T. Habermann, M. Hackstein, H. Hess, T. Hüyük, P. R. John, J. Jolie, D. Judson, A. Jungclaus, N. Karkour, R. Kempley, S. Leoni, B. Melon, R. Menegazzo, C. Michelagnoli, T. Mijatović, B. Million, O. Möller, G. Montagnoli, D. Montanari, A. Nannini, D. R. Napoli, Zs. Podolyak, G. Pollarolo, A. Pullia, B. Quintana, F. Recchia, P. Reiter, D. Rosso, W. Rother, E. Sahin, M. D. Salsac, F. Scarlassara, K. Sieja, P. A. Söderström, A. M. Stefanini, O. Stezowski, S. Szilner, Ch. Theisen, B. Travers, and C. A. Ur. Lifetime measurements in neutron-rich ^{63,65}co isotopes using the agata demonstrator. *Phys. Rev. C*, 88:044326, Oct 2013.

[111] F. Recchia, C. J. Chiara, R. V. F. Janssens, D. Weisshaar, A. Gade, W. B. Walters, M. Albers, M. Alcorta, V. M. Bader, T. Baugher, D. Bazin, J. S. Berryman, P. F. Bertone, B. A. Brown, C. M. Campbell, M. P. Carpenter, J. Chen, H. L. Crawford, H. M. David, D. T. Doherty, C. R. Hoffman, F. G. Kondev, A. Korichi, C. Langer, N. Larson, T. Lauritsen, S. N. Liddick, E. Lunderberg, A. O. Macchiavelli, S. Noji, C. Prokop, A. M. Rogers, D. Seweryniak, S. R. Stroberg, S. Suchyta, S. Williams, K. Wimmer, and S. Zhu. Configuration mixing and relative transition rates between low-spin states in ^{68}ni. *Phys. Rev. C*, 88:041302, Oct 2013.

[112] F. Recchia, S. M. Lenzi, S. Lunardi, E. Farnea, A. Gadea, N. Mărginean, D. R. Napoli, F. Nowacki, A. Poves, J. J. Valiente-Dobón, M. Axiotis, S. Aydin, D. Bazzacco, G. Benzoni, P. G. Bizzeti, A. M. Bizzeti-Sona, A. Bracco, D. Bucurescu, E. Caurier, L. Corradi, G. de Angelis, F. Della Vedova, E. Fioretto, A. Gottardo, M. Ionescu-Bujor, A. Iordachescu, S. Leoni, R. Mărginean, P. Mason, R. Menegazzo, D. Mengoni, B. Million, G. Montagnoli, R. Orlandi, G. Pollarolo, E. Sahin, F. Scarlassara, R. P. Singh, A. M. Stefanini, S. Szilner, C. A. Ur, and O. Wieland. Spectroscopy of odd-mass cobalt isotopes toward the $n = 40$ subshell closure and shell-model description of spherical and deformed states. *Phys. Rev. C*, 85:064305, Jun 2012.

[113] S. Leoni, B. Fornal, N. Mărginean, M. Sferrazza, Y. Tsunoda, T. Otsuka, G. Bocchi, F. C. L. Crespi, A. Bracco, S. Aydin, M. Boromiza, D. Bucurescu, N. Cieplicka-Oryńczak, C. Costache, S. Călinescu, N. Florea, D. G. Ghiţă, T. Glodariu, A. Ionescu, Ł.W. Iskra, M. Krzysiek, R. Mărginean, C. Mihai, R. E. Mihai, A. Mitu, A. Negreţ, C. R. Niţă, A. Olăcel, A. Oprea, S. Pascu, P. Petkov, C. Petrone, G. Porzio, A. Şerban, C. Sotty, L. Stan, I. Ştiru, L. Stroe, R. Şuvăilă, S. Toma, A. Turturică, S. Ujeniuc, and C. A. Ur. Multifaceted quadruplet of low-lying spin-zero states in ^{66}Ni: Emergence of shape isomerism in light nuclei. *Phys. Rev. Lett.*, 118:162502, Apr 2017.

[114] B. Olaizola, L. M. Fraile, H. Mach, A. Poves, F. Nowacki, A. Aprahamian, J. A. Briz, J. Cal-González, D. Ghiţa, U. Köster, W. Kurcewicz, S. R. Lesher, D. Pauwels, E. Picado, D. Radulov, G. S. Simpson, and J. M. Udías. Search for shape-coexisting 0^+ states in ^{66}Ni from lifetime measurements. *Phys. Rev. C*, 95:061303, Jun 2017.

[115] B.P. Crider, C.J. Prokop, S.N. Liddick, M. Al-Shudifat, A.D. Ayangeakaa, M.P. Carpenter, J.J. Carroll, J. Chen, C.J. Chiara, H.M. David, A.C. Dombos, S. Go, R. Grzywacz, J. Harker, R.V.F. Janssens, N. Larson, T. Lauritsen, R. Lewis, S.J. Quinn, F. Recchia, A. Spyrou, S. Suchyta, W.B. Walters, and S. Zhu. Shape coexistence from lifetime and branching-ratio measurements in 68,70ni. *Physics Letters B*, 763:108 – 113, 2016.

[116] A. Dijon, E. Clément, G. de France, G. de Angelis, G. Duchêne, J. Dudouet, S. Franchoo, A. Gadea, A. Gottardo, T. Hüyük, B. Jacquot, A. Kusoglu, D. Lebhertz, G. Lehaut, M. Martini, D. R. Napoli, F. Nowacki, S. Péru, A. Poves, F. Recchia, N. Redon, E. Sahin, C. Schmitt, M. Sferrazza, K. Sieja, O. Stezowski, J. J. Valiente-Dobón, A. Vancraeyenest, and Y. Zheng. Discovery of a new isomeric state in ^{68}ni: Evidence for a highly deformed proton intruder state. *Phys. Rev. C*, 85:031301, Mar 2012.

[117] M. Bernas, Ph. Dessagne, M. Langevin, J. Payet, F. Pougheon, and P. Roussel. Magic features of 68ni. *Physics Letters B*, 113(4):279 – 282, 1982.

[118] S. Suchyta, S. N. Liddick, Y. Tsunoda, T. Otsuka, M. B. Bennett, A. Chemey, M. Honma, N. Larson, C. J. Prokop, S. J. Quinn, N. Shimizu, A. Simon, A. Spyrou, V. Tripathi, Y. Utsuno, and J. M. VonMoss. Shape coexistence in ^{68}Ni. *Phys. Rev. C*, 89:021301, Feb 2014.

[119] Jytte Elseviers. Probing the semi-magicity of 68ni via the 66ni(t,p)68ni two-neutron transfer reaction in inverse kinematics, 2014.

[120] F. Flavigny, J. Elseviers, A. N. Andreyev, C. Bauer, V. Bildstein, A. Blazhev, B. A. Brown, H. De Witte, J. Diriken, V. N. Fedosseev, S. Franchoo, R. Gernhäuser, M. Huyse, S. Ilieva, S. Klupp, Th. Kröll, R. Lutter, B. A. Marsh, D. Mücher, K. Nowak, T. Otsuka, J. Pakarinen, N. Patronis, R. Raabe, F. Recchia, P. Reiter, T. Roger, S. Sambi, M. Seidlitz, M. D. Seliverstov, B. Siebeck, Y. Tsunoda, P. Van Duppen, M. Vermeulen, M. Von Schmid, D. Voulot, N. Warr, F. Wenander, and K. Wimmer. Microscopic structure of coexisting 0^+ states in ^{68}Ni probed via two-neutron transfer. *Phys. Rev. C*, 99:054332, May 2019.

[121] W. F. Mueller, B. Bruyneel, S. Franchoo, M. Huyse, J. Kurpeta, K. Kruglov, Y. Kudryavtsev, N. V. S. V. Prasad, R. Raabe, I. Reusen, P. Van Duppen, J. Van Roosbroeck, L. Vermeeren, L. Weissman, Z. Janas, M. Karny, T. Kszczot, A. Płochocki, K.-L. Kratz, B. Pfeiffer, H. Grawe, U. Köster, P. Thirolf, and W. B. Walters. β decay of ^{66}Co, ^{68}Co, and ^{70}Co. *Phys. Rev. C*, 61:054308, Apr 2000.

[122] C. J. Chiara, R. Broda, W. B. Walters, R. V. F. Janssens, M. Albers, M. Alcorta, P. F. Bertone, M. P. Carpenter, C. R. Hoffman, T. Lauritsen, A. M. Rogers, D. Seweryniak, S. Zhu, F. G. Kondev, B. Fornal, W. Królas, J. Wrzesiński, N. Larson, S. N. Liddick, C. Prokop, S. Suchyta, H. M. David, and D. T. Doherty. Low-spin states and the non-observation of a proposed 2202-kev, 0^+ isomer in ^{68}ni. *Phys. Rev. C*, 86:041304, Oct 2012.

[123] F. Flavigny, D. Pauwels, D. Radulov, I. J. Darby, H. De Witte, J. Diriken, D. V. Fedorov, V. N. Fedosseev, L. M. Fraile, M. Huyse, V. S. Ivanov, U. Köster, B. A. Marsh, T. Otsuka, L. Popescu, R. Raabe, M. D. Seliverstov, N. Shimizu, A. M. Sjödin, Y. Tsunoda, P. Van den Bergh, P. Van Duppen, J. Van de Walle, M. Venhart, W. B. Walters, and K. Wimmer. Characterization of the low-lying 0^+ and 2^+ states in ^{68}Ni via β decay of the low-spin ^{68}Co isomer. *Phys. Rev. C*, 91:034310, Mar 2015.

[124] B Olaizola, L M Fraile, H Mach, A Poves, A Aprahamian, J A Briz, J Cal-González, D Ghiţa, U Kster, W Kurcewicz, S R Lesher, D Pauwels, E Picado, D Radulov, G S Simpson, and J M Udías. Beta decay of 66mn to the n = 40 nucleus 66fe. *Journal of Physics G: Nuclear and Particle Physics*, 44(12):125103, nov 2017.

[125] S. N. Liddick, B. Abromeit, A. Ayres, A. Bey, C. R. Bingham, B. A. Brown, L. Cartegni, H. L. Crawford, I. G. Darby, R. Grzywacz, S. Ilyushkin, M. Hjorth-Jensen, N. Larson, M. Madurga, D. Miller, S. Padgett, S. V. Paulauskas, M. M. Rajabali, K. Rykaczewski, and S. Suchyta. Low-energy level schemes of $^{\mathbf{66,68}}$fe and inferred proton and neutron excitations across $\mathbf{Z = 28}$ and $\mathbf{N = 40}$. *Phys. Rev. C*, 87:014325, Jan 2013.

[126] Yusuke Tsunoda, Takaharu Otsuka, Noritaka Shimizu, Michio Honma, and Yutaka Utsuno. Novel shape evolution in exotic ni isotopes and configuration-dependent shell structure. *Phys. Rev. C*, 89:031301, Mar 2014.

[127] M. Stryjczyk, Y. Tsunoda, I. G. Darby, H. De Witte, J. Diriken, D. V. Fedorov, V. N. Fedosseev, L. M. Fraile, M. Huyse, U. Köster, B. A. Marsh, T. Otsuka, D. Pauwels, L. Popescu, D. Radulov, M. D. Seliverstov, A. M. Sjödin, P. Van den Bergh, P. Van Duppen, M. Venhart, W. B. Walters, and K. Wimmer. β^- decay study of the ^{66}Mn$-^{66}$Fe$-^{66}$Co$-^{66}$Ni decay chain. *Phys. Rev. C*, 98:064326, Dec 2018.

[128] C. J. Chiara, D. Weisshaar, R. V. F. Janssens, Y. Tsunoda, T. Otsuka, J. L. Harker, W. B. Walters, F. Recchia, M. Albers, M. Alcorta, V. M. Bader, T. Baugher, D. Bazin, J. S. Berryman, P. F. Bertone, C. M. Campbell, M. P. Carpenter, J. Chen, H. L. Crawford, H. M. David, D. T. Doherty, A. Gade, C. R. Hoffman, M. Honma, F. G. Kondev, A. Korichi, C. Langer, N. Larson, T. Lauritsen, S. N. Liddick, E. Lunderberg, A. O. Macchiavelli, S. Noji, C. Prokop, A. M. Rogers, D. Seweryniak, N. Shimizu, S. R. Stroberg, S. Suchyta, Y. Utsuno, S. J. Williams, K. Wimmer, and S. Zhu. Identification of deformed intruder states in semimagic ^{70}Ni. *Phys. Rev. C*, 91:044309, Apr 2015.

[129] C. J. Prokop, B. P. Crider, S. N. Liddick, A. D. Ayangeakaa, M. P. Carpenter, J. J. Carroll, J. Chen, C. J. Chiara, H. M. David, A. C. Dombos, S. Go, J. Harker, R. V. F. Janssens, N. Larson, T. Lauritsen, R. Lewis, S. J. Quinn, F. Recchia, D. Seweryniak, A. Spyrou, S. Suchyta, W. B. Walters, and S. Zhu. New low-energy 0^+ state and shape coexistence in ^{70}Ni. *Phys. Rev. C*, 92:061302, Dec 2015.

[130] A.I. Morales, G. Benzoni, H. Watanabe, Y. Tsunoda, T. Otsuka, S. Nishimura, F. Browne, R. Daido, P. Doornenbal, Y. Fang, G. Lorusso, Z. Patel, S. Rice, L. Sinclair, P.-A. Sderstrm, T. Sumikama, J. Wu, Z.Y. Xu, A. Yagi, R. Yokoyama, H. Baba, R. Avigo, F.L. Bello Garrote, N. Blasi, A. Bracco, F. Camera, S. Ceruti, F.C.L. Crespi, G. de Angelis, M.-C. Delattre, Zs. Dombradi, A. Gottardo, T. Isobe, I. Kojouharov, N. Kurz, I. Kuti, K. Matsui, B. Melon, D. Mengoni, T. Miyazaki, V. Modamio-Hoybjor, S. Momiyama, D.R. Napoli, M. Niikura, R. Orlandi, H. Sakurai, E. Sahin, D. Sohler, H. Schaffner, R. Taniuchi, J. Taprogge, Zs. Vajta, J.J. Valiente-Dobn, O. Wieland, and M. Yalcinkaya. Type ii shell evolution in a=70 isobars from the n̆226540 island of inversion. *Physics Letters B*, 765:328 – 333, 2017.

[131] S. N. Liddick, B. Abromeit, A. Ayres, A. Bey, C. R. Bingham, M. Bolla, L. Cartegni, H. L. Crawford, I. G. Darby, R. Grzywacz, S. Ilyushkin, N. Larson, M. Madurga, D. Miller, S. Pad-

gett, S. Paulauskas, M. M. Rajabali, K. Rykaczewski, and S. Suchyta. Low-energy structure of $^{66}_{27}$co$_{39}$ and $^{68}_{27}$co$_{41}$ populated through β decay. *Phys. Rev. C*, 85:014328, Jan 2012.

[132] I. Celikovic, A. Dijon, E. Clement, G. de France, P. Van Isacker, J. Ljungvall, C. Fransen, G. Georgiev, A. Gorgen, A. Gottardo, M. Hackstein, T. W. Hagen, C. Louchart, P. Napiorkowski, A. Obertelli, F. Recchia, W. Rother, S. Siem, B. Sulignano, P. Ujic, J. J. Valiente-Dobon, and M. Zielinska. Lifetime measurements of zn isotopes around n = 40. *Acta Phys.Pol.*, B44:375, 2013.

[133] I. Celikovic. *Nuclear structure around doubly-magic nuclei: lifetime measurements in the vicinity of ^{68}Ni and search for isomers around ^{100}Sn.* Theses, Université de Caen, December 2013. Expérience GANIL/VAMOS/EXOGAM.

[134] Ritu Chaudhary, N.K. Makhnotra, Rani Devi, and S.K. Khosa. Study of electromagnetic properties and structure of yrast bands in neutron-rich 70ŏ201376zn isotopes. *Nuclear Physics A*, 939:53 – 70, 2015.

[135] B. Pritychenko, J. Choquette, M. Horoi, B. Karamy, and B. Singh. An update of the b(e2) evaluation for 01+ŏ219221+ transitions in evenŏ2013even nuclei near nŏ23czŏ223c28. *Atomic Data and Nuclear Data Tables*, 98(4):798 – 811, 2012.

[136] C. Louchart, A. Obertelli, A. Görgen, W. Korten, D. Bazzacco, B. Birkenbach, B. Bruyneel, E. Clément, P. J. Coleman-Smith, L. Corradi, D. Curien, G. de Angelis, G. de France, J.-P. Delaroche, A. Dewald, F. Didierjean, M. Doncel, G. Duchêne, J. Eberth, M. N. Erduran, E. Farnea, C. Finck, E. Fioretto, C. Fransen, A. Gadea, M. Girod, A. Gottardo, J. Grebosz, T. Habermann, M. Hackstein, T. Huyuk, J. Jolie, D. Judson, A. Jungclaus, N. Karkour, S. Klupp, R. Krücken, A. Kusoglu, S. M. Lenzi, J. Libert, J. Ljungvall, S. Lunardi, G. Maron, R. Menegazzo, D. Mengoni, C. Michelagnoli, B. Million, P. Molini, O. Möller, G. Montagnoli, D. Montanari, D. R. Napoli, R. Orlandi, G. Pollarolo, A. Prieto, A. Pullia, B. Quintana, F. Recchia, P. Reiter, D. Rosso, W. Rother, E. Sahin, M.-D. Salsac, F. Scarlassara, M. Schlarb, S. Siem, P. P. Singh, P.-A. Söderström, A. M. Stefanini, O. Stézowski, B. Sulignano, S. Szilner, Ch. Theisen, C. A. Ur, J. J. Valiente-Dobón, and M. Zielinska. Collective nature of low-lying excitations in ^{70,72,74}zn from lifetime measurements using the agata spectrometer demonstrator. *Phys. Rev. C*, 87:054302, May 2013.

[137] unpublished LISE experiment, 2019.

[138] W. Nazarewicz, J. Dudek, R. Bengtsson, T. Bengtsson, and I. Ragnarsson. Microscopic study of the high-spin behaviour in selected a ŏ2243 80 nuclei. *Nuclear Physics A*, 435(2):397 – 447, 1985.

[139] C.J. Gross, J. Heese, K.P. Lieb, S. Ulbig, W. Nazarewicz, C.J. Lister, B.J. Varley, J. Billowes, A.A. Chishti, J.H. McNeill, and W. Gelletly. Band crossings and near-rigid rotation in 76kr and 78kr. *Nuclear Physics A*, 501(2):367 – 400, 1989.

[140] P. Bonche, H. Flocard, P.H. Heenen, S.J. Krieger, and M.S. Weiss. Self-consistent study of triaxial deformations: Application to the isotopes of kr, sr, zr and mo. *Nuclear Physics A*, 443(1):39 – 63, 1985.

[141] M. Bender, P. Bonche, and P.-H. Heenen. Shape coexistence in neutron-deficient kr isotopes: Constraints on the single-particle spectrum of self-consistent mean-field models from collective excitations. *Phys. Rev. C*, 74:024312, Aug 2006.

[142] J. Libert, M. Girod, and J.-P. Delaroche. Microscopic descriptions of superdeformed bands with the gogny force: Configuration mixing calculations in the a=190 mass region. *Phys. Rev. C*, 60:054301, Sep 1999.

[143] S. Goriely, S. Hilaire, M. Girod, and S. Péru. First gogny-hartree-fock-bogoliubov nuclear mass model. *Phys. Rev. Lett.*, 102:242501, Jun 2009.

[144] S. Hilaire, M. Girod, and S. Goriely. Nuclear structure properties with the gogny force. *Journal of the Korean Physical Society*, 59:1506–1509, 2011.

[145] S. Péru and M. Martini. Mean field based calculations with the gogny force: Some theoretical tools to explore the nuclear structure. *The European Physical Journal A*, 50(5), 2014.

[146] M. Girod, J. P. Delaroche, D. Gogny, and J. F. Berger. Hartree-fock-bogoliubov predictions for shape isomerism in nonfissile even-even nuclei. *Phys. Rev. Lett.*, 62:2452–2455, May 1989.

[147] J. Dechargé and D. Gogny. Hartree-fock-bogolyubov calculations with the $d1$ effective interaction on spherical nuclei. *Phys. Rev. C*, 21:1568–1593, Apr 1980.

[148] A. Lemasson, H. Iwasaki, C. Morse, D. Bazin, T. Baugher, J. S. Berryman, A. Dewald, C. Fransen, A. Gade, S. McDaniel, A. Nichols, A. Ratkiewicz, S. Stroberg, P. Voss, R. Wadsworth, D. Weisshaar, K. Wimmer, and R. Winkler. Observation of mutually enhanced collectivity in self-conjugate $^{\mathbf{76}}_{\mathbf{38}}\mathrm{sr}_{\mathbf{38}}$. *Phys. Rev. C*, 85:041303, Apr 2012.

[149] H. Iwasaki, A. Lemasson, C. Morse, A. Dewald, T. Braunroth, V. M. Bader, T. Baugher, D. Bazin, J. S. Berryman, C. M. Campbell, A. Gade, C. Langer, I. Y. Lee, C. Loelius, E. Lunderberg, F. Recchia, D. Smalley, S. R. Stroberg, R. Wadsworth, C. Walz, D. Weisshaar, A. Westerberg, K. Whitmore, and K. Wimmer. Evolution of collectivity in ^{72}Kr: Evidence for rapid shape transition. *Phys. Rev. Lett.*, 112:142502, Apr 2014.

[150] A. M. Hurst, P. A. Butler, D. G. Jenkins, P. Delahaye, F. Wenander, F. Ames, C. J. Barton, T. Behrens, A. Bürger, J. Cederkäll, E. Clément, T. Czosnyka, T. Davinson, G. de Angelis, J. Eberth, A. Ekström, S. Franchoo, G. Georgiev, A. Görgen, R.-D. Herzberg, M. Huyse, O. Ivanov, J. Iwanicki, G. D. Jones, P. Kent, U. Köster, T. Kröll, R. Krücken, A. C. Larsen, M. Nespolo, M. Pantea, E. S. Paul, M. Petri, H. Scheit, T. Sieber, S. Siem, J. F. Smith, A. Steer, I. Stefanescu, N. U. H. Syed, J. Van de Walle, P. Van Duppen, R. Wadsworth, N. Warr, D. Weisshaar, and M. Zielińska. Measurement of the sign of the spectroscopic quadrupole moment for the 2_1^+ state in ^{70}Se: No evidence for oblate shape. *Phys. Rev. Lett.*, 98:072501, Feb 2007.

[151] J. Henderson, C. Y. Wu, J. Ash, P. C. Bender, B. Elman, A. Gade, M. Grinder, H. Iwasaki, E. Kwan, B. Longfellow, T. Mijatović, D. Rhodes, M. Spieker, and D. Weisshaar. Localizing the shape transition in neutron-deficient selenium. *Phys. Rev. Lett.*, 121:082502, Aug 2018.

[152] A.D. Ayangeakaa, R.V.F. Janssens, C.Y. Wu, J.M. Allmond, J.L. Wood, S. Zhu, M. Albers, S. Almaraz-Calderon, B. Bucher, M.P. Carpenter, C.J. Chiara, D. Cline, H.L. Crawford, H.M.

David, J. Harker, A.B. Hayes, C.R. Hoffman, B.P. Kay, K. Kolos, A. Korichi, T. Lauritsen, A.O. Macchiavelli, A. Richard, D. Seweryniak, and A. Wiens. Shape coexistence and the role of axial asymmetry in 72ge. *Physics Letters B*, 754:254 – 259, 2016.

[153] S. M. Fischer, C. J. Lister, and D. P. Balamuth. Unravelling the band crossings in ^{68}Se and ^{72}Kr : the quest for $t = 0$ pairing. *Phys. Rev. C*, 67:064318, Jun 2003.

[154] E. Clment, A. Grgen, W. Korten, A. Brger, A. Chatillon, Y. Le Coz, Ch. Theisen, M. ZieliŎ144ska, B. Blank, P.J. Davies, S.P. Fox, J. Gerl, G. Georgiev, S. Grvy, J. Iwanicki, D.G. Jenkins, F. Johnston-Theasby, P. Joshi, I. Matea, P.J. Napiorkowski, F. de Oliveira Santos, M.G. Pellegriti, and R. Wadsworth. A new device for combined coulomb excitation and isomeric conversion electron spectroscopy with fast fragmentation beams. *Nuclear Instruments and Methods in Physics Research Section A: Accelerators, Spectrometers, Detectors and Associated Equipment*, 587(2):292 – 299, 2008.

[155] A. Obertelli, T. Baugher, D. Bazin, J. P. Delaroche, F. Flavigny, A. Gade, M. Girod, T. Glasmacher, A. Goergen, G. F. Grinyer, W. Korten, J. Ljungvall, S. McDaniel, A. Ratkiewicz, B. Sulignano, and D. Weisshaar. Shape evolution in self-conjugate nuclei, and the transitional nucleus ^{68}Se. *Phys. Rev. C*, 80:031304, Sep 2009.

[156] G Rainovski, H Schnare, R Schwengner, C Plettner, L Kubler, F Dnau, I Ragnarsson, J Eberth, T Steinhardt, O Thelen, M Hausmann, A Jungclaus, K P Lieb, A Mller, G de Angelis, A Gadea, D R Napoli, A Algora, D G Jenkins, R Wadsworth, A Wilson, W Andrejtscheff, and V I Dimitrov. Shape coexistence at high spin in the n = z + 2 nucleus 70 se. *Journal of Physics G: Nuclear and Particle Physics*, 28(10):2617, 2002.

[157] T. Hayakawa, Y. Toh, M. Oshima, A. Osa, M. Koizumi, Y. Hatsukawa, Y. Utsuno, J. Katakura, M. Matsuda, T. Morikawa, M. Sugawara, H. Kusakari, and T. Czosnyka. Projectile coulomb excitation of ^{78}Se. *Phys. Rev. C*, 67:064310, Jun 2003.

[158] A.E. Kavka, C. Fahlander, A. Bcklin, D. Cline, T. Czosnyka, R.M. Diamond, D. Disdier, W.J. Kernan, L. Kraus, I. Linck, N. Schulz, J. Srebrny, F.S. Stephens, L.E. Svensson, B. Varnestig, E.G. Vogt, and C.Y. Wu. Coulomb excitation of 76,80,82se. *Nuclear Physics A*, 593(2):177 – 211, 1995.

[159] K. Wimmer, W. Korten, T. Arici, P. Doornenbal, P. Aguilera, A. Algora, T. Ando, H. Baba, B. Blank, A. Boso, S. Chen, A. Corsi, P. Davies, G. de Angelis, G. de France, D.T. Doherty, J. Gerl, R. Gernhuser, D. Jenkins, S. Koyama, T. Motobayashi, S. Nagamine, M. Niikura, A. Obertelli, D. Lubos, B. Rubio, E. Sahin, T.Y. Saito, H. Sakurai, L. Sinclair, D. Steppenbeck, R. Taniuchi, R. Wadsworth, and M. Zielinska. Shape coexistence and isospin symmetry in aŏ20ac=Ŏ20ac70 nuclei: Spectroscopy of the tzŏ20ac=Ŏ20acŏ2c6Ŏ20191 nucleus 70kr. *Physics Letters B*, 785:441 – 446, 2018.

[160] F. Becker, A. Petrovici, J. Iwanicki, N. Amzal, W. Korten, K. Hauschild, A. Hurstel, Ch. Theisen, P.A. Butler, R.A. Cunningham, T. Czosnyka, G. de France, J. Gerl, P. Greenlees, K. Helariutta, R.-D. Herzberg, P. Jones, R. Julin, S. Juutinen, H. Kankaanp, M. Muikku, P. Nieminen, O. Radu, P. Rahkila, and Ch. Schlegel. Coulomb excitation of 78kr. *Nuclear Physics A*, 770(3):107 – 125, 2006.

[161] J. Ljungvall, A. Görgen, M. Girod, J.-P. Delaroche, A. Dewald, C. Dossat, E. Farnea, W. Korten, B. Melon, R. Menegazzo, A. Obertelli, R. Orlandi, P. Petkov, T. Pissulla, S. Siem, R. P. Singh, J. Srebrny, Ch. Theisen, C. A. Ur, J. J. Valiente-Dobón, K. O. Zell, and M. Zielińska. Shape coexistence in light se isotopes: Evidence for oblate shapes. *Phys. Rev. Lett.*, 100:102502, Mar 2008.

[162] M. Girod, J.-P. Delaroche, A. Grgen, and A. Obertelli. The role of triaxiality for the coexistence and evolution of shapes in light krypton isotopes. *Physics Letters B*, 676(1):39 – 43, 2009.

[163] Michael Bender and Paul-Henri Heenen. Configuration mixing of angular-momentum and particle-number projected triaxial hartree-fock-bogoliubov states using the skyrme energy density functional. *Phys. Rev. C*, 78:024309, Aug 2008.

[164] K. Langanke, D.J. Dean, and W. Nazarewicz. Shell model monte carlo studies of nuclei in the a$\check{2}$23c80 mass region. *Nuclear Physics A*, 728(1):109 – 117, 2003.

[165] M. Hasegawa, K. Kaneko, T. Mizusaki, and Y. Sun. Phase transition in exotic nuclei along the n=z line. *Physics Letters B*, 656(1):51 – 55, 2007.

[166] B. Bounthong. *Calculs microscopiques pour les noyaux exotiques de masse moyenne et lourde. Physique Nuclaire Thorique [nucl-th].* PhD thesis, Universit de Strasbourg, 2016.

[167] Peter Möller, Arnold J. Sierk, Ragnar Bengtsson, Hiroyuki Sagawa, and Takatoshi Ichikawa. Global calculation of nuclear shape isomers. *Phys. Rev. Lett.*, 103:212501, Nov 2009.

[168] J. P. Delaroche et al. Structure of even-even nuclei using a mapped collective hamiltonian and the d1s gogny interaction. *Phys. Rev. C*, 81:014303, Jan 2010.

[169] K. Becker et al. Gamma-gamma angular correlation measurements of transitions in ^{98}sr and ^{98}zr and confirmation of shape coexistence in ^{98}sr. *Z.Phys.*, A319:193, 1984.

[170] A.G Smith et al. The influence of n11/2 occupancy on the magnetic moments of collective 2_1^+ states in a 100 fission fragments. *Phys. Lett. B*, 591(1-2):55 – 60, 2004.

[171] D. Cline et al. Error estimation in non-linear least squares analysis of data. *Nucl. Inst. and Meth.*, 82(0):291 – 293, 1970.

[172] J. Dechargé and D. Gogny. Hartree-fock-bogolyubov calculations with the $d1$ effective interaction on spherical nuclei. *Phys. Rev. C*, 21:1568–1593, Apr 1980.

[173] J.F. Berger et al. Time-dependent quantum collective dynamics applied to nuclear fission. *Comp. Phys. Com.*, 63(1-3):365 – 374, 1991.

[174] Tomas R. Rodriguez. Structure of krypton isotopes calculated with symmetry-conserving configuration-mixing methods. *Phys. Rev. C*, 90:034306, Sep 2014.

[175] A. Petrovici, K.W. Schmid, and Amand Faessler. Microscopic aspects of shape coexistence in 72kr and 74kr. *Nuclear Physics A*, 665(3):333 – 350, 2000.

[176] R. Broda, B. Fornal, W. Królas, T. Pawłat, D. Bazzacco, S. Lunardi, C. Rossi-Alvarez, R. Menegazzo, G. de Angelis, P. Bednarczyk, J. Rico, D. De Acuña, P. J. Daly, R. H. Mayer, M. Sferrazza, H. Grawe, K. H. Maier, and R. Schubart. $n = 40$ neutron subshell closure in the ^{68}Ni nucleus. *Phys. Rev. Lett.*, 74:868–871, Feb 1995.

[177] O. Sorlin, S. Leenhardt, C. Donzaud, J. Duprat, F. Azaiez, F. Nowacki, H. Grawe, Zs. Dombrádi, F. Amorini, A. Astier, D. Baiborodin, M. Belleguic, C. Borcea, C. Bourgeois, D. M. Cullen, Z. Dlouhy, E. Dragulescu, M. Górska, S. Grévy, D. Guillemaud-Mueller, G. Hagemann, B. Herskind, J. Kiener, R. Lemmon, M. Lewitowicz, S. M. Lukyanov, P. Mayet, F. de Oliveira Santos, D. Pantalica, Yu.-E. Penionzhkevich, F. Pougheon, A. Poves, N. Redon, M. G. Saint-Laurent, J. A. Scarpaci, G. Sletten, M. Stanoiu, O. Tarasov, and Ch. Theisen. $^{68}_{28}ni_{40}$: Magicity versus superfluidity. *Phys. Rev. Lett.*, 88:092501, Feb 2002.

[178] M. Honma, T. Otsuka, T. Mizusaki, and M. Hjorth-Jensen. New effective interaction for f_5pg_9-shell nuclei. *Phys. Rev. C*, 80:064323, Dec 2009.

[179] J. Xiang, J. M. Yao, Y. Fu, Z. H. Wang, Z. P. Li, and W. H. Long. Novel triaxial structure in low-lying states of neutron-rich nuclei around $a \approx 100$. *Phys. Rev. C*, 93:054324, May 2016.